



DISSERTAÇÃO DE MESTRADO

**Channel modeling for Through-The-Earth  
(TTE) Communication Systems**

**Josua Daniel Pena Carreno**

**Brasília, Fevereiro de 2016**

**UNIVERSIDADE DE BRASÍLIA**

FACULDADE DE TECNOLOGIA

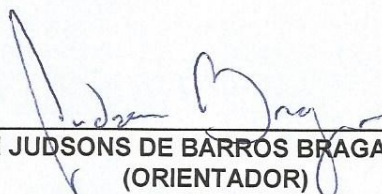
**UNIVERSIDADE DE BRASÍLIA  
FACULDADE DE TECNOLOGIA  
DEPARTAMENTO DE ENGENHARIA ELÉTRICA**

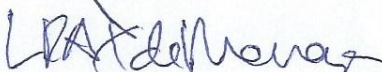
**CHANNEL MODELING FOR THROUGH-THE-EARTH (TTE)  
COMMUNICATION SYSTEMS**

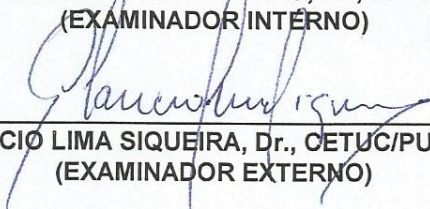
**JOSUA DANIEL PENA CARRENO**

DISSERTAÇÃO DE MESTRADO SUBMETIDA AO DEPARTAMENTO DE ENGENHARIA ELÉTRICA DA FACULDADE DE TECNOLOGIA DA UNIVERSIDADE DE BRASÍLIA, COMO PARTE DOS REQUISITOS NECESSÁRIOS PARA A OBTENÇÃO DO GRAU DE MESTRE.

APROVADA POR:

  
\_\_\_\_\_  
ADONIRAN JUDSONS DE BARROS BRAGA, Dr., ENE/UNB  
(ORIENTADOR)

  
\_\_\_\_\_  
LEONARDO R. A. X. MENEZES, Dr., ENE/UNB  
(EXAMINADOR INTERNO)

  
\_\_\_\_\_  
GLAUCIO LIMA SIQUEIRA, Dr., CETUC/PUC-Rio  
(EXAMINADOR EXTERNO)

Brasília, 19 de fevereiro de 2016.

## FICHA CATALOGRÁFICA

CARRENO, JOSUA DANIEL PENA

Channel modeling for Through-The-Earth (TTE) Communication Systems [Distrito Federal] 2016.

xvi, 97 p., 210 x 297 mm (ENE/FT/UnB, Mestre, Engenharia Elétrica, 2016).

Dissertação de Mestrado - Universidade de Brasília, Faculdade de Tecnologia.

Departamento de Engenharia Elétrica

1. TTE

2. Effective conductivity

3. Underground communication

4. Underground propagation channel

I. ENE/FT/UnB

II. Título (série)

## REFERÊNCIA BIBLIOGRÁFICA

CARRENO, J.D.P. (2016). *Channel modeling for Through-The-Earth (TTE) Communication Systems* .

Dissertação de Mestrado, Publicação: PPGEE-617/16, Departamento de Engenharia Elétrica,

Universidade de Brasília, Brasília, DF, 97 p.

## CESSÃO DE DIREITOS

AUTOR: Josua Daniel Pena Carreno

TÍTULO: Channel modeling for Through-The-Earth (TTE) Communication Systems .

GRAU: Mestre em Engenharia Elétrica ANO: 2016

É concedida à Universidade de Brasília permissão para reproduzir cópias desta Dissertação de Mestrado e para emprestar ou vender tais cópias somente para propósitos acadêmicos e científicos. Os autores reservam outros direitos de publicação e nenhuma parte dessa Dissertação de Mestrado pode ser reproduzida sem autorização por escrito dos autores.



Josua Daniel Pena Carreno

Depto. de Engenharia Elétrica (ENE) - FT

Universidade de Brasília (UnB)

Campus Darcy Ribeiro

CEP 70919-970 - Brasília - DF - Brasil

*To Ana and Jonathan for supporting me every day of my live*

*Josua Daniel Pena Carreno*

## ACKNOWLEDGEMENTS

*I would like to thank:*

*Judson Braga for being a good teacher and a strict leader*

*Savio Neves, Lucas Sousa e Silva and Henrique Berilli for always keeping a positive attitude and being excellent colleagues.*

*Professors Andre Noll and Leonardo Aguayo, for always having a constructive critic and giving good ideas to solve problems*

*Felipe Duerno for teaching me new programming languages and helping me out with all simulations*

*José Pereira Filho, Boanerges Ribeiro, Márcio Sales and Leandro Machado for being beside me in one of the hardest experiences of my life*

*André Vieira, Guilherme Santos, Jesús Gonzalez, Johanel Da Silva, Karla Bocaranda, Laila Wanick, Linniker Corado, Luciano Grossi, Pauli Ramirez, Reni Santos, Sinamaica Henriquez, Sirius Bocaranda, and Uirá Godoi for maintaining our friendship all these years no matter what distance is between us*

*Professor Gladys Bruzual, for supporting me since the first day at Engineering School  
Gustavo Sandri, je suis très heureux de t'avoir comme mon ami et professeur particulier de français*

*Arthur Sudre, for upholding me even without understanding my work*

*And my grandmother and my father for taking care of me from heaven.*

***Special thanks to:*** *"Instituto Tecnológico Vale" (ITV) and "Coordenação de Aperfeiçoamento de Pessoal de Nível Superior" (CAPES) for supporting this study.*

*Josua Daniel Pena Carreno*

---

## **RESUMO**

Este trabalho apresenta modelagem de canal em ambientes de comunicação TTE a partir de modelos analíticos estabelecidos, medidas e simulações eletromagnéticas. Para estes cenários, apresenta-se como contribuição original os resultados estatísticos tanto para a condutividade elétrica efetiva quanto para a atenuação sofrida pelo campo magnético durante a propagação. Os resultados de simulação obtidos aqui, além de confirmarem o comportamento do canal empírico, extrapolam para frequências não estudadas via ferramentas estatísticas.

---

## **ABSTRACT**

This dissertation presents channel modeling in TTE communication environments from well-established analytic models, measurements and electromagnetic simulations. For those scenarios, the main original contribution are the statistical results for the effective electric conductivity as well as the attenuation experimented by magnetic field while propagating Through-The-Earth. The simulation results present here, in addition to confirming the behavior of empirical models, extrapolate to frequencies not studied via statistical tools.

## RESUMO ESTENDIDO

A comunicação com e entre operários que trabalham em espaços confinados sempre foi tema de vital importância para a indústria da mineração, devido a que através de sistemas de comunicação pode se manter contato em tempo real com todos os membros das equipes e transferir informações de apoio durante casos de emergência. Mais recentemente, com a crescente automação na mineração, também é importante se garantir a comunicação entre os diferentes equipamentos e a superfície, Existem vários sistemas de comunicação disponíveis em minas subterrâneas do mundo, sendo que, sistemas baseados em cabos coaxiais ou fibra ótica são os mais utilizados. Porém estes não são eficientes em casos de desastre, podendo sofrer quebras e isolar os operários [1], como em explosões, incêndios, inundações e soterramentos, além de serem pouco flexíveis em ambientes cuja topologia muda o tempo todo.

A grande maioria dos sistemas de comunicação sem fio utiliza topologias de comunicação em radiofrequência (RF) baseadas em antenas radiantes, campo distante e meio de transmissão com características elétricas próximas as do vácuo. No caso em que rochas, solo, água e outros materiais de condutividade elétrica não desprezível se tornam o meio de propagação entre as pontas de comunicação, a alta taxa de atenuação de ondas eletromagnéticas em altas frequências não permite o uso desses sistemas acima citados [2].

Comunicações através da terra ou TTE, do inglês, *Through-the-earth*, consistem no uso de ondas eletromagnéticas para estabelecer um enlace entre a superfície e a mina subterrânea utilizando a terra como meio de propagação. A transmissão é normalmente feita por indução magnética em frequências abaixo de 30 kHz, sujeitas a ruídos atmosféricos e a harmônicos produzidos por equipamentos, limitando o desempenho de comunicação, especialmente no enlace de subida [2].

Uma regulamentação do congresso americano exigindo um sistema de comunicação de emergência em minas subterrâneas de carvão que opere em caso de acidentes, chamada lei *Mine Improvement and New Emergency Response Act (MINER Act)*, impulsionou a pesquisa e o desenvolvimento das comunicações TTE. Segundo a lei, este sistema deve ser sem fio, bidirecional, prover comunicação entre a superfície e o subterrâneo da mina e ser capaz de rastrear as pessoas presas no subterrâneo [3].

Pode-se também utilizar comunicações subterrâneas diferentes do TTE sendo essas cabeadas (TTW, *Through-the-wire*) e/ou sem fio (TTA, *Through-the-air*). Entre as possíveis aplicações, pode-se citar: automação das máquinas presentes na mineração; acionamento de explosivos; comunicação entre mineiros por dados ou de voz; monitoramento da mina por vídeo; monitoramento do estado dos mineiros; detecção de níveis elevados de gases danosos aos mineiros, o monitoramento e coordenação em tempo real da frota e pessoal.

Neste trabalho apresentamos alguns conceitos sobre comunicações em minas, motivados pela grande importância da indústria da mineração no Brasil e sua rápida evolução tecnológica, aliada

à pequena produção científica desta área no país. Este trabalho traz uma visão geral sobre estudos, modelos e equipamentos em torno de comunicações subterrâneas.

## **CONDIÇÕES PARA A COMUNICAÇÃO EM MINAS SUBTERRÂNEAS**

Uma mina pode ser definida como uma massa individual de substância mineral ou fóssil, em lavra, esteja ela na superfície terrestre ou no interior da terra e que tenha um valor econômico [4]. Geralmente, minas subterrâneas são muito úmidas, com umidade relativa do ar podendo chegar a 90% ou mais. Água corrosiva, poeira, gases explosivos e tóxicos, como dióxido de carbono e metano, são substâncias que podem afetar não só o bem estar de operários, mas também a vida útil e regulagem de equipamentos, incluindo os de comunicação.

Esse cenário guarda algumas semelhanças com a aplicações da construção civil, como túneis e metrô, mas com condições mais hostis. Porém, uma característica particular de minas subterrâneas é a sua expansão em função da retirada de minério estéril. A expansão do espaço de cobertura pode levar à necessidade do aumento da infraestrutura de telecomunicações [5]. Isto é especialmente verdade em comunicações TTA, que tem o ar da mina como meio de propagação. Outro aspecto da mina que também influencia as comunicações TTA é a sua forma e tipo de acesso. Escavações que formem minas abertas sustentadas por pilares trazem condições de propagação de ondas diferentes daquelas minas em túnel que tendem a criar um efeito de guia de onda com baixo índice de perda de propagação.

Com respeito às características elétricas do meio, minas diferem uma das outras não apenas pelo mineral explorado, mas também pela proporção deste mineral em relação a outros materiais, como os que compõem o capeamento (*overburden*) que separa a superfície do corpo útil de minério. A variação da condutividade elétrica do meio, em função desta proporção, influencia bastante a perda de propagação no canal, e pode definir o tipo de equipamento e configurações escolhidas para o funcionamento de sistemas de comunicação TTE. Para comunicações em rádio-frequência dentro das minas, como em TTA e, em alguns casos, em TTW, a condutividade das paredes da mina influencia os coeficientes de reflexão e difração e, por consequência, a dispersão temporal do canal de propagação.

## **USO, TÉCNICAS E EQUIPAMENTOS**

Há três principais categorias de comunicação em minas que se destacam: TTW, TTA e TTE, discutidas a seguir.



## **TTW: através do cabo**

Sistemas de comunicação TTW usam meios guiados [5] tanto para comunicação dentro da mina quanto entre superfície e mina. Um dos mais antigos instrumentos para comunicação em minas é o telefone de magneto [6], baseado em linha cabeada para comunicação de voz. Um gerador de magneto composto por ímãs é acionado manualmente por uma alavanca produzindo tensão alternada de 100 V entre 15 e 20 Hz, que após sua transmissão pelo cabo aciona os sinos dos outros telefones conectados. Estabelecida a conexão, baterias são usadas para garantir a alimentação dos equipamentos de comunicação de voz.

Fibras ópticas permitem altas taxas de transmissão de dados a grandes distâncias dentro da mina podendo chegar até 70 km sem necessidade de regeneração do sinal. Por ser uma ferramenta de grande capacidade, é utilizada para monitoramento em tempo real das diversas atividades da mina como sistema contra incêndio, sistemas automáticos entre outros [7].

Por sua vez, o *leaky feeder* é um cabo irradiante híbrido entre a transmissão por cabo (TTW) e a transmissão pelo ar (TTA). Utiliza um cabo coaxial fendido para transmitir e receber a informação dentro do túnel. Este cabo, em vez de ter uma malha protetora, possui uma camada de cobre com perfurações que atuam como um arranjo de antenas de abertura. Devido à perda ao longo do cabo, é necessário ter amplificadores regularmente espaçados tipicamente entre 350 e 500 m de distância. Os cabos fendidos funcionam em ambas as direções de comunicação, usualmente nas bandas VHF e UHF [8].

## **TTA: Através do ar**

Para comunicação dentro da mina, sistemas sem fio (TTA) se tornam mais vantajosos que TTW pela facilidade de instalação e adaptação à expansão da mina. Nos dias de hoje, os sistemas de comunicação TTA em minas são, em sua maioria, adaptações de um ou vários sistemas de comunicação sem fio para curto alcance como Zigbee, WiFi, RFID, etc. [9]. Visto que os equipamentos de rádio utilizados não trazem novidades em relação aos dispositivos RF usados em outras aplicações, esta seção se foca nas propostas de protocolos de redes para comunicação TTA encontradas na literatura.

Considerando a disposição dos nós e a falta de infraestrutura em minas, muitos trabalhos indicam a utilização de redes *ad hoc*. Um dos fatores investigados é o desempenho de protocolos, principalmente aqueles de controle de acesso ao meio ou de roteamento. Na área dos protocolos de controle de acesso ao meio, pode-se citar [10], o qual realiza uma análise de desempenho do protocolo MINECOM, baseado em TDMA-TDD (*time division multiple access - time division duplexing*).

Percebe-se que muitos trabalhos partem do pressuposto da utilização de padrões ou tecnologias que especifiquem os protocolos de camadas inferiores, como por exemplo o IEEE 802.15.4 ou alguma vertente do IEEE 802.11. Com relação a protocolos de roteamento, Jing [11] desenvolve um protocolo híbrido de roteamento para nós móveis baseados no protocolo GEAR (*geo-*

*graphical and energy aware routing*). Neste protocolo, os nós móveis possuem sua comunicação restrita a apenas alguns nós em função da distância e direção de movimento entre eles. Ao se realizar essas restrições, consegue-se aumentar o tempo de vida desses nós móveis.

Em [12, 13, 14], análises do desempenho dos protocolos DSDV (*destination-sequenced distance-vector*) e AODV (*ad hoc on-demand distance vector*) são feitas, levando em consideração a taxa de perda de pacotes, o atraso fim a fim e a vazão em transmissões de vídeo, enquanto que [15] realiza o estudo da utilização do protocolo OLSR (*optimized link state routing*) e do padrão IEEE 802.11n para prover a transmissão de vídeo e voz em minas. Bons resultados de vazão, latência e *jitter* da rede são encontrados.

Já em [16], há o desenvolvimento de um protocolo de roteamento *multi-hop* que utiliza um algoritmo recursivo entre os nós vizinhos para possibilitar a seleção de um caminho que possua uma menor quantidade de saltos, levando em consideração a métrica RSSI (*received signal strength indicator*). Para verificar o protocolo, testes foram realizados utilizando o transmissor MG2455 da *Radio Pulse*. Jiang [17] desenvolve um protocolo de roteamento que leva em consideração a disposição dos túneis em minas, em que há um túnel principal e alguns ramos. Considerando a disposição dos nós e a formação de *clusters* entre eles nesses túneis-ramos, o autor sugere uma forma de realocamento de nós para cada *cluster* a fim de equilibrar a rede.

Zheng [18] descreve a disposição de redes de sensores subterrâneas, assim como as dificuldades existentes no canal sem fio subterrâneo e, por fim, explicita os obstáculos e áreas de pesquisas para as camadas de rede, considerando também um desenvolvimento *cross-layered* como um possível mitigador dos desafios encontrados em redes subterrâneas.

### **TTE: Através da terra**

Nos anos que seguiram o *MINER Act*, o NIOSH (*National Institute for Occupational Safety and Health*) apoiou o desenvolvimento de uma série de tecnologias de comunicação e rastreamento em minas subterrâneas [3]. Cinco protótipos foram desenvolvidos por cinco empresas: *Alertek*, *E-Spectrum Technologies*, *Lockheed Martin*, *Stolar* e *Ultra Electronics*. Quatro protótipos baseiam-se na detecção de campos magnéticos utilizando antenas *loop* e uma na detecção de campos elétricos.

Os sistemas TTE desenvolvidos se mostraram capazes de prover comunicação unidirecional e, em alguns casos, bidirecional, de voz e texto em até 300 m (voz) e 600 m (texto) de profundidade, aproximadamente. Para transmitir voz, os protótipos utilizaram frequências de 3150 Hz a 4820 Hz. Alguns protótipos possuíam também um modo de localização baseado em triangulação, em que apenas um tom é transmitido no enlace de subida. Utilizando receptores dispostos na superfície é possível localizar a posição do transmissor por meio do tratamento do sinal recebido.

Utilizou-se em alguns protótipos modulação analógica SSB (*single side band*), e em outros modulação digital PSK (*phase shift keying*) e/ou FSK (*frequency shift keying*). Além disso, em alguns protótipos, técnicas de cancelamento de ruído foram testadas [3]. Algumas empresas

conseguiram transformar seus projetos em produtos comerciais [19].

O *Flex Alert*, fabricado pela canadense *Mine-Radio Systems*, é um sistema de comunicação unidirecional entre galerias subterrâneas e a superfície, utilizado para dar suporte na evacuação de operários em caso de emergência. Utiliza um campo magnético a baixa frequência que transporta informação a um receptor posicionado no capacete dos mineiros. É composto por uma antena tipo *loop* de 10 a 120 m de comprimento posicionada estrategicamente sobre a mina. Quando há alguma emergência, um sinal é emitido da superfície para todos os mineiros fazendo a lâmpada do capacete piscar sinalizando a evacuação [7].

O *Dispositivo Pessoal de Emergência (PED)* da australiana *MineSite Technology* é um sistema de comunicação unidirecional que permite a transmissão de mensagens de texto específicas às pessoas que se encontram no interior da mina sem uso de cabos. Mesmo fornecendo comunicação só superfície-mina, pode ser utilizado um cabo irradiante (*leaky feeder*) para completar a comunicação no link de subida [7]. O sistema também é usado para detonação remota de explosivos e controle remoto de equipamentos.

Após seus testes em conjunto com a NIOSH, a *Lockheed Martin* comercializa a *MagneLink MCS*, que é um sistema TTE autossuficiente e bidirecional que oferece suporte a voz, texto e localização baseado em ondas magnéticas de baixa frequência. Testes a 500 metros de profundidade validaram as aplicações de voz e texto, em que uma antena de 130 metros de comprimento e outra com múltiplas voltas foram usadas na superfície e na mina, respectivamente.

A canadense *Vital Alert* [20] desenvolveu recentemente o sistema digital *Canary* de rádio TTE bidirecional para comunicação de dados e voz. O receptor da *Canary* é implementado em rádio definido por software, sendo facilmente reconfigurável para operar entre frequências de 300 Hz a 9 kHz. O dispositivo permite modulação adaptativa com taxas que variam de 9 bps a 1 kbps.

Em se tratando de processamento de sinais, [2] sugere o uso de modulação MSK (*minimum shift keying*). O autor também sugere técnicas de combate ao ruído atmosférico e de códigos corretores de erros, para conferir maior robustez ao sistema. O autor afirma melhorar a razão sinal-ruído (RSR) de 10 a 30 dB após a caracterização do ruído utilizando múltiplas antenas ortogonais e a aplicação de técnicas como cancelamento adaptativo de ruído, detecção por máxima verossimilhança e realimentação de decisão. A falta de estudos mais recentes em processamento de sinais para comunicação TTE pode indicar que ainda exista um ganho de desempenho a ser alcançado via tratamento de sinais em investigações futuras.

## PROPAGAÇÃO EM COMUNICAÇÃO TTE

O modo de transmissão TTE mais promissor é ilustrado na Figura 1, onde antenas *loop* na superfície e no subsolo trocam informação via indução magnética. As dimensões e massa de cada uma das antenas, corrente de excitação e frequência de operação definem a qualidade e alcance de transmissão, e podem variar de acordo com o objetivo do sistema, profundidade e características

do solo [21].

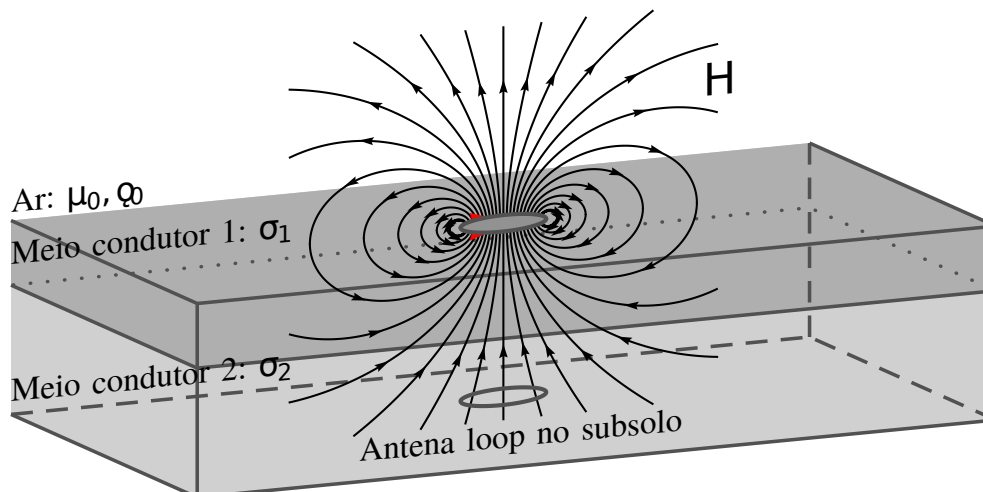


Figure 1: Representação esquemática de sistema de comunicação TTE, operando em *downlink*. As dimensões típicas das antenas são da ordem de dezenas de metros.

Devido às propriedades intrínsecas do solo, a penetração de ondas de rádio em meio condutor obedece à equação de difusão  $\nabla^2 H = \mu\sigma\partial H/\partial t$ , em vez da equação de onda  $\nabla^2 H = \mu\epsilon(\partial^2 H)/(\partial t^2)$  com o campo decaindo exponencialmente em função da distância percorrida, frequência de operação e condutividade elétrica do meio. O grau de decaimento é frequentemente associado à função da profundidade pelicular  $\delta = \sqrt{2/(\omega\mu\sigma)}$ , que representa a distância na qual a intensidade de uma onda plana reduz a  $1/e$  de seu valor. Ou seja, a taxa de decaimento em função da distância  $x$  é expressa por  $e^{-x/\delta}$ . Portanto, a profundidade pelicular é inversamente proporcional à raiz quadrada da frequência, o que justifica o uso de frequências baixas, usualmente abaixo de 30kHz, para comunicação TTE. Essas observações são verdadeiras para meio bom condutor. [22] considera um bom condutor todo material que satisfaça  $\sigma/(\epsilon\omega) \gg 1$ .

Para irradiar ondas eletromagnéticas em frequências tão baixas, as antenas deveriam ser quilométricas para entrarem em ressonância. Em comunicação TTE, a transferência de potência reativa via indução magnética (ou elétrica) corresponde à quase totalidade da potência transmitida. A propagação em meio condutor ou dielétrico também altera algumas propriedades básicas da onda, como a velocidade de propagação  $v_{rocha}$  e o comprimento de onda  $\lambda_{rocha}$ . Em um bom condutor, a contribuição da permissividade real pode ser desprezada e o comprimento de onda que atravessa as rochas da mina pode ser escrito como  $\lambda_{rocha} = 2\pi\delta$ , o que em comunicação TTE operando a 10 kHz com  $\sigma = 10^{-3}\text{S/m}$  pode reduzir em 30 vezes o comprimento de onda em relação ao ar. Desta forma, afirmar que comunicação TTE sempre ocorre em campo próximo pode não ser correto.

## Zonas de Campo

Classicamente, as zonas de campo para transmissão no vácuo ou no ar são divididas em *campo próximo reativo*, *campo próximo radiante*, *zona de transição* e *campo distante* [23]. Nas duas

primeiras zonas, o campo é resultado da interferência de ondas de diversos pontos da antena, como se fossem vários pequenos dipolos contribuindo na formação do campo. Em campo distante, onde os campos elétrico e magnético estão em fase e possuem uma relação fixa entre si, a antena de transmissão é vista como um ponto radiante e seu campo pode ser visto como uma frente de onda plana. Na zona de transição, ambos os comportamentos podem ser observados. Em um meio condutor, Gibson [22] propôs uma subdivisão diferente para as zonas de campo.

Em regiões muito próximas à antena de transmissão, o campo possui uma natureza *quase-estática* seguindo leis da estática como a atenuação pelo inverso do cubo da distância, apesar da variação no tempo. A partir do chamado *campo próximo*, onde, assim como em quase-estático, inexistente irradiação, o meio condutor começa a contribuir em atenuação de campo. Na zona de *campo distante*, apesar das perdas devidas ao meio, o campo obedece à lei de atenuação com inverso linear da distância. Campo distante, no caso, não quer dizer que a radiação parte da antena diretamente, e sim pela indução de correntes parasitas [24] no meio condutivo provocada pelo campo magnético da antena, as quais geram novos campos. Por fim, a zona de transição é uma região arbitrária entre os campos próximo e distante.

A Tabela 3.1 traz as zonas de campo e suas condições para dois tipos de meio. Um sistema operando no espaço livre a 10 kHz ( $\lambda_0=30$  km) com separação entre antenas de 300 m se encontra em campo próximo reativo ( $\frac{\lambda_0}{2\pi} \approx 4775$  m), enquanto que em meio condutor com  $\sigma = 10^{-3}$  S/m e  $\mu = \mu_0$ ,  $\frac{\lambda_{rocha}}{2\pi} = \delta \approx 160$  m < 300 m. Ou seja, trata-se de zona de transição e está mais próximo do campo distante do que do campo próximo.

<i>Modelo</i>	<i>Tipo de aproximação</i>	<i>Condições</i>
Vácuo	Campo próximo reativo	$r < \frac{\lambda_0}{2\pi}$
	Campo próximo radiante	$\frac{\lambda_0}{2\pi} < r < \lambda_0$
	Zona de transição	$\lambda_0 < r < 2\lambda_0$
	Campo distante	$r > 2\lambda_0$ ou $2D^2/\lambda_0$
Meio condutivo	Quase estático	$r \ll \frac{\lambda_{rocha}}{2\pi}$
	Campo próximo	$r^2 \ll \left(\frac{\lambda_{rocha}}{2\pi}\right)^2$
	Zona de transição	$r \approx \frac{\lambda_{rocha}}{2\pi}$
	Campo distante	$r \gg \frac{\lambda_{rocha}}{2\pi}$

Table 1: Zonas de campo no vácuo e em meio condutor

### Modelo de Campo Magnético $H$

O momento magnético de uma antena *loop* indica a eficiência de transmissão indutiva em função das características do transmissor como o número de voltas do *loop*, a corrente RMS nos filamentos da antena de transmissão e a área do *loop*. O aumento de momento magnético tem por custo o aumento da potência dissipada em calor nos filamentos da antena. A aproximação mais simples para o campo magnético variante no tempo gerado por uma antena *loop* se faz considerando o vácuo como meio homogêneo infinito ignorando qualquer condição de contorno [25]. O modelo traz as componentes vertical e horizontal do campo magnético sendo usadas, na maioria das vezes, em comunicação coaxial e coplanar entre dois *loops*, respectivamente, e que

dependem do momento magnético, distância e frequência. A adaptação para um meio infinito condutivo (MIC) para ambos os enlaces de subida e descida é feita modificando-se apenas o número de onda em função da distância pelicular  $\delta$ . Wait formulou expressões analíticas do campo magnético de antenas circulares com corrente uniforme distinguindo os meios superfície e subterrâneo, nos chamados modelos de semi-espço homogêneo (SEH), para os enlaces de subida [26] e de descida [27]. Nestes modelos existe reciprocidade entre os dois enlaces apenas para o campo vertical, e não o horizontal, diferentemente do modelo MIC. Durkin [28] sugere que exista na interface entre a terra e o ar uma barreira de transposição que possa ser modelada por uma fina camada de condutividade ainda maior que aquela do semi-espço homogêneo abaixo dela. Chamamos este modelo de semi-espço homogêneo com superfície condutora, em que a espessura da camada de interface e sua condutividade são parâmetros de entrada.

# INDEX

<b>1</b>	<b>INTRODUCTION</b>	<b>1</b>
<b>2</b>	<b>BASIC CONCEPTS</b>	<b>4</b>
2.1	MINE	4
2.2	UNDERGROUND MINE COMMUNICATION	5
2.2.1	TTW: THROUGH-THE-WIRE	5
2.2.2	TTA: THROUGH-THE-AIR	7
2.3	PROTOCOLS USED FOR UNDERGROUND COMMUNICATION	8
2.4	EQUIPMENT FOR UNDERGROUND COMMUNICATION	9
2.5	NUMERICAL SIMULATIONS OF MAGNETIC TRANSMISSION ENVIRONMENTS	10
<b>3</b>	<b>PROPAGATION IN UNDERGROUND TTE COMMUNICATION SYSTEMS</b>	<b>12</b>
3.1	FIELD ZONES	12
3.2	ANTENNA MODELING FOR TTE COMMUNICATIONS	13
3.3	THEORETICAL MODELS FOR TTE PROPAGATION	15
3.3.1	INFINITE CONDUCTIVE MEDIUM (IC)	15
3.3.2	HOMOGENEOUS HALF-SPACE MODEL (HHS)	16
3.3.3	THIN SHEET MODEL (TS)	17
3.3.4	MULTI-LAYER MODEL	18
3.4	CHANNEL MODELING AND OPTIMUM OPERATION FREQUENCY	20
3.5	SOIL CONDUCTIVITY	23
<b>4</b>	<b>ANALYSIS OF ANALYTIC MODELS, MEASUREMENTS AND SIMULATIONS</b>	<b>26</b>
4.1	THEORETICAL MODELS FOR H-FIELD AND TRANSFER FUNCTION	26
4.1.1	MAGNETIC FIELD	26
4.1.2	TRANSFER FUNCTION	27
4.2	HHS AND TS MODELS CURVES	28
4.3	PRELIMINARY SIMULATION RESULTS	29
4.3.1	SCENARIO I: FIXED NUMBER OF LAYERS	30
4.3.2	SCENARIO II: RANDOM NUMBER OF LAYERS	31
4.4	ELECTRIC CONDUCTIVITY CHARACTERIZATION THROUGH MEASUREMENTS IN UNDERGROUND MINES	32
4.4.1	EQUIVALENT ELECTRIC CONDUCTIVITY OVER ALL FREQUENCIES AND DEPTHS	35
4.4.2	EQUIVALENT ELECTRIC CONDUCTIVITY ESTIMATION AS A FUNCTION OF FREQUENCY	36

4.4.3	EQUIVALENT ELECTRIC CONDUCTIVITY ESTIMATION AS A FUNCTION OF MINE DEPTH .....	40
4.5	MULTI-LAYER STATISTICAL MODEL THROUGH ELECTROMAGNETIC FIELD SIMULATIONS .....	42
4.5.1	H-FIELD VARIATION AS A FUNCTION OF DEPTH AND FREQUENCY .....	43
4.5.2	H-FIELD MEDIAN FITTING .....	45
4.5.3	EQUIVALENT CONDUCTIVITY .....	47
4.6	ISSUES SOLVED WHILE USING THE COMMERCIAL SIMULATOR .....	50
<b>5</b>	<b>CONCLUSION .....</b>	<b>62</b>
	<b>BIBLIOGRAPHICAL REFERENCES .....</b>	<b>64</b>
	<b>APPENDIX .....</b>	<b>68</b>
<b>I</b>	<b>MINER ACT OF 2006 .....</b>	<b>69</b>
<b>II</b>	<b>3D MAGNETIC FIELD SIMULATION ON CST STUDIO SUITE .....</b>	<b>71</b>
<b>III</b>	<b>ROOT MEAN SQUARE ERROR (RMSE) .....</b>	<b>74</b>
<b>IV</b>	<b>LOGNORMAL DISTRIBUTION .....</b>	<b>75</b>
<b>V</b>	<b>STATISTICAL PARAMETERS USED .....</b>	<b>76</b>
<b>VI</b>	<b>NUMERIC METHODS FOR ELECTROMAGNETIC MODELING .....</b>	<b>78</b>
VI.1	FDTD .....	78
VI.2	METHOD OF MOMENTS (MOM) .....	79
VI.3	FINITE ELEMENT METHOD (FEM) .....	80
<b>VII</b>	<b>MAGNETIC FIELD MEASUREMENTS FROM 94 AMERICAN COAL MINES .....</b>	<b>83</b>
<b>VIII</b>	<b>H-FIELD STATISTICAL DISTRIBUTIONS FOR FREQUENCY AND DEPTH .....</b>	<b>89</b>



# FIGURE LIST

1	Representação esquemática de sistema de comunicação TTE, operando em <i>down-link</i> . As dimensões típicas das antenas são da ordem de dezenas de metros. ....	xii
2.1	Surface and underground mines .....	5
2.2	Magnetic telephone .....	6
2.3	Fiber optics.....	6
2.4	Leaky Feeder .....	7
2.5	TE and TM modes in waveguides .....	7
3.1	Through-The-Earth communication .....	12
3.2	Field regions for typical Antennae Adapted from: OSHA [29] .....	13
3.3	Channel transfer function.....	14
3.4	Infinite Conductive Medium IC.....	16
3.5	HHS Geometry.....	17
3.6	Thin sheet configuration .....	18
3.7	Stratified soil for Multi-layer model .....	19
3.8	Geometry used in the calculation of the magnetic field between two circular loop antennae. The angle $\alpha$ formed by orthogonal vectors to the planes determined by the two antennae is the result of rotations around the $\hat{x}'$ e $\hat{y}'$ axis. ....	21
3.9	Equivalent conductivity for 630 Hz for 94 coal mines .....	24
3.10	Estimated Apparent conductivities (S/m) change with overburden depth interval (m) for various $\sigma d$ at 630 Hz.....	24
4.1	H-field from a loop antenna for coaxial and co-planar configuration.....	27
4.2	Channel transfer function.....	27
4.5	H-field TS and HHS models .....	29
4.12	Conductivities over all frequencies and depths.....	35
4.13	Conductivities over all depths for 630 Hz .....	36
4.14	Conductivities over all depths for 1050 Hz .....	37
4.15	Conductivities over all depths for 1950 Hz .....	37
4.16	Conductivities over all depths for 3030 Hz .....	38
4.17	Conductivities over all depths (normalized in frequency) .....	39
4.18	$\mu$ parameter: polynomial 3rd order extrapolation .....	40
4.19	Conductivities for each frequency as a function of depth.....	40
4.26	H-field median fitting.....	46
4.27	H-field median fitting.....	47
4.28	H-field median fitting.....	49
4.3	H-field TS and HHS models variation of parameters $\sigma d$ .....	51

4.4	Simulation scenario for <b>HHS</b> model simulation .....	52
4.6	H-field statistical characterization at 50 m .....	53
4.7	H-field statistical characterization at 110 m.....	54
4.8	H-field statistical characterization at 150 m.....	55
4.9	H-field statistical characterization at 50 m .....	56
4.10	H-field statistical characterization at 110 m.....	57
4.11	H-field statistical characterization at 150 m.....	58
4.20	Conductivities (normalized in frequency and depth) .....	59
4.21	Multi-layer TTE scenario.....	59
4.22	H-field variation for a single mine.....	60
4.23	H-field variation for a single mine.....	60
4.24	H-field variation as a function of depth .....	61
4.25	H-field variation as a function of frequency .....	61
II.1	Tetrahedral meshing .....	72
II.2	Border conditions.....	72
II.3	Magnetic field inside substrates.....	73
II.4	Current result in linear scale .....	73
VI.1	Basic Element of FDTD Space segmentation .....	79
VI.2	FEM segmentation example .....	81
VIII.1	H-field statistical characterization at 20 m and 657.9 Hz.....	89
VIII.2	H-field statistical characterization at 20 m and 4328.8 Hz .....	90
VIII.3	H-field statistical characterization at 20 m and 10000 Hz .....	91
VIII.4	H-field statistical characterization at 150 m and 657.9 Hz .....	92
VIII.5	H-field statistical characterization at 150 m and 4328.8 Hz.....	93
VIII.6	H-field statistical characterization at 150 m and 10000 Hz .....	94
VIII.7	H-field statistical characterization at 300 m and 657.9 Hz .....	95
VIII.8	H-field statistical characterization at 300 m and 4328.8 Hz.....	96
VIII.9	H-field statistical characterization at 300 m and 10000 Hz .....	97

# TABLE LIST

1	Zonas de campo no vácuo e em meio condutor .....	xiii
3.1	Comparison between near and far field for free space and a conductive medium. ...	14
3.2	Logarithmic regression model.....	25
4.1	Statistical characteristics for H-field in stratified medium with fix number of layers	31
4.2	Statistical characteristics for H-field in stratified medium with random number of layers .....	31
4.3	Surface Vertical Magnetic Field signal levels vs. Overburden Depth from 94 Coal Mine Sites Normalized by magnetic moment .....	32
4.4	RMSE error over all frequencies and distances .....	36
4.5	RMSE error of conductivity distribution over all depths for each frequency .....	38
4.6	Log-normal extrapolation .....	39
4.7	RMSE error of conductivity distribution for each frequency for depths between 0 and 100 meters .....	41
4.8	RMSE error of conductivity distribution for each frequency for depths between 100 and 200 meters .....	41
4.9	RMSE error of conductivity distribution for each frequency for depths between 200 and 500 meters .....	41
4.10	$\mu$ parameter in dB for Log-normal distribution of conductivity .....	41
4.11	$\sigma$ parameter in dB for Log-normal distribution of conductivity .....	42
4.12	$\mu$ parameter in dB for Log Normal Distribution 1 .....	42
4.13	H-field distribution for each pair of depth/frequency .....	44
4.14	RMSE of field distribution for each pair of depth/frequency .....	44
4.15	Mean values for H-field for three depths and three frequencies.....	44
4.16	Standard deviation values for H-field for three depths and three frequencies.....	44
4.17	H-field median coefficients.....	45
V.1	Burr parameters .....	76
V.2	Extreme value parameters .....	76
V.3	Generalized Pareto parameters .....	76
V.4	Log-logistic parameters .....	77
V.5	Log-normal parameters .....	77
V.6	Normal parameters .....	77
VII.1	Surface Vertical Magnetic Field signal levels vs. Overburden Depth from 94 Coal Mine Sites .....	83
VII.2	In-mine Collins Transmitter RMS Magnetic Moment at Fundamental Operation frequency vs. Frequency and Depth from 94 Coal Mine Sites .....	86

# LIST OF SYMBOLS

## LATIN SYMBOLS

$Md$       Magnetic moment      [ $A/m^2$ ]

## GREEK SYMBOLS

$\delta$       Skin Depth  
 $\mu_0$       Vacuum Magnetic Permeability

## ABBREVIATIONS

CST      Computer Simulation Technology  
DSP      Digital Signal Processor  
EFIE      Electric Field Integral Equation  
FDTD      Finite-Difference Time-Domain  
FEM      Finite Element Method  
FSK      Frequency Shift Keying  
GPD      Generalized Pareto Distribution  
HHS      Homogeneous Half-Space  
IC      Infinite Conductive Medium  
ISI      InterSymbol Interference  
MFIE      Magnetic Field Integral Equation  
MoM      Method of Moments  
NIOSH      National Institute for Occupational Safety and Health (United States of America)  
PEC      Perfect Electric Conductor  
PMC      Perfect Magnetic Conductor  
PSK      Phase Shift Keying  
RF      Radio Frequency  
RFID      Radio Frequency IDentification  
RMSE      Random Mean Square Error  
SSB      Single Side Band  
TS      Thin Sheet model  
TTA      Through-The-Air  
TTE      Through-The-Earth  
TTW      Through-The-Wire  
VBA      Visual Basic for Applications

# 1 INTRODUCTION

A mine can be defined as a mass of mineral or fossil substance, under excavation, whether it is superficial or underground and that its production has economical value [4]. Usually, underground mines are very humid, with the relative air humidity close to 90%. Corrosive water, dust, explosive and toxic gases as carbon and methane dioxide, are substances that can affect workers and machinery, including communication systems. The channel modeling in such media permit a more precise strategy for communication in mines, however it must take into account soil complexity and heterogeneity.

Such scenario is similar to several civil construction applications as subway tunnels, but in more hostile conditions. Nevertheless, a particular characteristic of underground mines is its expansion as a function of ore extraction. This cover area expansion can impel the necessity of continuous increasing telecommunication infrastructure. This is specially correct in TTA (Through-the-Air) Communications where the air inside the mine is the propagation medium. Another mine characteristic which influences TTA communication is mine shape and type of access. Excavations forming open mines supported by pillars give different propagation conditions from tunneled mines which tends to create a waveguide effect with low propagation loss index.

Regarding to electric characteristics of medium, mines are different from one another not just from mineral's perspective, but also from the proportion of different materials and humidity. Variation of electrical conductivity in medium, arouses substantially propagation losses and can define the type of equipment to be used as well as working configuration of TTE (Through-The-Earth) communication systems. For radio-frequency communications inside mines, as TTA and, in some cases, TTW (Through-The-Wire), mine tunnel walls conductivity can affect reflection and diffraction coefficients and, consequently, time dispersion of the propagation channel.

The majority of wireless communication systems use radio-frequency topology based on radiating antennae, far-field and transmission medium with characteristics close to vacuum conditions. When rocks, soil, water, and other materials with non-neglecting electric conductivity, are the propagation medium, such conditions can not be used. That is because exists a significant attenuation rate of electromagnetic waves at high frequencies which does not allow the use of TTA communication systems.

Through-The-Earth communication systems consist on using electromagnetic waves to establish a link between surface and the underground mine using soil as propagation medium. Generally, transmission is realized by magnetic induction at frequencies below 30 kHz, and it is subject to atmospheric noise and harmonics produced by equipment inside the mine. That condition limits communication performance specially in up-link transmission.

Communicating with personnel working in confined spaces has been always an important issue for mining industry. Through the use of communication system it is possible to keep real-time

contact with all team members and transmitting back-up information in emergency situations.

Among with the growing of automation in mining industry, it is also important to guarantee communication between different equipment and surface control station. Even when the most used systems for underground communication are wired, they are not efficient in cases of emergency, due to their vulnerability to break during explosions, fires, floods, and burial.

A regulation from the congress of the United States of America was extended demanding reliable systems for emergency situations in underground mines. Such regulation was named as Mine Improvement and New Emergency Response Act (MINER Act) and prompted research on TTE communication. According to this statute, such system must be wireless, bidirectional, provide communication from surface to underground mine and vice versa, and track people buried.

Some models were created in order to model the TTE propagation. Those models have different levels of complexity, starting from a simple homogeneous channel model to a much more close-to-reality model yet extremely complicated to implement. The simplest approximation for transmission of a magnetic field created by a loop antenna electrically small is made by considering vacuum as a homogeneous medium, neglecting any boundary condition, and assuming uniform distributed current on the loop. Then, that homogeneous medium can be altered to replace the vacuum by an Infinite Conductive (IC) medium.

Wait in [26] and [27] upgrades that simplification and proposed a model to describe a Homogeneous Half-Space (HHS) model where one antenna is located in air over a homogeneous soil of electric conductivity  $\sigma$  different from vacuum, and the other antenna is buried at a certain distance from surface. Later, Hill and Wait in [30] proposed a model that modifies Wait's HHS model by introducing a conductive barrier between air and soil. Such barrier has a higher electric conductivity than the homogeneous soil where the receiver antenna is buried due to the use of electric equipment and cables on surface and in low depths. Finally in 2014, Lincan in his doctorate thesis [31] proposed a more complex and laborious model that characterized the propagation medium as a stratified soil with different electrical conductivities for each layer. This model also contemplates the configuration of two loop antennae with one of them buried at a certain distance.

In the consulted literature there are few studies related to effective or equivalent electric conductivity in stratified soils from underground mines. Actually, some simplifications are made as supposing homogeneous materials or using weighted arithmetic mean for producing an equivalent conductivity and then use the homogeneous model.

This investigation aims the statistical characterization of electric conductivity and magnetic field attenuation in underground mines. The statistic models are based on measurements carried out in 94 different coal mines in the United States in 1970's and electromagnetic simulations using numerical methods

This dissertation is organized as follows: Chapter II introduces a brief revision of general concepts related to mining and underground communication; Chapter III brings a revision about propagation models for TTE communication systems; Chapter IV presents the scenarios chosen

to simulate propagation in underground mines as well as the analysis of results from those simulations; and finally in Chapter V can be found the conclusions and some proposals for future researches related to TTE.

## 2 BASIC CONCEPTS

This chapter addresses the most relevant topics found in literature related to underground communication (UC). A complete review is beyond the scope of this document. Therefore, the aim of this section is to explain the ideas associated to this work basis. Further information will be found in following chapters.

Sections 2.1 and 2.2 introduce the concepts of mine and communication in underground mines. Section 2.3 presents part of communication protocols used for UC. In section 2.4 some commercial equipment are presented.

### 2.1 MINE

Before talking about Underground Communication, it is important to classify a mine. There are two types of mines depending on where the mineral is located and how it is exploited, both types are:

#### **Surface mine:**

According to [32], if the mineral is on the surface or close to it, that mine is classified as surface mine. Such kind of mine is exploited through open pits or open cast methods, generally mining in benches or steps. Also, this type of mine is the most predominant used around the world, has high productivity, is low operating cost, and provides good safety conditions.

#### **Underground mine:**

Also, according to [32] if the mineral is several meters under surface it is denominated underground mine. Depending on the type of wall and roof support technique used, those mines can be classified as unsupported, supported or caves. That classification is listed as follows:

- **Unsupported mines:** are those where mineral deposits are roughly tabular. They are generally associated with strong ore and surrounding rock, making possible the absence of artificial pillars for assisting in the support of the openings.
- **Supported mines:** are those with weak rock structure which creates the need of artificial supports. The most used construction method is called "Cut-and-fill" that consists in filling the voids created while taking horizontal slices of mineral with rock waste, tailings, cemented tailings, or other suitable materials, in order to support the walls.
- **Caved mines:** according to [33], such mines are characterized by caving and extraction of massive volumes of rock that can result in the formation of a surface depression whose morphology depends on mineral extraction process, mass of rock, and ground surface to-



pography.

In figure 2.1 are presented images related to such kind of mines.

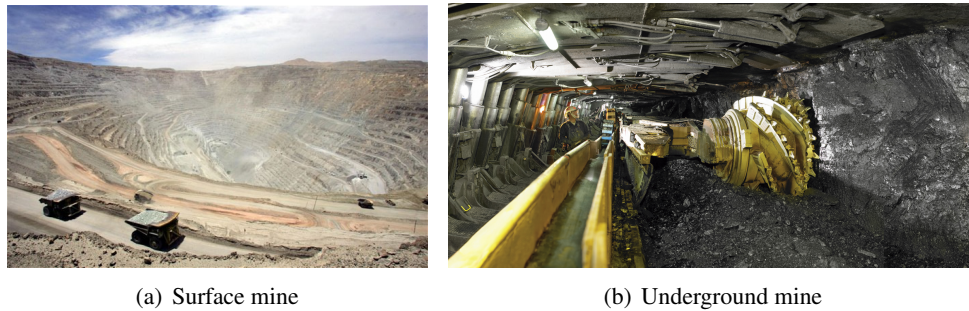


Figure 2.1: Surface and underground mines.

Sources: a) Madeline Ratcliffe [34] b) ASSOCIATED PRESS [35]

## 2.2 UNDERGROUND MINE COMMUNICATION

### 2.2.1 TTW: Through-The-Wire

Communication systems using guided media as coaxial cables, copper stranded wire, fiber optics, or waveguides are called Through-The-Wire systems [5]. In mining industry several TTW systems have been used, some of them are mentioned as follows:

- **Magnetic telephone:** This device is constituted by: a battery, a manual generator, bells, a switchhook, a cable coupling, a transmitter, and a receiver. The battery provides direct current to the transmitter and, by actuating the lever, an alternate current of almost 100 V 15-20 Hz is generated. Then, that current is able to activate the receiver's bells and the communication can be initiated. The main problem of this system is that it can not be used by several telephones due to weak signal generated [6]. Figure 2.2 shows a magnetic telephone used in underground mines.



Figure 2.2: Magnetic telephone  
Source: ATM MINING TELEPHONES [36]

- **Fiber optics:** Such system work as waveguides where light is confined within the fiber core. Usually those fibers are made of plastic or glass. The latter type has a wider bandwidth, less losses and is more expensive than plastic fibers [37]. They allow high data transmission rates within long distances inside the mine. Due to the fact of being a great capacity tool, it is used for real-time monitoring of several activities in the interior of a mine. Such activities are: fire protection system, CCTV, automatic systems, etc. [7]

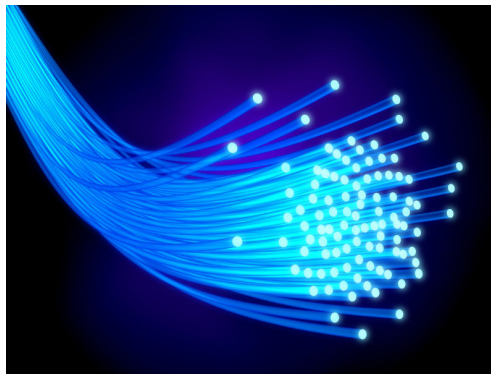


Figure 2.3: Fiber optics  
Source: Inteligencia em negócios [38]

- **Leaky feeder:** According to [39], a system with irradiating cables, commonly known as leaky feeders, is a hybrid technology between a Through-The-Wire and a Through-The-Air system. It uses a modified coaxial cable for transmitting and receiving information inside a tunnel. This cable instead of having a protective woven shield it has a copper layer with several slits acting as an aperture antennae array. Due to losses along cables, it is necessary to use signal amplifiers regularly positioned from 350 to 500 m. That signal is usually received via mobile devices carried by miners. The inverse process is realized by the same cable and it also transmits the signal to other places inside the mine. As stated in [8] this system uses frequencies VHF (150 MHz) and UHF (450 MHz).



Figure 2.4: Leaky Feeder  
Source: CDCP [39]

## 2.2.2 TTA: Through-The-Air

Through-The-Air communication inside a mine is more effective than TTW due to its easy installation and adaptation to mine's expansion. A particular characteristic of underground mines is expansion as a result of mineral extraction. This creates the necessity of upgrading telecommunication settings and/or infrastructure [5]. Another aspects that influence TTA communication are: mine shape and type of access. Excavations forming open mines supported by pillars give propagation conditions differing from tunnel mines.

Nowadays, TTA communication for underground mines are, mostly, adaptations of one or several small-range wireless communication systems such as the following [9]:

- **Tunnels as waveguides:** Underground mines tend to create the effect of waveguides with a low propagation loss index. This has been studied by Forooshane et al. in [21]. The authors present six analytic models for describing propagation inside tunnels. The simplest model presented in the article supposes signals propagating in TM as well in TE mode. Figure 2.5 shows both propagation modes.

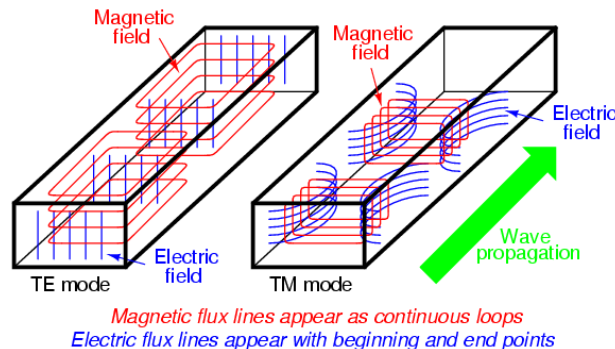


Figure 2.5: TE and TM modes in waveguides  
Source: Physics Stack Exchange [40]

- **Zigbee:** According to [41], this is a wireless system distributed under IEEE recommendation 802.15.4 for low-power consumption and low-cost personal area networks. Operation frequencies are from industrial, scientific and medical radios (ISM), where 2,4 GHz is the most used around the world. These networks are used as a backbone for transmission of RFID signals.
- **Wireless LAN:** Such systems are based on IEEE 802.11 recommendation and work at non licensed frequencies for providing high data rate transmission [42]. Usually those systems are used for ad hoc networks and in underground mines are a simple and non-expensive

solution. The Wi-Fi Alliance is a global non-profit association which works to guarantee interoperability and security protection for 802.11 standard. As one of the most used technologies for indoor data transmission, it is a useful solution for underground communication.

- **RFID:** Radio-Frequency Identification is a method that uses RFID labels, tag readers, routers and radio-bases for detecting individual, objects or devices unequivocally. The latter have RFID tags containing small chips with specifically information. They can be either active or passive. For mine communication the active tags can have a 100 m range and passive 8 m. Routers are located in every mine level in order to mediate between radio stations and RFID tags. RFID readers receive information from tags and rout it to base-station making easier miner position monitoring [9].

### 2.3 PROTOCOLS USED FOR UNDERGROUND COMMUNICATION

The majority of protocols used in underground communication are applied in TTA transmission. Some of them can be adapted to TTE communication networks. Considering a mobile network inside a mine with limited infrastructure, several works suggest the use of *ad hoc* networks. One of investigated factor is protocol performance, especially those used for media access or routing control. In media control access protocol it is possible to cite [10] where the performance of MINECOM protocol is analyzed. Such protocol is bases on TDMA-TDD (Time Division Multiple Access - Time Division Duplexing).

Regarding routing protocols, Jing [11] developed a hybrid routing protocol for mobile nodes based on GEAR (Geographical and Energy Aware Routing). On that protocol, mobile nodes have restricted communication to some other nodes as a function of distance and movement direction between them. While doing such restrictions, it is possible to increase the lifetime of those mobile nodes.

Chetan and Wu in [12, 14] present two performance analysis of DSDV (Destination-Sequenced Distance-Vector) and AODV (Ad hoc On-demand Distance Vector). Those analysis consider package loss rate, end-to-end delay and video transmission spreading; while in [15] the OLSR (Optimized Link State Routing) protocol and IEEE 802.11n standard are analyzed for voice and video transmission in mines. Good results on spreading, latency and jitter on network are found as well.

In [16], the author develops a multi-hop routing protocol that uses a recursive algorithm between neighbor nodes for permitting the selection of the smallest number of path hops. Such selection considers the RSSI (Received Signal Strength Indicator) metric, and, for verifying the protocol, tests using the MG2455 transmitter from Radio Pulse were realized.

Jiang in [17] developed a routing protocol that considers mine tunnel disposition as a main tunnel with several branch tunnels. Observing node disposition and cluster formation through

those branches, the author suggests reallocating nodes for every cluster in order to balance the network.

Zheng in [18] describes the disposition of Underground Sensor Networks as well as problems at wireless underground channels. Finally, the author mentions the obstacles and the further works for network layers, considering also the development of a cross-layered structure as a possible mitigating solution for underground network issues.

## 2.4 EQUIPMENT FOR UNDERGROUND COMMUNICATION

In the following years after the MINER Act (see Appendix I), the American NIOSH (National Institute for Occupational Safety and Health) supported the development of a series of communication technologies and tracking for underground mines [3]. Five prototypes were developed by five different companies: **Alertek**, **E-Spectrum Technologies**, **Lockheed Martin**, **Stolar**, and **Ultra Electronics**. Four of them are based on magnetic field detection via loop antennae and the other detects electric fields.

Those TTE systems show the capability of unidirectional communication and, in some cases, bidirectional communication for voice and text transmission up to 300 m (voice) and 600 m (text). For voice transmission, those prototypes use frequencies of 3150 Hz and 4820 Hz.

Some prototypes have a location mode based on triangulation, where only a tone is used in up-link node. Using receivers located on mine's surface it is possible to locate transmitter's position treating the received signal.

In some prototypes the analogical modulation SSB (Single Side Band) was used, and in others were used digital modulation PSK (Phase Shift Keying) and/or FSK (Frequency Shift Keying). Additionally, some companies tested noise cancellation techniques for their prototypes [3].

Also, a few enterprises could transform their prototypes into commercial products [19]. Some of those commercial products are listed below.

- **Flex Alert**: Is an unidirectional communication system, between underground galleries and above ground facilities, used in emergency situations. This system is composed by a loop antenna of 10 to 120 m long strategically located on mine surface. It sends an electromagnetic field at low frequencies to a receiver situated on miners' helmets which activates helmet's lamp and a secondary LED [42].
- **TeleMag**: Is a bidirectional communication system operating at frequencies between 3 and 8 kHz which uses the single-side band (SSB) modulation technique and tracking DSP<sup>1</sup>-based filters for attenuating noise induced by transmitted signal harmonics. That combination of technologies improves Signal-to-Noise ratio.

---

<sup>1</sup>Digital Signal Processor

Also, it is a fixed base-to-base system where transmitting and receiving antennae are filamentary loops. This device has been tested at up to 100 m depth, even though theoretical calculations indicate that it is possible to reach up to 330 m.

Main advantages of this system are: bidirectional communication and compatibility with other devices inside and outside mine. Disadvantages are: the system does not accomplish the prerogatives from the American MSHA <sup>2</sup>(Mine Safety and Health Administration) [42]

- **Personal Emergency Device (PED)**: Is an unidirectional communication system that allows transmission of specific text messages to inside mine personnel wirelessly. Even though it provides only down-link communication, a leaky feeder cable can be used for completing both ends [42]. This system can also be used for remote detonation of explosives and remote controlling of equipment.
- **MagneLink MCS**: this system was commercialized after joint tests with NIOSH by **Lockheed Martin**. It is a self-sufficient and bidirectional system that supports voice, text and localization based on low-frequency magnetic waves. Validating tests, using a transmitting antenna with a diameter of 130 m and a receiving antenna with multiple turns, were realized for voice and text transmission up to 500 m depth.
- **Vital Alert**: this device was developed by the Canadian Enterprise **Vital Alert** [20] and commercialized using the name "Canary". It is a bidirectional digital communication system for voice and data transmission. The receiver is implemented through software defined radio which simplifies reconfiguration in order to operate at frequencies from 300 Hz to 9 kHz. Also, it permits adaptive modulation with rates varying from 9 bps to 1 kbps.

## 2.5 NUMERICAL SIMULATIONS OF MAGNETIC TRANSMISSION ENVIRONMENTS

Numerical method usage for calculation of magnetic fields, magnetic field densities, impedance, etc. from Maxwell equations has been essential to antennae design and complex propagation media modeling. The most used techniques for such calculations are listed by Todd in [43] and are presented in Appendix VI.

Such methods are usually separated in two main groups of solvers: Differential Equation (DE) solvers and Integral Equation (IE) solvers. Finite-difference time-domain (FDTD) and Finite element method (FEM) are DE solvers with different solution techniques, the first in time and the later in frequency domain, that generally require the same computational power (computer power) to solve problems. Because each of these solutions discretizes the problem and requires a radiation volume, generally their problem sizes are comparable. The IE solver named method of moments (MoM) does not require a radiation boundary by imposing certain boundary conditions to the structure in its solution technique. However, because of these imposed boundary conditions

---

<sup>2</sup>The MSHA establishes that all electric equipment, used near a mine access or inside it, must be designed, built and installed in such way that it does not cause an explosion and/or fire, or another accident.

this technique is not useful for complex 3D volumes of non metallic surfaces, and clearly cannot be used to solve TTE radiation problems. Simulations of TTE environments in low frequencies have been carried out using FDTD [44] and FEM [45] solvers with adequate performances. In this dissertation, all numerical calculations are based on FEM solver.

### 3 PROPAGATION IN UNDERGROUND TTE COMMUNICATION SYSTEMS

Through-The-Earth communication uses ground as propagation medium for electromagnetic waves carrying the transmitted information. The most general representation of such systems is shown in Figure 3.1, where there is an above-ground antenna and another inside the underground gallery. Antennae dimension will vary according to operation characteristics and system's main objective [21].

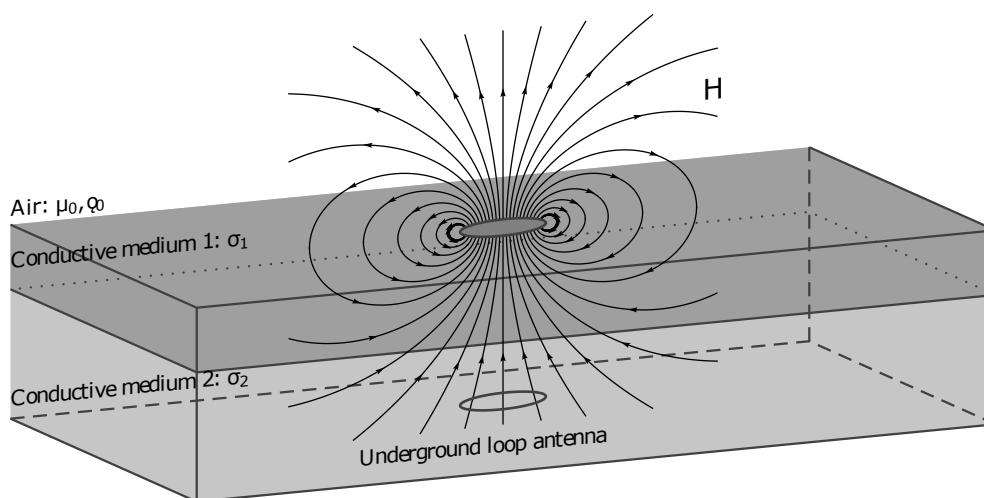


Figure 3.1: Through-The-Earth communication.

Due to intrinsic characteristics of soil, radio-frequency waves dissipation and finite electric conductivity, electromagnetic waves penetration is modeled by the diffusion equation  $\nabla^2 H = \mu\sigma\partial H/\partial t$  instead of wave equation  $\nabla^2 H = \mu\epsilon(\partial^2 H)/(\partial t^2)$ . The magnetic field decays exponentially with traveled distance through material medium and such decay can be expressed as a function of skin depth  $\delta$ <sup>1</sup>. For a uniform conductive medium, the skin depth is the distance at which the intensity of a propagating plane wave decays to  $e^{-1}$  of its value. Also, in a conductive medium the skin depth is inversely proportional to frequency square root, so it is necessary to use low frequencies in order to guarantee less propagation losses within soil. Such low frequencies usually are VLF (3-30 kHz) and sometimes LF (30-300 kHz) [22].

#### 3.1 FIELD ZONES

Traditionally, field zones for transmission in vacuum conditions or in air are divided in Reactive Near Field, Radiant Near Field, Transition Zone and Far-field [23]. In the first two zones, the

<sup>1</sup> $\delta = \frac{2}{\mu_0\sigma\omega}$  where  $\mu_0$  is the magnetic conductivity of vacuum,  $\sigma$  electrical conductivity of soil,  $\omega$  the angular frequency



field is a consequence of interference produced by different points on the antenna, which acts as an array of small dipoles contributing to resulting field. In far-field, where magnetic and electric field have orthogonal phases and have a fix relation between each other, the transmitting antenna is seen as a radiating point and its field is seen as a plane wave front. In transition zone, both behaviors can be observed. in a conductive medium, Gibson [22] proposed a different subdivision for field zones.

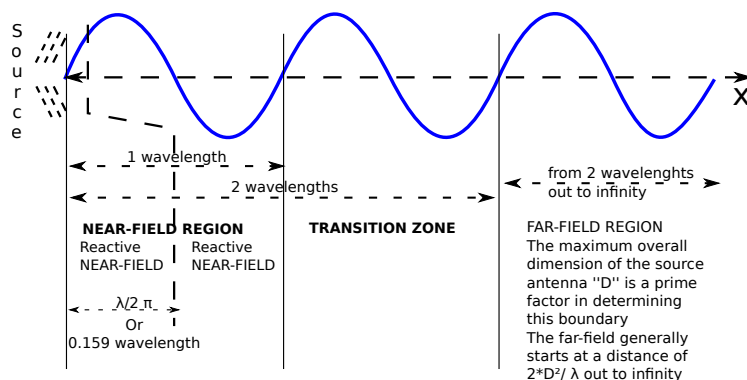


Figure 3.2: Field regions for typical Antennae  
Adapted from: OSHA [29]

In close to transmitting antenna regions, the field presents "quasi-static" behavior and follows electrostatic laws as attenuation as a function of inverse cube of distance even when it is varying in time. From near-field and ahead, the conductive medium begins to contribute to field attenuation. In far-field, despite there are losses due to surrounding medium, the field obeys the linear attenuation law as a function of distance inverse. Still in far-field, the field received is not only the one generated by the transmitting antenna, but also those generated by parasitic currents [24] induced in the conductive medium by the original field. Finally, the transition zone is an arbitrary region between near and far-field.

Table 3.1 presents the field zones and their characteristics for two types of medium. A system operating in free space at 10 kHz ( $\lambda = 30$  km) with a separation of 300 m between antennae is Reactive Near-Field ( $\frac{\lambda_0}{2\pi} \approx 4775$  m). In a conductive medium with an electric conductivity  $\sigma = 10^{-3}$  S/m and magnetic permeability  $\mu = \mu_0$ , the wavelength is reduced to approximately <sup>2</sup> 160 m which is less than the distance between the antennae.

### 3.2 ANTENNA MODELING FOR TTE COMMUNICATIONS

The type and size of antennae for TTE communications depend on the desired range of the communications infrastructure and on the available physical space on site. As discussed earlier, antennae based on magnetic field, such as loops, are preferred over antennae based on electric field, such as electric dipoles or monopoles, because electric fields have higher attenuation rates

---

<sup>2</sup>  $\frac{\lambda_{rock}}{2\pi} = \delta \approx 160 \text{ m} < 300 \text{ m}$

<i>Model</i>	<i>Type of approximation</i>	<i>Conditions</i>
Vacuum	Reactive near field	$0 < r < \frac{\lambda_0}{2\pi}$
	Radiant near field	$\frac{\lambda_0}{2\pi} < r < \lambda_0$
	Transition zone	$\lambda_0 < r < 2\lambda_0$
	Far field	$r > 2\lambda_0$
Conductive Medium	Quasi-static	$r \ll \frac{\lambda_{rocha}}{2\pi}$
	Near field	$r^2 \ll \left(\frac{\lambda_{rocha}}{2\pi}\right)^2$
	Transition zone	$r = \frac{\lambda_{rocha}}{2\pi}$
	Far field	$r \gg \frac{\lambda_{rocha}}{2\pi}$

Table 3.1: Comparison between near and far field for free space and a conductive medium.

in the conductive medium at low frequencies[22].

The magnetic moment produced by an antenna can depend on the material that constitutes the antenna and on the antenna geometry. In systems that use loop antennae and that need to have a moderate range ( $> 300$  m), it may be necessary to employ a few dozen meters long transmission antennae. Small loops with 1 or more turns are often used in short range communications in mines and caves. Such loops have the disadvantage of presenting significantly higher impedances than bigger antennae having the same linear length.

Another type of antenna used in receivers in TTE communications is the ferrite rod [22]. It is constituted by a thin coil with many turns and a core made of a magnetic material whose magnetic permeability is tens times larger than vacuum permeability. The higher number of turns and the core material compensates the small cross area section of the antenna. This structure, although usually long (between 10 cm and 2 meters), can offer higher mobility to the radio equipment and is normally used at the underground where the atmospheric noise is weaker. At the surface, the atmospheric noise is more problematic and, as a result, it is necessary to employ bigger structures such as loop antennae connected to low noise amplifiers and noise coupling circuits. Figure 3.3 represents an ferrite rod antenna.



Figure 3.3: Ferrite rod antenna  
Source: Souterweb [46]

Comparing the ferrite and the loop as transmitting antenna, a single turn loop antenna with 200 g of mass and 1 m of diameter produces a magnetic moment  $m_d = 30Am^2$  dissipating 10 W. Whereas, a small ferrite rod with a little more than 1 cm of radius and 20 cm of length produces

an equivalent magnetic moment dissipating double of power. However, an antenna with 8,5 kg and 50 meters of diameter can produce up to  $m_d = 30kAm^2$  dissipating 100 W. It is important to highlight the difficulty of using ferrite rods in light receptors for personal mobile communication due to high consumption of power, which does not prevent its use in heavier receivers used in mobile machinery.

### 3.3 THEORETICAL MODELS FOR TTE PROPAGATION

Magnetic moment  $m_d = N_{tx}I_{tx}S_{tx}$  of a loop antenna indicates the inductive transmission capacity as a function of transmitter characteristics.  $N_{tx}$  is the number of turns of the transmitter loop,  $I_{tx}$  is the RMS value of a tone of electric current at the transmission antenna, and  $S_{tx}$  represents the loop area. According to this formula, it is possible to note that the increase of magnetic moment also increases power dissipated as heat in the windings of the loop ( $P_{tx} = R_{tx}I_{tx}^2$ ), where the loop resistance  $R_{tx}$  increases with  $N_{tx}$  and/or  $S_{tx}$ . Even though this power is dissipated and not radiated, it determines the current value used in magnetic field generation and then, it is associated indirectly with power transmission.

The simplest approximation for a magnetic field created by a loop antenna electrically small is made by considering vacuum as a homogeneous medium, neglecting any boundary condition [25] and assuming uniform distributed current on the loop. At a very close distance to source ( $r \ll \lambda/2\pi$ ), the intensity of a time varying magnetic field is similar to a static field calculated by Biot-Savart law [24]. On vacuum condition operation at 10 kHz, this distance is about hundreds of meters. For a loop antenna, the quasi-static magnetic field can be described by:

$$H_{qe} = \frac{m_d}{4\pi r^3} \{2 \cos(\theta) \hat{r} + \sin(\theta) \hat{\theta}\}, \quad (3.1)$$

Where  $\hat{r}$ ,  $\hat{\theta}$  are vectors in radial and elevation spherical coordinates. As stated in section 3.1, the H-field is altered as a function of medium characteristics. So the equation (3.1) is modified to include them. The following subsections shows four different field models describing more complex scenarios and other field equations.

#### 3.3.1 Infinite Conductive Medium (IC)

Adapting a vacuum infinite plane model [25] to a Conductive Infinite Medium (IC) is realized by altering only the wave-number  $k_{rock} = (1 - j)/\delta$ . This field approximation for both up-link and down-link, in spherical coordinates, is described in its phasorial fashion by [22]:

$$H = \frac{m_d}{4\pi r^3} e^{-jT} e^{-T} \{2 \cos \theta (1 + (1 + j)T) \hat{r} + \sin \theta (1 + (1 + j)T + 2jT^2) \hat{\theta}\}, \quad (3.2)$$

Where  $T = r/\delta = r\sqrt{\mu\sigma\omega/2}$  represents a range normalized by skin-depth and contemplates soil losses contribution. The parameter  $T$  can also be interpreted as a spacial frequency normalized by a known range  $r$ . The following Figure represents this configuration if the boundaries of the image are ignored.

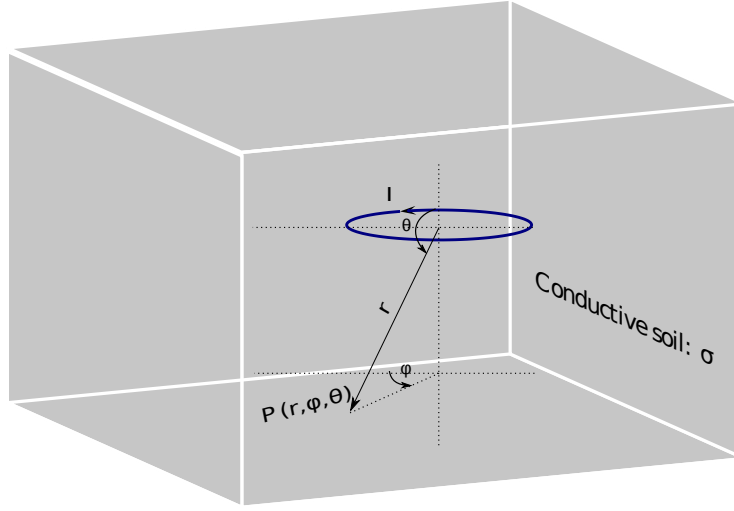


Figure 3.4: Infinite Conductive Medium IC with constant  $\sigma$ .

### 3.3.2 Homogeneous Half-Space model (HHS)

According to Wait in [27] this configuration considers a small wire loop antenna in a horizontal plane over ground at some height  $h_0$  and H-field is measured at a distance  $h$  under earth surface. It is used the cylindrical coordinate system  $(\rho, \phi, z)$  and earth is represented as a homogeneous Half-Space with a conductivity  $\sigma$ . All displacement currents are neglected due to the assumption of all distances involved are smaller than free-space wavelength. Hence, both H-field components up-link  $H_{up}$  and down-link  $H_{down}$  in cylindrical coordinates in both radial  $\hat{\rho}$  (horizontal field) and profundity  $\hat{z}$  (vertical field) are given, respectively, by:

$$H_{up} = \frac{m_d}{2\pi h^3} \int_0^\infty \beta(x) \{J_0(Dx)\hat{z} - J_1(Dx)\hat{\rho}\} dx, \quad (3.3)$$

$$H_{down} = \frac{m_d}{2\pi h^3} \int_0^\infty \beta(x) \left\{ J_0(Dx)\hat{z} - J_1(Dx) \frac{(x^2 + j2\mathcal{T}^2)^{1/2}}{x} \hat{\rho} \right\} dx, \quad (3.4)$$

where

$$\beta(x) = \frac{J_1(Ax)}{Ax/2} \frac{x^3}{(x^2 + j2\mathcal{T}^2)^{1/2} + x + \chi} e^{-Zx} e^{-(x^2 + j2\mathcal{T}^2)^{1/2}}, \quad (3.5)$$

and  $A = a/h$ ,  $D = \rho/h$ ,  $Z = h_0/h$ ,  $\mathcal{T} = h/\delta$ ,  $\delta = \sqrt{\frac{2}{\omega\mu\sigma_a}}$ ,  $a$  is the loop radius,  $J_0$  e  $J_1$  are Bessel functions of the first kind, and  $\chi$  is an auxiliar variable which is set to zero for this model. Figure 3.5 shows this configuration.

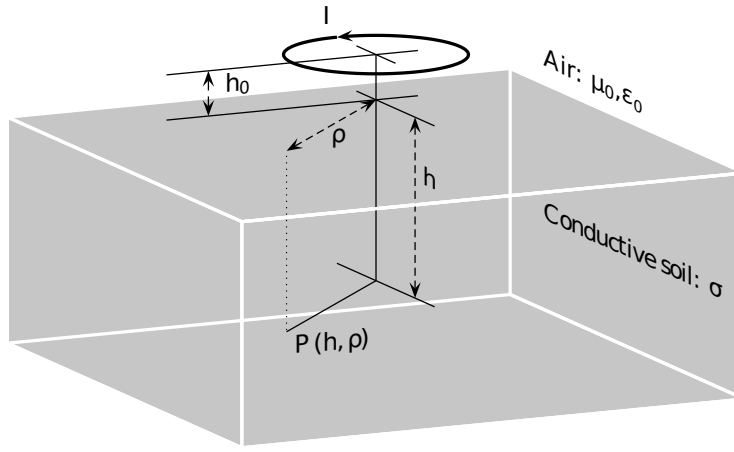


Figure 3.5: Geometry used for the calculation of the magnetic field at the point  $P(h, \rho)$  for a circular loop antenna at  $h_0$  above ground.

It is observable that exists reciprocity between the two links for the vertical field, but not for the horizontal field that, in fact, could be ignored in a configuration in which the antennae are coaxially aligned, i.e., when  $\rho = 0$  (or  $\mathcal{T} = T$ ) making  $J_1(Dx) = 0$ . Likewise, in the infinite medium model (3.2), for  $\theta = 180^\circ$  in coaxial configuration, the elevational field component disappears, and only the vertical field component remains at the  $\hat{r}$  direction. In contrast with the infinite medium model, where the loop must have sufficiently small dimensions to ensure that the current has spatial uniformity, the homogeneous half-space models have the correction factor  $J_1(Ax)$  which compensates for the size variation of the antenna.

### 3.3.3 Thin sheet model (TS)

Hill and Wait [30] suggests that at the interface between earth and air exists a barrier that could be modeled by a thin layer of greater conductivity than the conductivity of the homogeneous half-space below it. This model replaces the term  $\chi = 0$  with  $\chi = j2\mathcal{T}^2\sigma_m d$ ,  $d = \frac{h_1}{h}$  in the denominators of (3.3) and (3.4), where  $h_1$  and  $\sigma_m$  represent the height and the conductivity of the thin interface layer, respectively, as seen in Figure 3.6. Hence, the equation( 3.5) becomes:

$$\beta(x) = \frac{J_1(Ax)}{Ax/2} \frac{x^3}{(x^2 + j2\mathcal{T}^2)^{1/2} + x + j2\mathcal{T}^2\sigma_m d} e^{-Zx} e^{-(x^2 + j2\mathcal{T}^2)^{1/2}}, \quad (3.6)$$

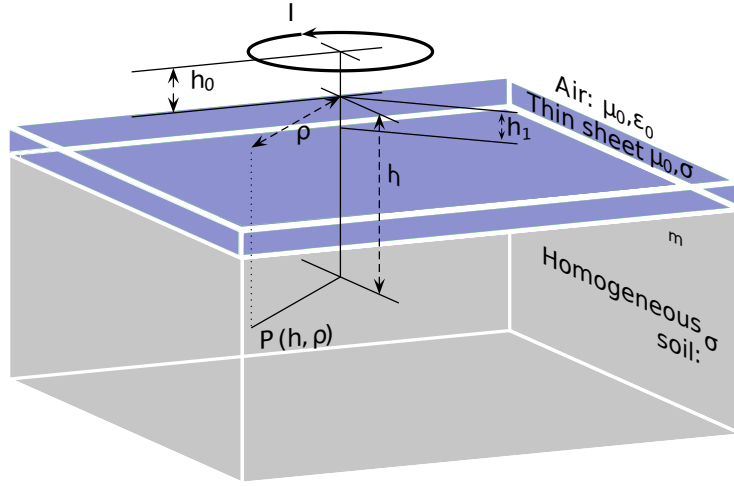


Figure 3.6: Geometry used for calculation of the magnetic field at the point  $P(h, \rho)$  for a circular loop antenna at  $h_0$  above a thin sheet of conductive material.

This high conductive layer is justified by the usual presence of cables, equipment, salt and other conductive materials on surface or in lower depth positions.

### 3.3.4 Multi-layer model

In 2014 Lincan presented in [31] a complex model for describing magnetic and electric propagation for a multi-layered TTE communication system. Similar to the HHS model, two loop antennae located above and underground, transmit and receive a signal through a stratified soil with several different electric conductivities as shown in Figure 3.7.

The following equations describe H and E-field for such medium in cylindrical coordinate system:

$$\mathbf{E} = j\mu\omega \frac{\partial \Pi^*}{\partial \rho} \hat{\phi} \quad (3.7)$$

$$\frac{\partial^2 \Pi^*}{\partial \rho \partial z} \hat{\rho} - (j\mu\omega\sigma - \epsilon\mu\omega^2 - \frac{\partial^2}{\partial z^2}) \Pi^* \hat{z} \quad (3.8)$$

Where  $\Pi^*$  varies according to every layer of material, and depends on transmitted signal  $T_i$  and reflected  $R_i$  as follows:

$$\Pi_0^* = \frac{IA_{wire}}{4\pi} \int_0^\infty T_0(\lambda) e^{-k_0 z} J_0(\lambda \rho) d\lambda \quad (3.9)$$

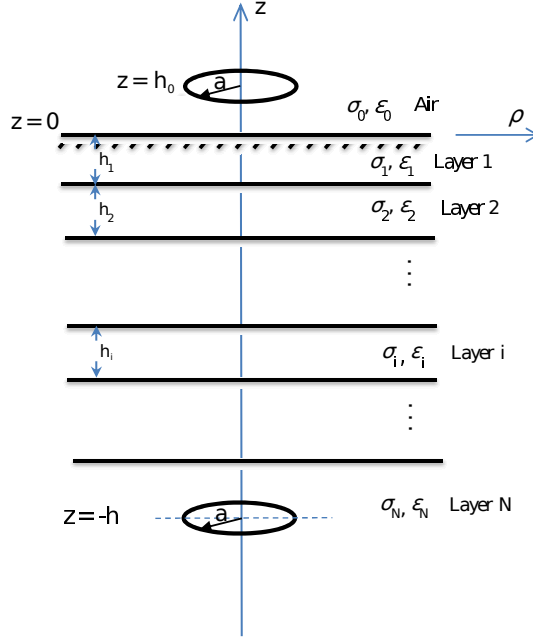


Figure 3.7: Stratified soil for Multi-layer model  
Adapted from: Lincan[31]

$$\Pi_i^* = \frac{IA_{wire}}{4\pi} \int_0^\infty (T_i(\lambda)e^{-k_1 z} + R_i(\lambda)e^{k_1 z}) J_0(\lambda\rho) d\lambda \quad (3.10)$$

$$\Pi_N^* = \frac{IA_{wire}}{4\pi} \int_0^\infty J_0(\lambda\rho) \left( \frac{\lambda}{k_N} e^{-k_N|z+h|} + R_N(\lambda)e^{k_N z} \right) d\lambda \quad (3.11)$$

The author make several approximations related to boundary conditions for every layer and determines that the only parameter that must be calculated is  $T_0(\lambda)$  through the following equation:

$$T_0(\lambda) = \frac{\lambda 2^N (\prod_{i=0}^{N-1} k_i) \left( e^{k_N(h-H'_N) - \sum_{i=1}^{N-1} k_i h_i} \right)}{L_0 + L_1 + L_2 \dots + L_{N-1}} \quad (3.12)$$

All  $L_i$  at denominator have no physical significance, although they can be interpreted as interaction within an arbitrary combination of m layers. Equations for every one of them are the followings:

$$L_0 = \prod_{i=0}^{N-1} (k_i + k_{i+1}), \quad (3.13)$$

$$L_1 = \sum_{p=1}^{N-1} \left\{ e^{-2k_p h_p} \prod_{i=0}^{N-1} (k_i + (-1)^{\delta^1} k_{i+1}) \right\}, \quad (3.14)$$

$$L_2 = \sum_{p=1, q=2, p < q}^{N-1} \left\{ e^{(-2k_p h_p - 2k_q h_q)} \prod_{i=0}^{N-1} (k_i + (-1)^{\delta^2} k_{i+1}) \right\}, \quad (3.15)$$

$$L_m = \sum_{\substack{p=1, q=2, r=3, \dots, t=m, \\ p < q < r < \dots < t}}^{N-1} \left\{ e^{(-2k_p h_p - 2k_q h_q - 2k_r h_r - \dots - 2k_t h_t)} \prod_{i=0}^{N-1} (k_i + (-1)^{\delta^m} k_{i+1}) \right\}, \quad (3.16)$$

$$L_{N-1} = e^{(-2k_p h_p - 2k_q h_q - 2k_r h_r - \dots - 2k_{N-1} h_{N-1})} \prod_{i=0}^{N-1} (k_i + (-1)^{\delta^{(N-1)}} k_{i+1}), \quad (3.17)$$

The author also elucidates that generally the term  $\delta m$  for  $L_m$  in (3.16) is the sum of the occurrence of  $k_i$  and  $k_{i+1}$  in the exponential term of  $e^{(-2k_p h_p - 2k_q h_q - 2k_r h_r - \dots - 2k_t h_t)}$ . For obvious reasons, this model is extremely complicated to implement for more than three layers and it is unpractical to use in real mining conditions where several random layers are found.

All models cited above are on frequency domain, since  $\delta$  varies with  $\omega$ . It is worth noting that any linear and nonlinear transmitter distortion are excluded from the models.

### 3.4 CHANNEL MODELING AND OPTIMUM OPERATION FREQUENCY

In systems that operate in moderately low frequencies, it is more common to use voltage and current to parameterize quadripoles and, consequently, parameters based on impedance are used in this model. To analyze the propagation channel at frequencies below 30 kHz, it is useful to adopt the concept of transfer impedance between loops, that considers the phasor current  $I_{tx}(\omega)$  in the transmission loop and the induced voltage  $V_{rx}(\omega)$  at the receiving antenna:

$$Z(\omega) = V_{rx}(\omega)/I_{tx}(\omega). \quad (3.18)$$

According to Faraday's law, the induced voltage by a magnetic field that goes through a conductive closed loop depends on the temporal variation of the magnetic flux that enters the loop orthogonally [24]. As a result, the voltage induced at the antenna due to the magnetic field is given by:

$$\begin{aligned} V_{rx}(\omega) &= -j\omega N_{rx} \int_S \mu H \cdot d\mathbf{S} \\ &= -j\omega \mu N_{rx} S_{rx} H \cos(\varphi) \end{aligned} \quad (3.19)$$

where  $N_{rx}$  e  $S_{rx}$  are the number of turns and the area of the receiving loop, respectively, and  $\varphi$  is the angle between the magnetic field and the loop axis, that is orthogonal to its plane. We see in (3.19) that, although the field attenuates at high frequencies, the receiver causes the output signal to also be attenuated at low frequencies. Expressing  $\mathbf{H}$  in spherical coordinates,  $\mathbf{H}_r$  at the  $\hat{r}$



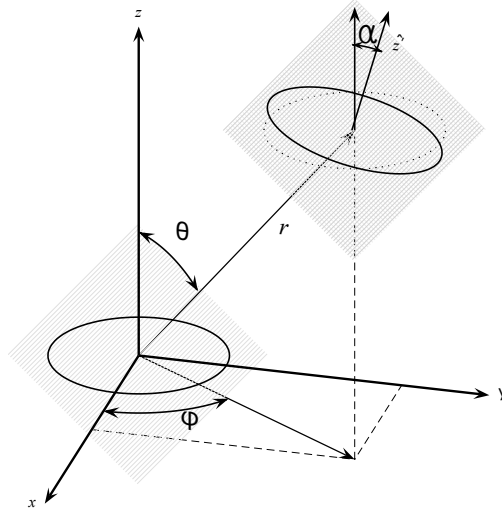


Figure 3.8: Geometry used in the calculation of the magnetic field between two circular loop antennae. The angle  $\alpha$  formed by orthogonal vectors to the planes determined by the two antennae is the result of rotations around the  $\hat{x}'$  e  $\hat{y}'$  axis.

direction, and  $\mathbf{H}_\theta$  at the  $\hat{\theta}$  direction, we have,

$$V_{rx}(\omega) = -j\omega\mu N_{rx}S_{rx} [H_r \cos(\theta - \theta_x) \cos(\theta_y) - H_\theta \sin(\theta - \theta_x) \cos(\theta_y)], \quad (3.20)$$

where  $\theta_x$  e  $\theta_y$  are rotation angles for the  $\hat{x}'$  and  $\hat{y}'$  axis, that are auxiliary axis created by the  $\phi - 90^\circ$  rotation of the  $\hat{z}$  axis, where  $\phi$  is the azimuthal angle. Figure 3.8 illustrates the described geometry.

In cylindrical coordinates, the voltage induced in function of the fields  $\mathbf{H}_z$  in the  $\hat{z}$  direction, and  $\mathbf{H}_\rho$ , in the  $\hat{\rho}$  direction, is given by:

$$V_{rx}(\omega) = -j\omega\mu N_{rx}S_{rx} [H_z \cos(\theta_x) \cos(\theta_y) + H_\rho \sin(\theta_x) \cos(\theta_y)]. \quad (3.21)$$

For a tonal current in the transmitter, the phasorial magnetic moment  $m_d(\omega) = N_{tx}S_{tx}I_{tx}(\omega)$  indicates the complex force of a transmitting antenna for a given frequency. Adapting the field equations and adopting the concept of transfer impedance  $Z(T) = V_{rx}(T)/I_{tx}(T)$ , at the normalized spatial frequency  $T$  (or  $\mathcal{T}$ ), we have:

$$Z_{IC}(T) = N_{tx}N_{rx}S_{tx}S_{rx} \left[ \sqrt{G_r^{tx}G_r^{rx}}F_r + \sqrt{G_\theta^{tx}G_\theta^{rx}}F_\theta \right] \quad (3.22)$$

as the transfer impedance for the **IC** model, where the normalized gain of the transmission and reception antennae polarized at the directions  $\hat{r}$  and  $\hat{\theta}$  are  $G_r^{tx} = \cos^2(\theta)$   $G_r^{rx} = \cos^2(\theta - \theta_x) \cos^2(\theta_y)$ ,  $G_\theta^{tx} = \sin^2(\theta)$  and  $G_\theta^{rx} = \sin^2(\theta - \theta_x) \sin^2(\theta_y)$ , and  $F_r$  e  $F_\theta$  are transfer functions for the propagation channel given, respectively, by:

$$F_r = \frac{T^2}{\pi\sigma r^5} e^{-T} \sqrt{1 + 2T + 2T^2} e^{j\{\tan^{-1}(\frac{T}{1+T}) - T - \frac{\pi}{2}\}} \quad \text{and} \quad (3.23)$$

$$F_\theta = \frac{T^2}{2\pi\sigma r^5} e^{-T} \sqrt{(1+T)^2 + (T+2T^2)^2} \times e^{j\{\tan^{-1}(\frac{T+2T^2}{1+T}) - T + \frac{\pi}{2}\}}. \quad (3.24)$$

In  $Z_{IC}(T)$ , all linear distortion is in  $F_r$  e  $F_\theta$ , including the derivative operation performed by the receiving loop antenna. This facilitates the separation of contributions throughout the network as a function of the type of linear system.

For the field approximations [26][27][28] that uses the homogeneous Half-Space model (**HHS**) and Thin Sheet (**TS**) model, the transfer impedance  $Z_{HHS}(\mathcal{T})$  and the transfer functions  $F_z$ ,  $F_\rho^{up}$  and  $F_\rho^{down}$  are given, respectively, by

$$Z_{HHS}(\mathcal{T}) = N_{tx}N_{rx}S_{tx}S_{rx} \left[ \sqrt{G_z^{rx}}F_z + \sqrt{G_\rho^{rx}}F_\rho \right], \quad (3.25)$$

$$F_z = \frac{\mathcal{T}^2}{\pi\sigma r^5} e^{-j\frac{\pi}{2}} \int_0^\infty \beta(x) J_0(Dx) dx, \quad (3.26)$$

$$F_\rho^{up} = \frac{\mathcal{T}^2}{\pi\sigma r^5} e^{-j\frac{\pi}{2}} \int_0^\infty \beta(x) J_1(Dx) dx, \quad e \quad (3.27)$$

$$F_\rho^{down} = \frac{\mathcal{T}^2}{\pi\sigma r^5} e^{-j\frac{\pi}{2}} \int_0^\infty \beta(x) J_1(Dx) \frac{(x^2 + j2T^2)^{1/2}}{x} dx, \quad (3.28)$$

where  $G_z^{rx} = \cos^2(\theta_x) \cos^2(\theta_y)$  and  $G_\rho^{rx} = \sin^2(\theta_x) \cos^2(\theta_y)$ . In this model, part of the antennae normalized gains are accounted for inside the channel transfer function and depend mainly on  $\rho$ ,  $h$ ,  $\theta_x$  and  $\theta_y$ .

The calculation of the power delivered to the receiver as a function of system parameters is important for a number of performance measurements in communications systems. The relationship between the dissipated powers in the first loop (transmission) and delivered to the second loop at the receiver is given by

$$\frac{P_{rx}}{P_{tx}} = \frac{|Z(T)|^2}{R_{tx}R_{rx}}, \quad (3.29)$$

from which we get

$$\sqrt{P_{rx,IC}} = \sqrt{P_{tx}} \Phi_{tx} \Phi_{rx} \left| \sqrt{G_r^{tx} G_r^{rx}} F_r + \sqrt{G_\theta^{tx} G_\theta^{rx}} F_\theta \right|, \quad (3.30)$$

$$\sqrt{P_{rx,HHS}} = \sqrt{P_{tx}} \Phi_{tx} \Phi_{rx} \left| \sqrt{G_z^{rx}} F_z + \sqrt{G_\rho^{rx}} F_\rho \right|, \quad (3.31)$$

where  $\Phi_{tx}$  and  $\Phi_{rx}$  are the specific apertures of the transmitting and receiving antennae, respectively. The specific aperture of a loop antenna is a function of its radius  $a$ , mass,  $M$ , mass density,  $\rho_l$ , and, wire conductivity  $\sigma_l$ , and is given by  $\Phi = 0.5a\sqrt{M\sigma_l/\rho_l}$ . The optimum frequency is an important parameter used to set the carrier frequency of modulated signals in TTE communication.

### 3.5 SOIL CONDUCTIVITY

In order to facilitate the estimation of field intensity as a function of depth and frequency, for a medium with high variation within its composition, some studies use the concept of equivalent or effective conductivity. Such definition is used among classical models shown above.

In consulted literature there are few studies related to effective or equivalent electric conductivity in stratified soils from underground mines. Generally, it is used a layered model where each layer has a different electric conductivity and magnetic permeability. Some simplifications are made as supposing a one layer homogeneous material as shown in [22]. Similarly, Lincan in [31] uses a weighted arithmetic mean for substituting a heterogeneous conductivity for an equivalent homogeneous conductivity. Equation (3.32) shows the calculation for the equivalent conductivity proposed by Lincan.

$$\sigma_{equivalent} = \frac{\sigma_n(x_t - \sum_{i=1}^{n-1} x_i)}{x_t} + \sum_{i=1}^{n-1} \frac{\sigma_i x_i}{x_t} \quad (3.32)$$

Where  $\sigma_i$  and  $x_i$  are electric conductivity and height of the  $i$ -th layer and  $x_t$  is total distance between surface and underground antenna. Measurements of magnetic field were used by Durkin in [47] and Lincan [31] to estimate the apparent conductivity seen by the transmitter using analytic models, with the intent to characterize the average and variability behavior of conductivity.

Both authors analyzed real electric conductivity data from 94 coal mines from the United States carried out by Little [48] in 1980 and can be seen in Figure 3.9 for frequency of 630 Hz. Durkin used the model **HHS** for the estimation and Lincan complemented the study by comparing **HHS** and **TS** models for creating a new estimation model. That model was named as **Q-factor** and starts with the calculation of  $Q_{thin}$  using a seed value for  $\sigma_0$  and  $\sigma_a$ . Then the result is equal to the magnitude of  $Q_{homo}$  calculated from the **HHS** model, and repeating it with a newer value for  $\sigma d$  until both sides of equation are the same.

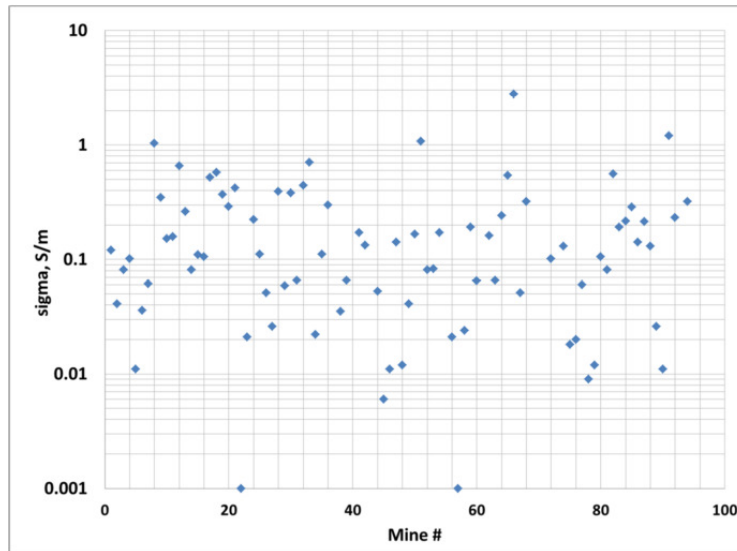


Figure 3.9: Equivalent conductivity for 94 real mines  
Source: Lincan [31]

Also, Lincan used a logarithmic regression for estimating an apparent conductivity  $\sigma_a$  for the real mines data through equation (3.33). It was stated that  $\sigma_a$  represents a random sample from a normal distribution with mean depending on frequency and depth, and variance independent of both magnitudes. Table 3.2 shows the values of regression coefficients a, b and c determined from the mine data.

$$\sigma_{apparent} = a + b * \log(freq) + c * \log(depth) \quad (3.33)$$

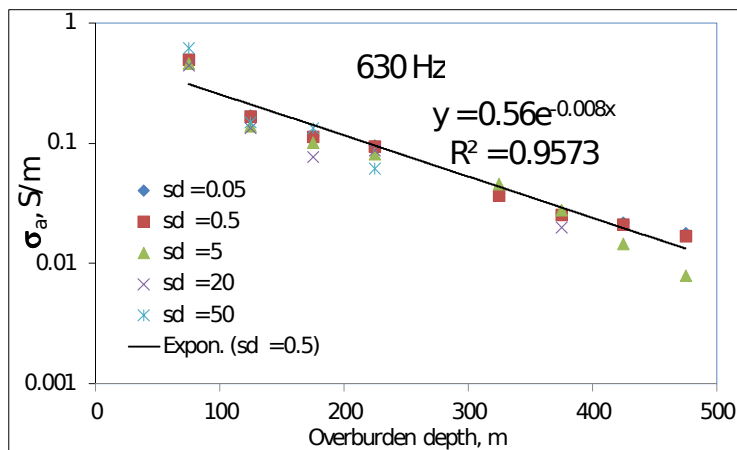


Figure 3.10: Estimated Apparent conductivities (S/m) change with overburden depth interval (m) for various  $\sigma d$  (appear as "sd" in plot legend) at 630 Hz. TS model. Source: Lincan [31]

For this model the author noticed that the frequency coefficient has the same order as depth, so frequency dependence for electric conductivity cannot be neglected for the apparent estimation.

Table 3.2: Regression model for apparent conductivity ( $\sigma_a$ , S/m) with respect to log (depth, m) and log (frequency, Hz)

Observations	a	b	c	Standard Error	R Square
238	2.1834	-0.2932	-0.5068	0.1479	0.4674

# 4 ANALYSIS OF ANALYTIC MODELS, MEASUREMENTS AND SIMULATIONS

This chapter presents magnetic field and propagation channel behavior of TTE systems based on analytic models, Monte Carlo simulations using a FEM solver and field measurements found in literature.

## 4.1 THEORETICAL MODELS FOR H-FIELD AND TRANSFER FUNCTION

Results presented in this and following sections are intent to be independent of transmission and reception parameters, such as antenna gain, electric current intensity, loop area, etc. Nevertheless, several values are informed in order to support further researches. These calculations were set for a ULF/VLF bands, specifically from 0.1 to 10 kHz. It is used a basic configuration formed by two loop antennae coaxially aligned with a homogeneous medium between them. Loop antenna radius has 1 m, soil electric conductivity is  $\sigma = 0,08792$  S/m, and distance through antennae is  $d = 327$  m.

### 4.1.1 Magnetic field

Figure 4.1 shows H-field intensity on the axis of a loop antenna ( $\theta = 0$  in spherical coordinates). The H-field has been normalized by the intensity of quasi-static field as a function of T for **IC** and **HHS** models. Also is presented the H-field for another point on loop's plane ( $\theta = \pi/2$ ) only for **IC** model due to the lack of adaptation to co-planar configuration of **HHS** model. It is shown the excess of losses (or gain) created by medium and antenna's structure, which is more severe than the one described through inverse cube law for the coaxial configuration. For the co-planar configuration, the losses only exceed the quasi-static field for  $T > 3.1$ .

In order to observe the non-normalized intensity of H-field in Figure 4.1, it is necessary to add a 60 dB/decade for a fix frequency. It is easy to see that for distances up to  $T=1/4$ , which is close to 40 m for a system operating at 1 kHz and a moderate electric conductivity  $\sigma = 10^{-2}$ , the models follow a very similar to quasi-static field behavior. After that, co-planar fields increase up to  $T \approx 3$ , and then, they start to decrease. Coaxial fields decrease for all T, at rates varying from 1.5 dB after the first  $\delta$  ( $T=1$ ), 4.5 dB from second to third  $\delta$ , and 8.7 dB/ $\delta$  for  $T \rightarrow \infty$ . Such convergence value of attenuation rate/ $\delta$  is typical for plane waves in far-field, and also is used to define  $\delta$ , since  $(20\log(e^{-\frac{r}{\delta}}=1))=-8.7$  dB).

For a fix distance, the spectrum, as a function of normalized frequency T, presents a low-pass filter behavior. Such filter has a band of 1.4 for coaxial configuration, and 2.8 for co-planar

configuration. Nevertheless, it will be shown in next section that those are not channel's spectrum shape for communication endpoints.

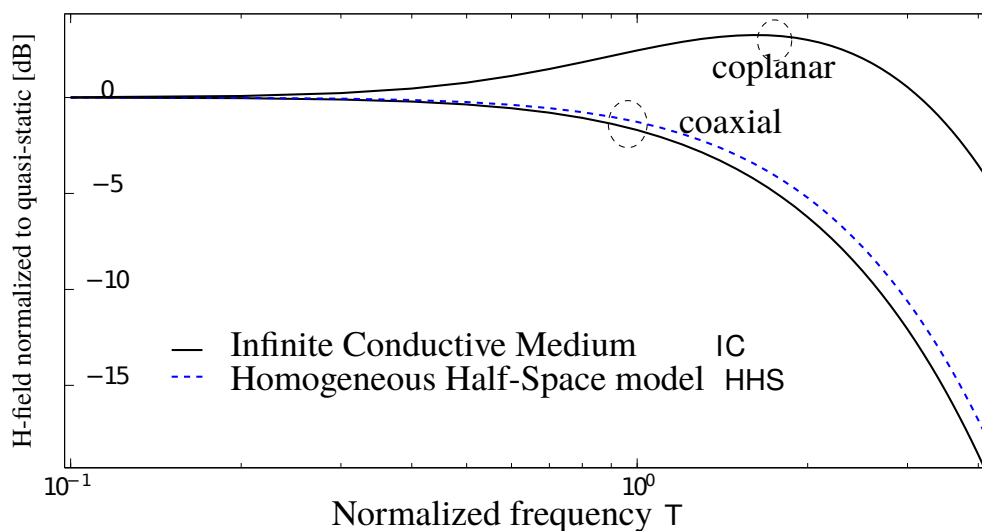


Figure 4.1: H-field from a loop antenna for coaxial and co-planar configurations according to IC and HHS up-link models)

#### 4.1.2 Transfer function

From equations in section 3.4 is possible to see that  $Z(T)$  and  $P_{rx}/P_{tx}$  carry intrinsic parameters of the loops used. Therefore, in order to understand the channel behavior, it is used the transfer function  $F$ . Although it depends on the shape of the antenna, it does not depend on its parameters. Figure 4.2 presents the magnitude spectrum of the channel transfer function for antennae at the coaxial and co-planar configurations.

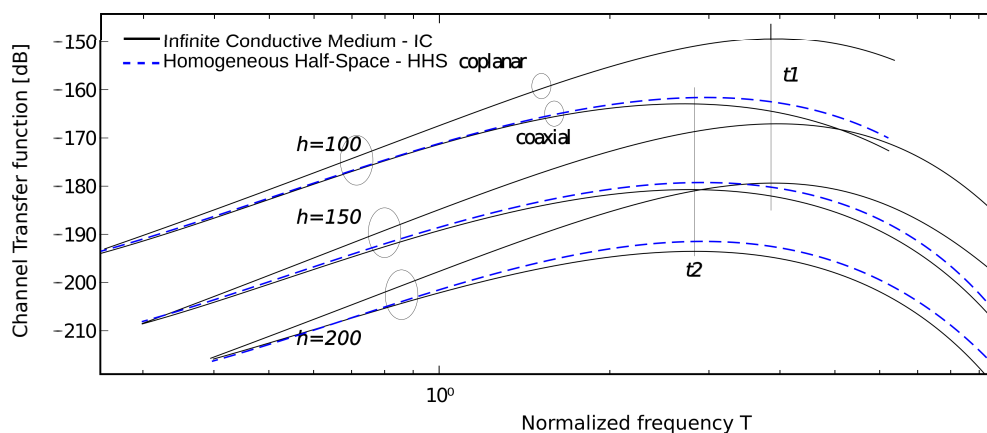


Figure 4.2: Channel transfer function for up-link between two loop antennae in coaxial and co-planar configurations for the IC and HHS models.

Is observed that the channels are band-pass and, for the coaxial configuration the normalized

optimal frequency is  $T_{opt} \approx 2.83$  with quality factor  $Q = 2.2$  and asymmetrical bandwidth with maximum at  $T_{opt}$ . For instance, considering a depth of  $r = 200$  and soil conductivity  $\sigma = 10^{-2}$  S/m, the optimal frequencies are  $f_{opt} \approx 5$  kHz and the bandwidth, in which there is less than 3 dB variation, is 11 kHz. For co-planar transmission,  $T_{opt} \approx 3.86$  with quality factor  $Q = 1.8$ .

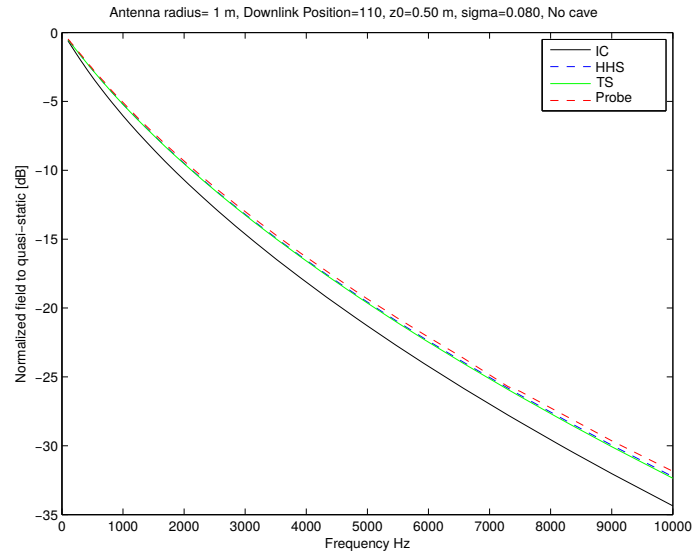
## 4.2 HHS AND TS MODELS CURVES

As stated in (3.6), **HHS** and **TS** models differ by the term  $\chi$  in which the **TS** model depends on the product  $\sigma d$ . The following figures show such difference for 2 values of  $\sigma d$  with a separation of antennae of 300 m.

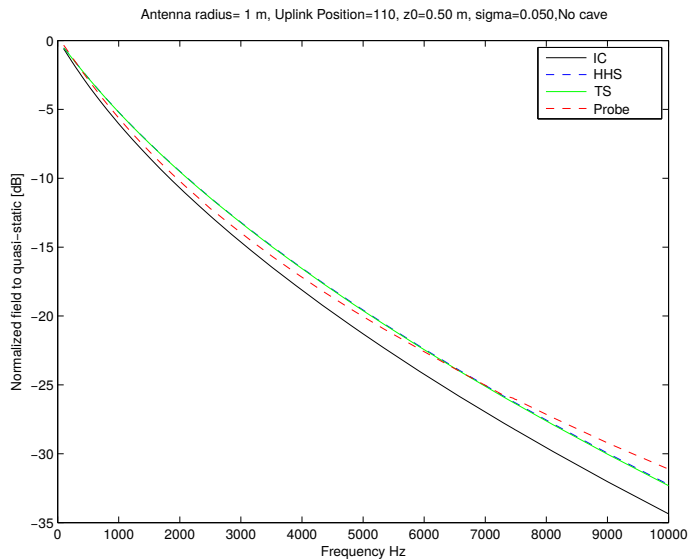
Taking into account those results, and using the same conditions expounded above in section 4.1, magnetic field intensities are shown in Figure 4.3, taking frequencies from 0.1 to 10 kHz and comparing them to theoretical models. From some other simulations is possible to infer that simulation accuracy is improved for higher frequencies when the environment's width representing soil is augmented.

Subsequently a TTE transmission simulation environment was built, choosing the Finite Element Method and setting the simulator program to frequencies for ULF/VLF bands, specifically from 0.1 to 10 kHz. A basic structure formed by two loop antennae coaxially aligned with a homogeneous medium between them was constructed, similarly that in Figure 4.4.





(a) HHS model



(b) Thin sheet model

Figure 4.5: H-field TS and HHS theoretical models compared to data from simulator

After comparing results obtained via simulator to **TS** and **HHS** models, it is possible to see that simulations from simulator suit theoretical equations. Thus, other results related to multi-layer environments should be equally valid even when there are not reliable theoretical models to compare.

### 4.3 PRELIMINARY SIMULATION RESULTS

Starting from data presented in figure 3.9 on section 3.5, it was identified the Log-normal as the statistical distribution of electric conductivity. This conductivities were estimated from 94

measurements carried out in different coal mines throughout the USA with depth varying from 21 to 472 m. The parameters for such distribution are:  $\mu = -2.3034$  dB and  $\sigma = 1.4554$  dB for a frequency of 630 Hz. That data is used for calculations in this section.

#### 4.3.1 Scenario I: fixed number of layers

This scenario has the following characteristics:

- `Antennae size`: both antennae have a square shape with 15 m side and square cross-section of  $1 \text{ cm}^2$ .
- `Antennae position`: the above ground antenna was set to be 50 cm over ground and in vacuum conditions. The second antenna was positioned at 150 m under surface of mine, inside a cave in vacuum condition.
- `Layer size`: all layers are 50 m side square shaped parallelepipeds with different heights, which depends on the number of layers and the height overall layers is 160 m,
- `Number of layers`: a fix number of ten layers with random heights according to a uniform distribution  $U(1, 10)$ ,
- `Probe position`: probes for measuring H-field distributed evenly at the antennae axes at a 10 m distance of each other and at center of each antenna,
- `Layer electromagnetic characteristics`: magnetic permeability was set as vacuum condition  $\mu_0 = 4\pi 10^{-7}$ ; electric conductivity was programmed to be a point of a random Log-Normal distribution according to the parameters presented above.
- `Number of trials`: 50 independent and random trials.

There were selected 3 probe positions: 50, 110 and 150 m, to study H-field behavior. Since parameters were extracted from a Log-normal distribution fitting to 630 Hz measurement data, it was selected 657 Hz for obtaining more realistic results.

In Figures 4.6 to 4.8 shows H-field intensity over all trials and the statistical characteristic at each vertical position.

According to those graphics, and theoretical estimations presented in previous chapters, it is possible to realized that H-field decays with distance as expected. Also, it is interesting to see that its statistical distribution changes as a function of distance as well. Characteristics of the first distribution for each distance are presented in table 4.1

Table 4.1: Statistical characteristics for H-field in stratified medium with fix number of layers

Distance	Extreme Value	Normal	Generalized Pareto
50 m	$\mu = 6.62212e-05$ $\sigma = 8.40553e-06$	-	-
110 m	-	$\mu = 2.93305e-06$ $\sigma = 1.6028e-06$	-
150 m	-	-	$k = -0.122508, \sigma = 2.97543e-07$ $\theta = 0$

### 4.3.2 Scenario II: random number of layers

For this section, it was used the same configuration presented in scenario I, but changing the distribution that sets the number of layers to a uniform random variable  $U(3, 30)$ . Also there were selected 3 probe positions at 50, 110 and 150 m, to study H-field behavior. Again, the frequency of 657 Hz was selected for obtaining more realistic results. Figures 4.9, 4.10 and 4.11 show H-field intensity and the statistical characteristic, presented in table 4.2, for all trials at each vertical position.

As well as in section 4.3.1 is easy to realized that H-field decays with distance and statistical distribution changes as a function of distance. Such variational behavior for both scenarios is also expected due to soil attenuation and skin depth penetration.

Table 4.2: Statistical characteristics for H-field in stratified medium with random number of layers

Distance	Extreme Value	Log-Logistic	Burr
50 m	$\mu = 6.71428e-05$ $\sigma = 9.14058e-06$	-	-
110 m	-	$\mu = -12.8007$ $\sigma = 0.305818$	-
150 m	-	-	$k = 0.761137, c = 2.53095$ $\alpha = 2.03539e-07$

#### 4.4 ELECTRIC CONDUCTIVITY CHARACTERIZATION THROUGH MEASUREMENTS IN UNDERGROUND MINES

As seen in previous chapters, there is insufficient real data related to electric conductivity  $\sigma$  in underground mines. The practical way to estimate  $\sigma$  is through H-field measurement. Using theoretical models presented in chapter 3 it is possible to estimate an equivalent  $\sigma$  at a specific distance for a particular mine.

Data presented in [48] and shown in figure 3.9 is the most complete information related to magnetic field in underground mines that can be found in literature so far. In this section are presented 3 methods of estimation of equivalent electric conductivity for higher frequencies. The H-field information presented in table 4.3 was used to build a database of electric conductivities for frequencies 630, 1050, 1950 and 3030 Hz through the **HHS** model. Data on this table was obtained by normalizing the H-field by the magnetic moment<sup>1</sup>.

Table 4.3: Surface Vertical Magnetic Field signal levels vs. Overburden Depth from 94 Coal Mine Sites Normalized by magnetic moment  
RMS Signal levels in dB reference 1  $\mu$ A/m. Adapted from [48]

Mine No.	State	Depth (m)	Frequency [Hz]			
			630	1050	1950	3030
1	KY	182.87	-43.3769	-47.3269	-51.4963	-53.3921
2	KY	122.83	-23.5197	-25.1526	-27.7640	-30.4328
3	KY	122.83	-25.5197	-27.4526	-30.5640	-37.4328
4	IL	243.83	-70.8551	-69.7041	-72.5501	-77.9792
5	KY	425.8	-60.4785	F <sup>2</sup>	-57.1947	-60.6969
6	KY	205.43	-39.6785	-40.6785	-44.1947	-63.5969
7	VA	158.49	-33.0526	-32.5122	-33.0732	-30.5023
8	KY	60.95	-14.1843	-19.6604	-17.5344	-7.2642
9	OH	80.46	-17.3576	-4.8771	-24.4049	-15.4841
10	OH	77.41	-12.2576	-27.8771	-15.9049	-9.8841
11	WV	80.46	-13.6845	-12.8338	-9.1491	-5.8495
12	WV	76.19	-19.9576	-5.3771	-12.0049	-23.9841
13	PA	103.93	-25.5618	-23.5361	-19.6781	-21.3190
14	PA	135.94	-29.0349	-29.9564	-37.0554	-43.6693
15	PA	182.87	-42.3789	-41.6048	-42.0140	-40.7563
16	PA	210	-48.5576	-49.8771	-48.4049	-53.1840
17	PA	72.84	-16.1533	-17.1712	-8.8727	-18.0194
18	PA	64	-11.7354	-21.7748	-6.9967	-6.6550

Continued on next page

<sup>1</sup>Two tables containing H-field and magnetic moment adapted to depths in meters can be seen in Appendix VII.

<sup>2</sup>SYMBOLS: N= No test measurement performed. F=Failure to detect transmitted signal

**Table 4.3 – continued from previous page**

Mine No.	State	Depth (m)	Frequency[Hz]			
			630	1050	1950	3030
19	PA	106.07	-29.3609	-28.6039	-29.0049	-29.7504
20	PA	103.93	-26.3859	-24.3789	-25.5485	-24.1918
21	PA	99.05	-27.6048	-31.0005	-35.6085	-44.4258
22	WV	173.43	-30.2809	-30.3155	-31.3303	-29.1061
23	VA	365.75	-70.8474	-71.8374	-70.8415	-67.8362
24	KY	82.29	-15.7914	-20.7155	-13.5783	-11.6042
25	VA	129.84	-28.5255	-28.3883	-35.4317	-33.5194
26	VA	210	-42.6053	-42.5727	-41.7208	-43.3400
27	VA	210	-39.1464	-40.3603	-40.2306	-38.7438
28	VA	157.88	-50.8408	-43.4443	-49.7550	-46.7597
29	VA	177.08	-36.7458	-37.0692	-35.6618	-34.6001
30	KY	99.05	-26.5618	-26.5361	-23.6780	-19.3190
31	VA	188.97	-39.9843	-39.6604	-39.5344	-36.0642
32	WV	100.88	-28.7405	-27.7903	-31.0101	-20.6639
33	WV	70.1	-16.9843	1.3655	-0.4382	-9.6684
34	WV	409.04	-68.2138	-71.6711	-79.3603	-79.8338
35	WV	99.05	-19.4377	-18.3155	-19.3645	-17.4672
36	WV	65.83	-9.3454	-11.2229	-12.2716	-3.8691
37	PA	145.99	-30.1913	-28.9766	-30.9514	-32.5155
38	WV	238.04	-44.9113	-47.2915	-54.9302	-67.8777
39	WV	154.83	-32.5618	-33.5361	-37.6780	-39.3190
40	AL	142.95	-22.8199	-25.7903	-28.8326	-30.7727
41	AL	147.82	-37.0576	-35.3771	-37.9049	-36.6841
42	AL	109.11	-23.2231	-20.5473	-22.0835	-20.8830
43	AL	89.91	-12.8197	-12.2526	-14.3640	-19.2328
44	AL	79.85	-11.1425	-17.3963	-16.3569	-9.6039
45	TN	288.03	-46.0418	-50.8775	-45.8897	-58.4649
46	TN	363.01	-55.0075	-58.0461	-58.4685	-68.9319
47	KY	79.85	-13.1100	-12.6959	-16.0727	-15.4976
48	KY	307.84	-49.4048	-52.1720	-52.1371	-52.6895
49	KY	145.99	-28.8322	-28.0589	-26.9967	-26.7311
50	IL	227.07	-58.2721	-67.1464	-56.2046	-68.8096
51	IL	85.03	-31.1224	-25.1774	-16.2556	-19.0968
52	IL	139.9	-29.6697	-31.9760	-33.4604	-36.2376
53	IL	197.81	-43.6139	-51.3562	-47.2783	-58.5393

Continued on next page

**Table 4.3 – continued from previous page**

Mine No.	State	Depth (m)	Frequency[Hz]			
			630	1050	1950	3030
54	IL	93.87	-19.3322	-40.5704	-27.9967	-27.7311
55	IL	88.08	-19.1913	-20.8766	-22.9514	-19.5155
56	WV	128.93	-23.6393	-23.9019	-24.3677	-23.1301
57	WV	320.03	-44.9966	-46.6765	-49.5473	-50.0835
58	WV	177.08	-33.2398	-34.2338	-35.3866	-36.0289
59	WV	117.95	-28.5576	-26.8771	-30.4049	-29.1840
60	WV	106.98	-20.2144	-20.2396	-17.6478	-16.3405
61	WV	257.86	N	N	N	N
62	WV	209.09	-53.4255	-53.6162	-53.9967	-56.7311
63	WV	147.82	-30.8436	-32.8698	-39.0716	-33.7317
64	WV	107.89	-26.4650	-24.5474	-23.8072	-20.4806
65	WV	71.01	-15.4255	-9.6162	-13.9967	-10.7311
66	WV	78.02	-43.4255	-25.6162	-8.9967	-34.7311
67	WV	128.01	-25.1612	-24.9454	-25.9143	-24.4788
68	WV	136.85	-40.3576	-39.2771	-41.3049	-42.2840
69	WV	131.06	F	F	-23.6923	-27.2979
70	WV	278.89	F	F	-63.0129	F
71	PA	72.84	-7.1457	-5.9878	-11.0101	-12.5956
72	PA	146.91	-32.9682	-33.2187	-35.6609	-34.3965
73	PA	190.8	F	-37.6767	-37.6696	F
74	PA	145.99	-34.4377	-35.3155	F	-37.9672
75	PA	200.55	-36.3522	-46.0922	-45.0251	-50.5885
76	UT	364.84	-57.8651	-56.2656	-68.4362	-75.1776
77	UT	304.79	-60.6271	-60.0182	-64.2923	-66.0979
78	UT	365.75	-53.2223	-56.6767	F	-60.8478
79	CO	427.02	-64.1550	-71.3323	F	F
80	OH	152.39	-34.6576	-47.8771	-46.4049	-57.1840
81	OH	182.87	-39.9326	-42.6429	-48.6805	-58.7121
82	OH	142.95	-51.6363	-49.8307	-53.2023	-59.9308
83	OH	164.89	-43.2231	-44.5473	-47.0835	-52.8830
84	OH	170.99	-46.6815	-37.8641	-42.2361	-45.9554
85	KY	79.24	-15.7245	-14.8003	-13.0409	-11.7092
86	KY	152.09	-36.4377	-36.3155	-38.3645	-38.9672
87	KY	121.91	-30.7245	-30.8003	-31.0409	-27.7092
88	KY	115.82	-25.5018	-25.1983	-24.1840	-24.1967

Continued on next page

**Table 4.3 – continued from previous page**

Mine No.	State	Depth (m)	Frequency[Hz]			
			630	1050	1950	3030
89	AL	197.81	-37.1425	-37.3963	-37.8569	-40.6039
90	AL	472.74	-68.2223	-72.6767	-71.3696	-71.8478
91	KY	57.91	-13.3257	-2.7350	-8.3609	-16.1878
92	KY	79.85	-14.9377	-24.3155	-23.3645	-14.9672
93	KY	21.03	11.2888	12.8932	-23.7903	16.7314
94	KY	99.97	-25.5061	-29.7144	-37.9102	-45.2139

#### 4.4.1 Equivalent electric conductivity over all frequencies and depths

Based on the magnetic field from Table 4.3 for every frequency and depths, it was estimated the equivalent electric conductivity using the **HHS** model. Figure 4.12 shows all  $\sigma$  estimated over all frequencies and depths:

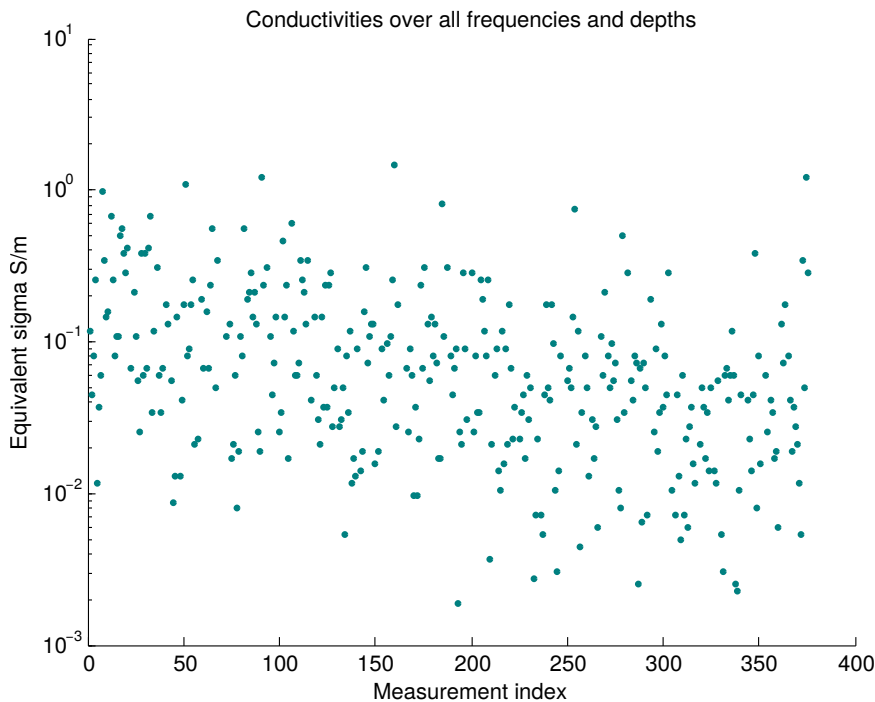


Figure 4.12: Conductivities over all frequencies and depths

From this data, it is possible to identify the statistical distribution for  $\sigma_e$ . Through a comparison between Random Mean Square Errors (RMSE) for several distributions, it was generated a classification Table 4.4 for deciding which distribution fits the best the data. For this method, it was identified the Log-normal distribution with parameters  $\mu = -2.87014$  dB and  $\sigma = 1.27042$  dB. Such parameters are fairly similar to those calculated in Section 4.3, which can sustain the

validity of this method.

Table 4.4: RMSE error over all frequencies and distances

Distribution	RMSE
Log-normal	0.0060106
Burr	0.0086287
Loglogistic	0.010472
GeneralizedExtremeValue	0.014665
Weibull	0.019625
Gamma	0.026832

#### 4.4.2 Equivalent electric conductivity estimation as a function of frequency

Considering all distances in which H-field was measured, it was estimated the conductivity for each frequency as seen in Figures 4.13 to 4.16. Again it was used the RMSE for creating Table 4.5. From these result, it is possible to infer that conductivity reduces when frequency rises. Such behavior may be associated to different field conditions (quasi-static, transition, far-field, etc.) suffered by fields with different frequencies in which simple models, such as **HHS** cannot respond.

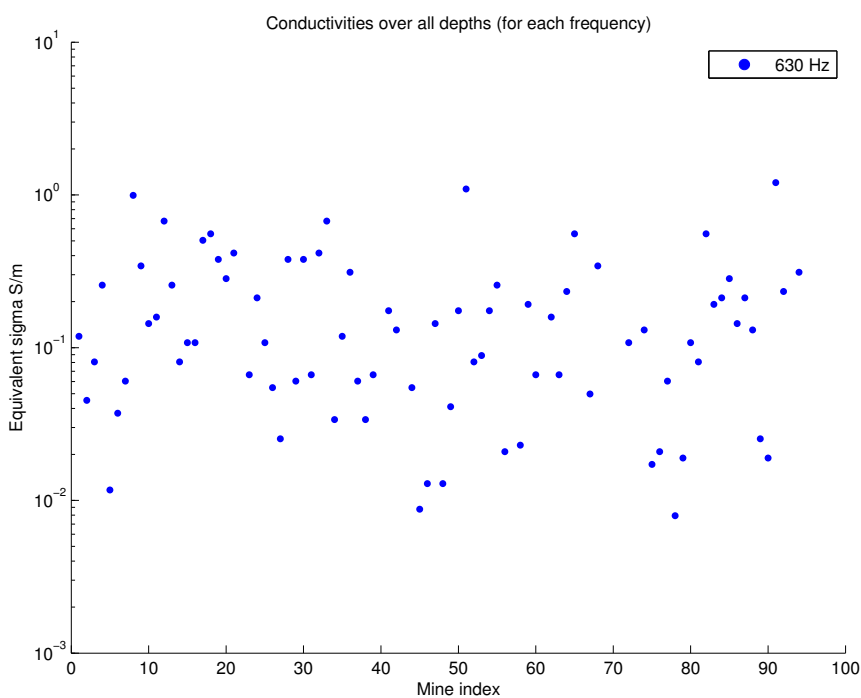


Figure 4.13: Conductivities over all depths 630 Hz



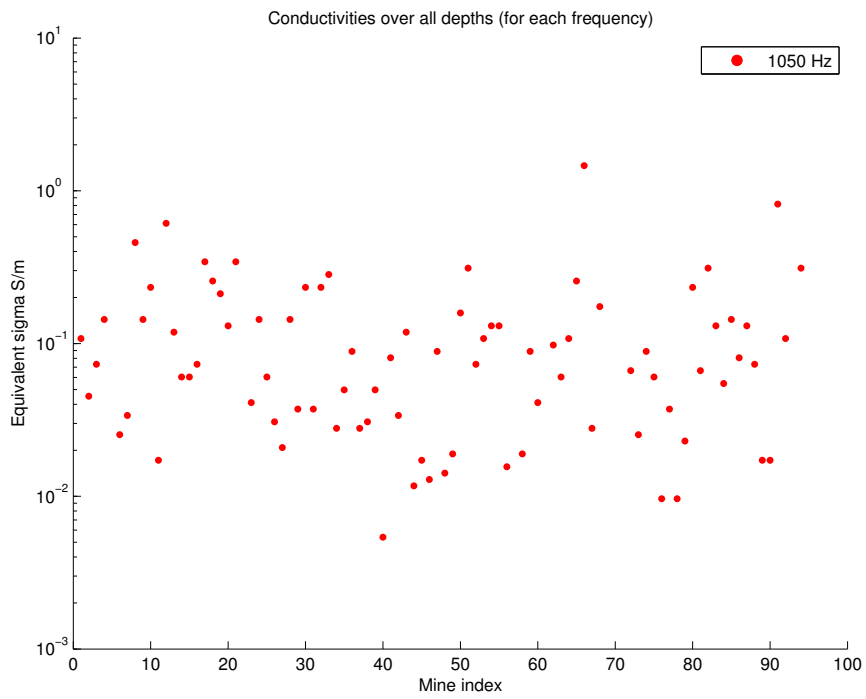


Figure 4.14: Conductivities over all depths 1050 Hz

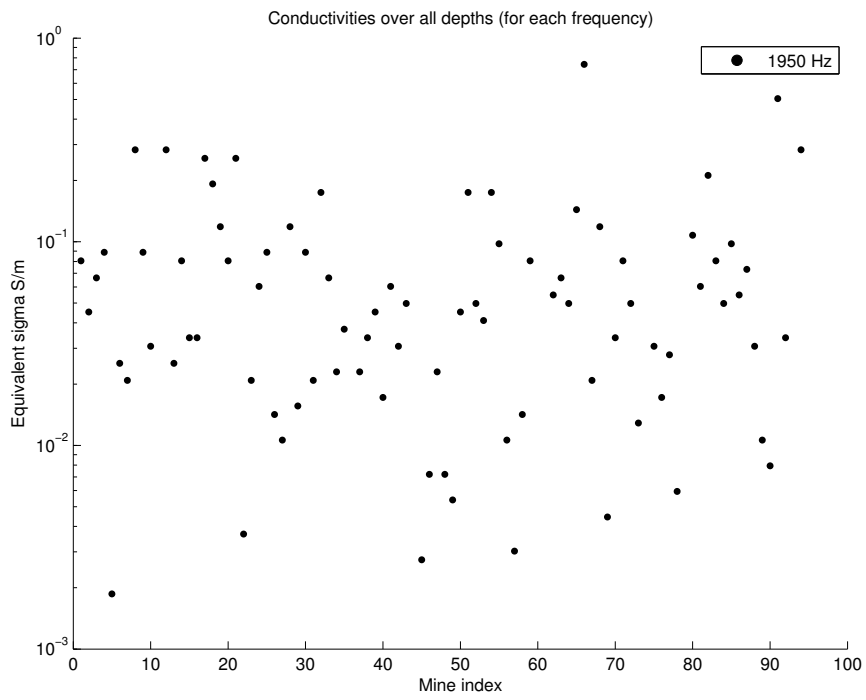


Figure 4.15: Conductivities over all depths 1950 Hz

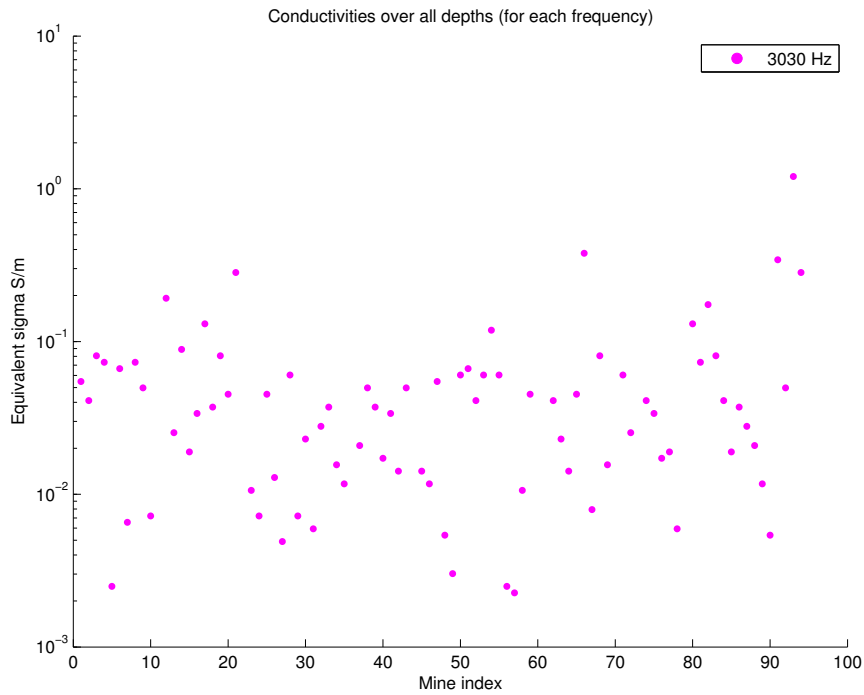


Figure 4.16: Conductivities over all depths 3030 Hz

Table 4.5: RMSE error of conductivity distribution over all depths for each frequency

Distribution	630 Hz	1050 Hz	1950 Hz	3030 Hz
Log-normal	0.015891	0.010706	0.013781	0.015545
Burr	0.011917	0.011181	0.010981	0.011891
Gamma	0.022089	0.02612	0.02733	0.035226
GeneralizedExtremeValue	0.022256	0.017913	0.013599	0.013227
Loglogistic	0.018732	0.012352	0.014193	0.011777
Weibull	0.01827	0.021948	0.022922	0.028261

From Table 4.5, it is observed that Log-normal distribution reaches a suitable fitting, and considering its symmetry in dB and simplicity, it is chosen for data normalization through its parameter  $\mu$ . Results for that normalization are shown in Figure 4.17. The characteristic parameters for Log-normal distribution are  $\mu=0$  dB  $\sigma= 1.1701$  dB. Comparing both results it is possible to realize that conductivities keep the same behavior. A remarkable difference that can be observed is that variation of equivalent  $\sigma$  is reduced after normalization in frequency.

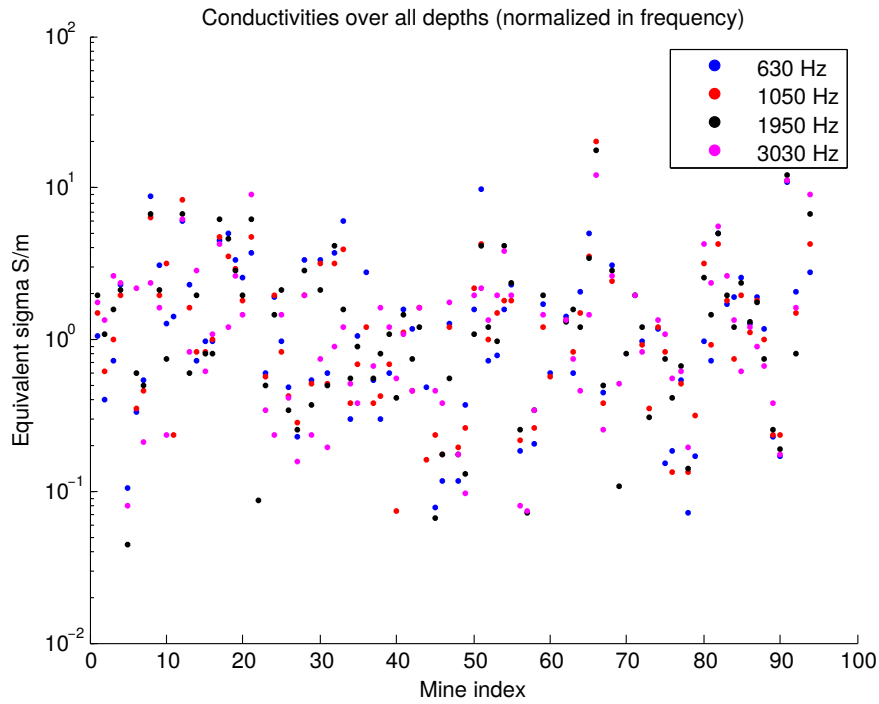


Figure 4.17: Conductivities over all depths (normalized in frequency)

#### 4.4.2.1 Extrapolation of Log-normal parameters for frequencies beyond 3030 Hz

An estimation of parameters  $\mu$  and  $\sigma$  of Log-normal distribution that describes equivalent conductivity is presented in Table 4.6 and in Figure 4.18. Such estimation was carried out by the means of cubic spline interpolation and, subsequently, extrapolation with a 3rd order polynomial.

Table 4.6: Log-normal Distribution parameters of conductivity: over all depths (for each frequency) and extrapolated Mu values from 4350Hz to 10kHz

Frequency	$\mu$ [dB]	$\sigma$ [dB]
<b>630</b>	-2.1911	1.1771
<b>1050</b>	-2.6202	1.1057
<b>1950</b>	-3.1759	1.2120
<b>3030</b>	-3.4768	1.2041
<b>4350</b>	-3.807	-
<b>5970</b>	-4.1922	-
<b>7850</b>	-4.6392	-
<b>10000</b>	-5.1503	-

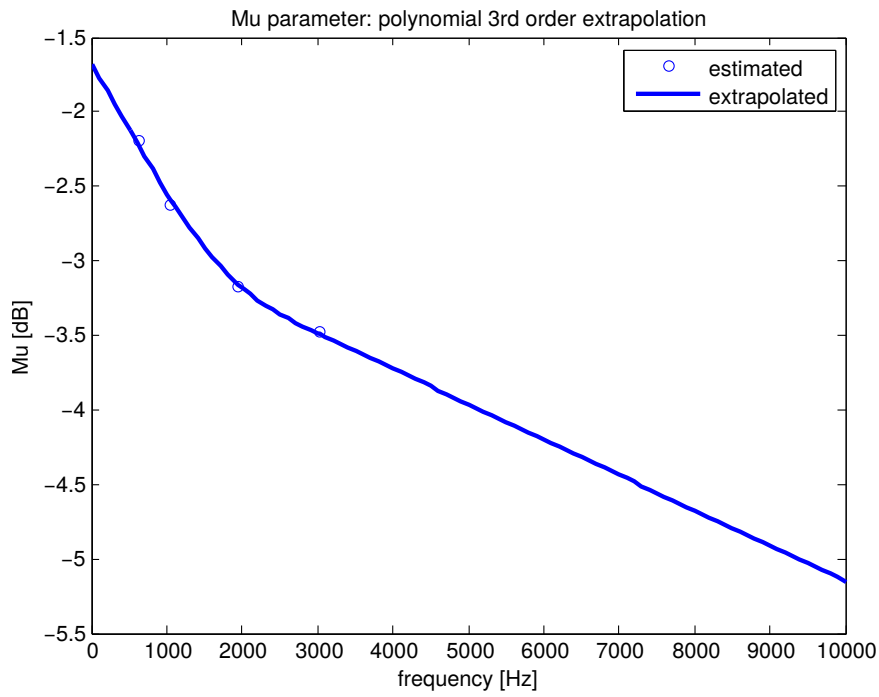


Figure 4.18:  $\mu$  parameter of Log-normal distribution for conductivity: polynomial 3rd order extrapolation

#### 4.4.3 Equivalent electric conductivity estimation as a function of mine depth

It is important to estimate the variation of conductivity as a function of mine depth. Again, using data from Section 4.4.1, it was estimated a curve for equivalent conductivities Figure 4.19.

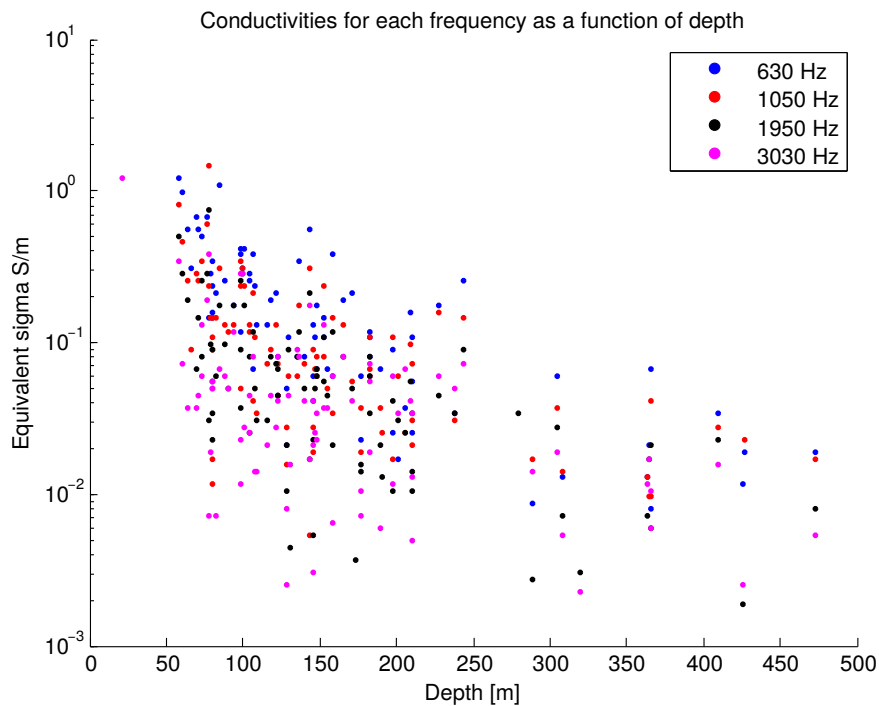


Figure 4.19: Conductivities for each frequency as a function of depth

Due to depth distribution in the database, there were calculated different statistical distributions for three groups of depths. The classification of fitting distributions can be found in tables 4.7 to 4.9 and parameters for fitting distributions are presented in Tables 4.10 and 4.11 According to this results, equivalent conductivity decreases as depth increases. This fact is usually related to higher conductivities inherent in surface or lower depths due to metal equipment/cables and soil salinization. However, simulation results in Section 4.5 will show that the dependence of equivalent conductivity on depth is also true even when there is not any upper layer with higher conductivity. In multi-layer conditions, the transitions through various layers appear to cause more attenuation to the field when it is in quasi-static or transition zone, leading to a pessimistic estimation of apparent conductivity for measurements at lower depths.

Table 4.7: RMSE error of conductivity distribution for each frequency for depths between 0 and 100 meters

<b>Distribution</b>	<b>630 Hz</b>	<b>1050 Hz</b>	<b>1950 Hz</b>	<b>3030 Hz</b>
<b>Log-normal</b>	0.026581	0.03822	0.036472	0.03152
<b>Burr</b>	0.033005	0.029182	0.03752	0.030142
<b>Gamma</b>	0.039023	0.040892	0.041438	0.051767
<b>Loglogistic</b>	0.029427	0.02913	0.038843	0.032266
<b>Weibull</b>	0.043136	0.042323	0.040548	0.043012

Table 4.8: RMSE error of conductivity distribution for each frequency for depths between 100 and 200 meters

<b>Distribution</b>	<b>630 Hz</b>	<b>1050 Hz</b>	<b>1950 Hz</b>	<b>3030 Hz</b>
<b>Log-normal</b>	0.024253	0.023005	0.043881	0.035353
<b>Burr</b>	0.028294	0.02049	0.023493	0.023014
<b>Gamma</b>	0.038121	0.025111	0.024466	0.023405
<b>Loglogistic</b>	0.028137	0.021599	0.041669	0.034128
<b>Weibull</b>	0.039953	0.029537	0.023432	0.024249

Table 4.9: RMSE error of conductivity distribution for each frequency for depths between 200 and 500 meters

<b>Distribution</b>	<b>630 Hz</b>	<b>1050 Hz</b>	<b>1950 Hz</b>	<b>3030 Hz</b>
<b>Log-normal</b>	0.044205	0.0483	0.052546	0.047364
<b>Burr</b>	Inf	Inf	0.035293	Inf
<b>Gamma</b>	0.063591	0.068918	0.036083	0.054153
<b>Loglogistic</b>	0.04792	0.050442	0.051208	0.049498
<b>Weibull</b>	0.056534	0.065842	0.035107	0.05294

Table 4.10:  $\mu$  parameter in dB for Log-normal distribution of conductivity

<b>Frequency [Hz]</b>	<b>D: 0 to 100 m</b>	<b>D: 100 to 200 m</b>	<b>D: 200 to 500 m</b>
630	-1.12	-2.2042	-3.3967
1050	-1.7223	-2.7709	-3.4683
1950	-2.1317	-3.2491	-4.1733
3030	-2.699	-3.5825	-4.1933

Table 4.11:  $\sigma$  parameter in dB for Log-normal distribution of conductivity

Frequency [Hz]	D: 0 to 100 m	D: 100 to 200 m	D: 200 to 500 m
630	0.77296	0.80186	1.0242
1050	1.0706	0.83934	0.84134
1950	0.92617	0.96328	1.0428
3030	1.2674	0.97317	1.069

An estimation of equivalent conductivity normalized as in frequency as in depth is shown in Figure 4.20. The statistical distribution obtained is Log-normal with parameters  $\mu = 0$  dB,  $\sigma = 0.94462$  dB.

Finally, it was used the extrapolation method explained in the previous section for estimating  $\mu$  parameter of equivalent conductivity distribution for some frequencies from 630 Hz to 10 kHz. From this data, it is possible to realize that  $\mu$  decreases as a function of distance and frequency.

Table 4.12:  $\mu$  parameter in dB for Log Normal Distribution (for each frequency and depth interval)

Frequency [Hz]	D: 0 to 100 m	D: 100 to 200 m	D: 200 to 500 m
630	-1.12	-2.2042	-3.3967
1050	-1.7223	-2.7709	-3.4683
1950	-2.1317	-3.2491	-4.1733
3030	-2.699	-3.5825	-4.1933
4350	-3.3459	-3.9373	-4.2111
5970	-4.1388	-4.3567	-4.1949
7850	-5.0589	-4.8434	-4.1762
10000	-6.1111	-5.4	-4.1548

## 4.5 MULTI-LAYER STATISTICAL MODEL THROUGH ELECTROMAGNETIC FIELD SIMULATIONS

With the estimations calculated in section 4.4, specially in Table 4.6 for the middle frequency, a simulation set was created in order to study H-field behavior in close-to-reality scenarios. The scenario used for that simulation is described as follows and it is shown in Figure 4.21:

- **Antennae size:** both antennae have a square shape with  $\sqrt{\pi}$  m side and square cross-section of  $1 \text{ cm}^2$ .
- **Antennae position:** the above ground antenna was set to be 50 cm over ground and in vacuum conditions. The second antenna was positioned at 300 m under surface of mine, inserted in the soil layer.
- **Layer size:** all layers are 50 m side square shaped parallelepipeds with different heights, which depends on the number of layers and the height overall layers is 310 m,

- Number of layers: a random number of layers  $X$  is selected from a uniform distribution  $U(3, 25)$ ,
- Heights of layers: a random height is chosen from a uniform distribution  $U(1, 300/x)$  where  $x$  is the number of layers sorted before,
- Probe position: probes for measuring H-field distributed evenly at the antennae axes at a 10 m distance of each other and at center of each antenna,
- Layer electromagnetic characteristics: magnetic permeability was set as vacuum condition  $\mu_0 = 4\pi 10^{-7}$ ; electric conductivity was programmed to be a point of a random Log-Normal distribution according to the extrapolated parameters from Table 4.6 for frequency of 4350 Hz,
- Frequency range: 0.1 to 10 kHz distributed in logarithmic steps,
- Number of trials: 150 independent and random trials.

#### 4.5.1 H-field variation as a function of depth and frequency

In order to have a general idea about the variation of H-field as a function of depth and frequency, it is interesting to see such variation for a single trial. Figure 4.22 shows that H-field decreases as depth and frequency augment.

Also, it is interesting to compare the simulated H-field to theoretical models of **TS** and **HHS**. In Figure 4.23 is shown the H-field for all frequencies and all trials, and **TS** and **HHS** overlapping them. Is possible to infer that both theoretical models cannot suit the simulated field for any configuration because H-field has a different behavior that is not predicted for them. Even if some conductive values are used to fit the H-field curve to the median of synthetic data for some frequencies those will not be valid for other frequencies or depths.

Furthermore, is important to give a closer view to H-field variations. Thus, there were selected three frequencies close to those from the extrapolated data (657.9, 4328.8 and 10000 Hz) and three depths (20, 150 and 300 m) from all available data. From now on, all fields are captured from synthetic or measured data are normalized to the magnetic moment of their transmitters to improve the comparisons  $M = I \times N \times Stx = 0.28 \times 1 \times \pi$ .

Field variation as a function of depth is shown in Figure 4.24. From it, it is possible to infer:

- For short depths, the H-field is affected homogeneously for all frequencies,
- For mid depths, the frequency starts to influence more significantly the attenuation of H-field and also it starts to augment its variation from mine to mine,
- For long depths, both H-field attenuation and variation are hoisted in higher intensity. Such stronger field dependence on frequency for deeper depths is natural and also is noticed in **IC**, **HHS** and **TS** models.

Now, regarding to H-field variation as a function of depth, Figure 4.25, shows this variation for three frequencies. It is possible to see that attenuation augments non-linearly with depth for all frequencies. Also, variation of H-field is more severe for deeper positions for all frequencies.

For each pair of frequency/depth there is a statistical distribution that fits the best the data. All fields are taken in dB to fit distributions due to the importance of fields on very low levels. Again, it was used the RMSE as decision parameter. The tables 4.14 and 4.13 show the distribution found and the RMSE for each combination. From the first one, it is possible to identify Burr as the most frequent distribution.

Table 4.13: H-field distribution for each pair of depth/frequency

Frequency	Depth		
	20 m	150 m	300 m
<b>657.9 Hz</b>	Burr	Extreme Value	Generalized Extreme Value
<b>4328.8 Hz</b>	Burr	Weibull	Lognormal
<b>10 kHz</b>	Burr	Burr	Lognormal

Table 4.14: RMSE of field distribution for each pair of depth/frequency

Frequency	Depth		
	20 m	150 m	300 m
<b>657.9 Hz</b>	0.0162	0.0147	0.0117
<b>4328.8 Hz</b>	0.0156	0.0162	0.0128
<b>10 kHz</b>	0.0158	0.0120	0.0109

Regarding mean and standard deviation, tables 4.15 and 4.16 resume those statistical parameters found. All related figures can be found in Appendix VIII.

Table 4.15: Mean value for H-field for three depths and three frequencies

Frequency	Depth		
	20 m	150 m	300 m
<b>657.9 Hz</b>	-102.0837	-152.7302	-178.4232
<b>4328.8 Hz</b>	-102.5094	-166.3229	-210.2905
<b>10 kHz</b>	-103.2016	-179.2336	-235.5912

Table 4.16: Standard deviation for H-field for three depths and three frequencies

Frequency	Depth		
	20 m	150 m	300 m
<b>657.9 Hz</b>	4.2795	3.2247	5.2173
<b>4328.8 Hz</b>	4.5272	8.5019	12.9196
<b>10 kHz</b>	4.9979	11.1981	17.2684



## 4.5.2 H-field median fitting

In order to describe H-field in a more general way, it was calculated the median of all trials as function of frequency and depth. Then, it was estimated the following empirical equation for H-field as a function of frequency and depth. Figure 4.26 shows the median values of H-field for each pair of frequency ( $f$ ) and depth ( $d$ ) and the fitting plane of the equation in (4.1)

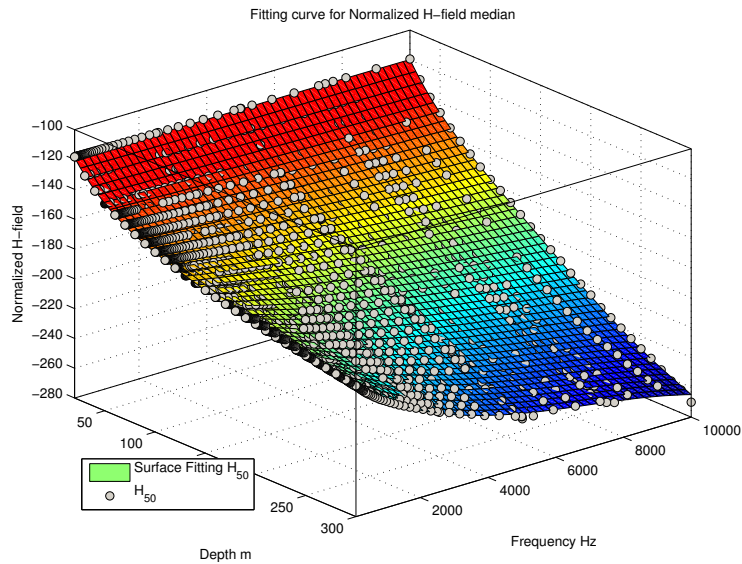
$$\mathbf{H}_{50}(d, f) = 20[a_1 + a_2 \times \log(\omega) + a_3 \times \log(d) + a_4 \times \log(e^{-T})] \quad [\mathbf{dB}] \quad (4.1)$$

For  $\omega = 2\pi f$  and  $T = d\sqrt{\frac{\omega\mu\sigma_0}{2}}$ .  $\sigma_0 = 0.025$  is the equivalent value of mean conductivity used in all simulations. This formula has R-square: 1.0000 and RMSE: 0.1506. The other coefficients are presented in Table 4.17

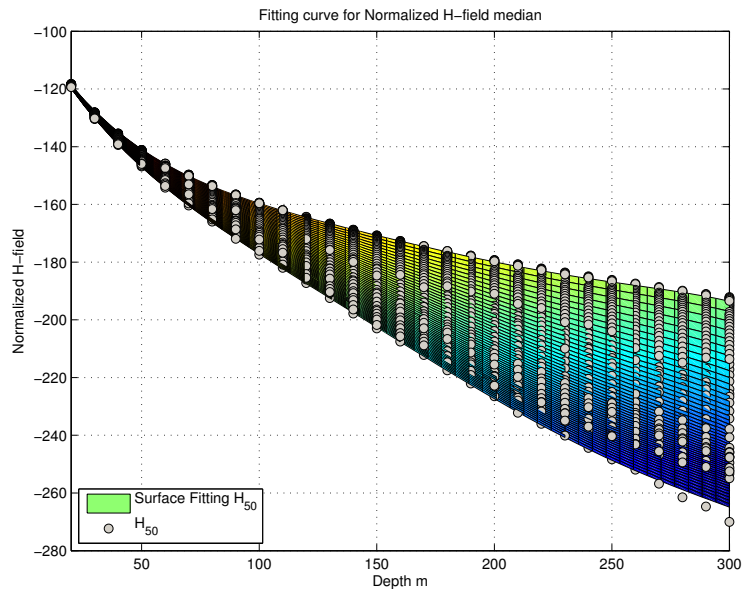
Table 4.17: H-field median coefficients

Coefficient	Value
$a_1$	-2.821
$a_2$	0.233
$a_3$	-2.335
$a_4$	1.053

It is important to remember that this equation fits the median of H-field data extracted from multi-layer simulations with conductivity following Log-normal distribution with parameters  $\mu = 3.807$  and  $\sigma = 1.196$ . These values are extrapolated from measured field data. Other less complex equations of lower order are easily computed bringing simplicity for the model at the cost of increasing the RMSE.



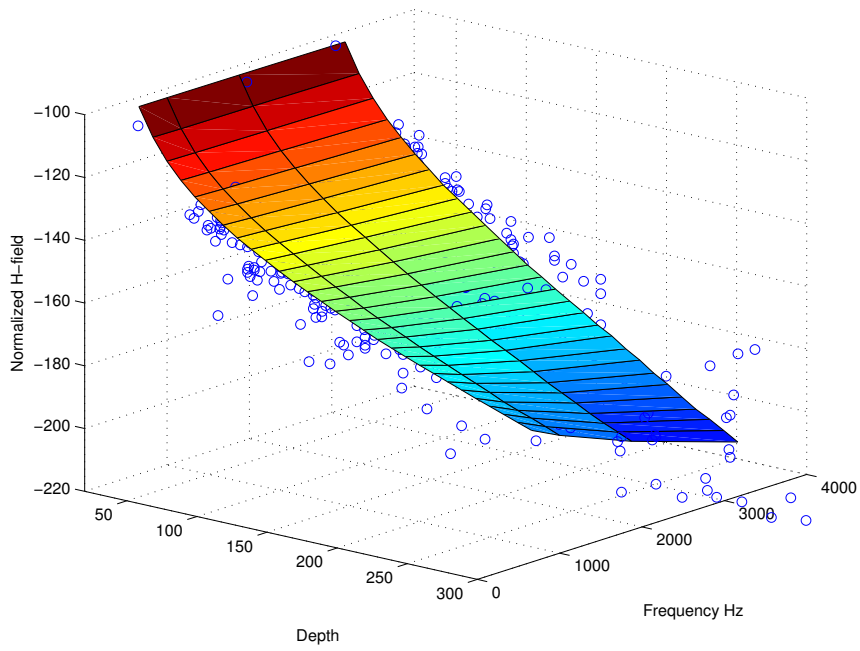
(a) 3D H-field median fitting



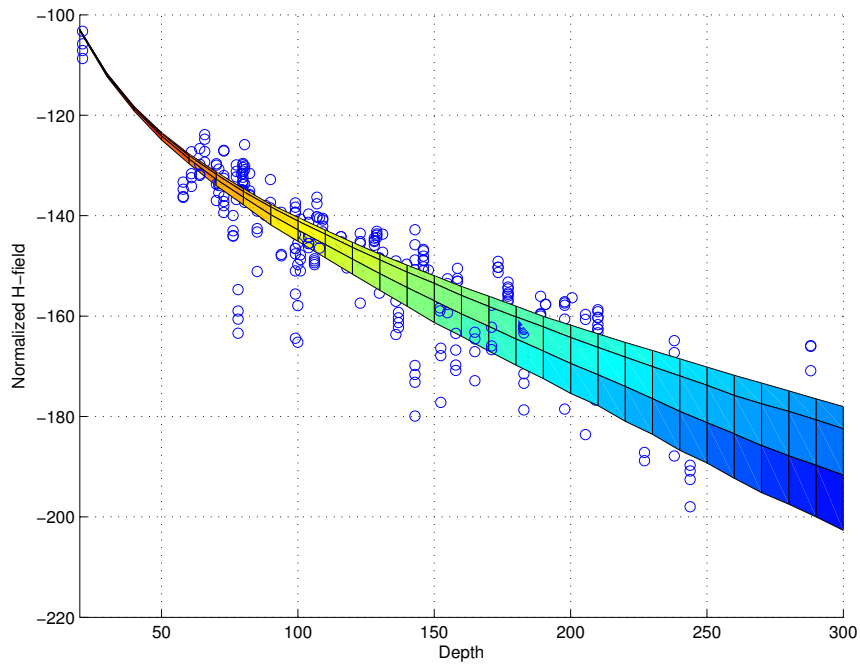
(b) 2D H-field median fitting

Figure 4.26: H-field median fitting

Figure 4.27 shows a comparison between H-field median calculated from simulations (surface) and measured data field from Table 4.3 only for the four frequencies employed in measurements. It is possible to infer that all simulations have resemblance to real data up to 250 m. Taking into account that data from simulations was taken from 20 to 300 m, it is possible to suggest that the model simulated is valid, including the choice of layer and conductivity distributions and their parameters.



(a) 3D view H-field median vs real data



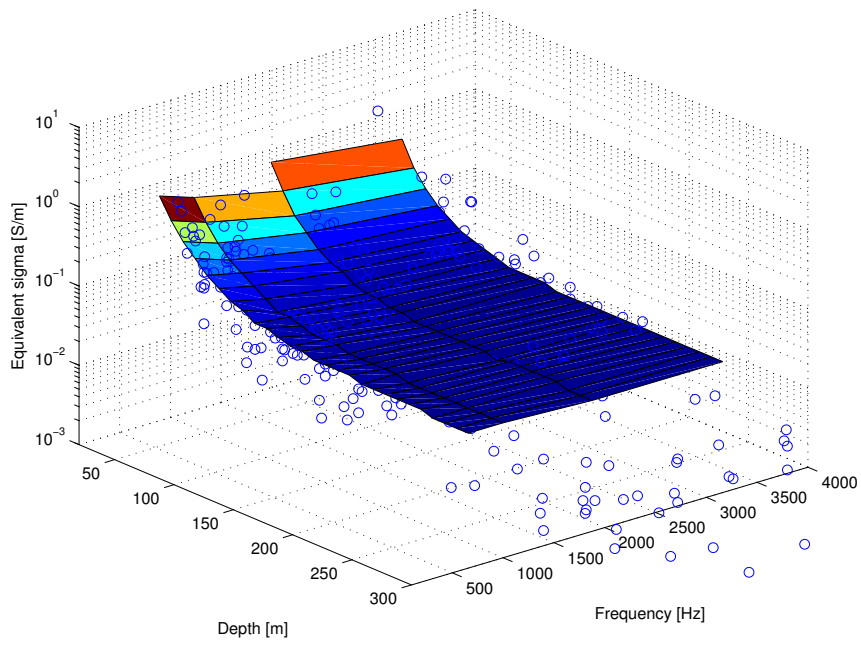
(b) 2D view H-field median vs real data

Figure 4.27: H-field median compared to real condition data

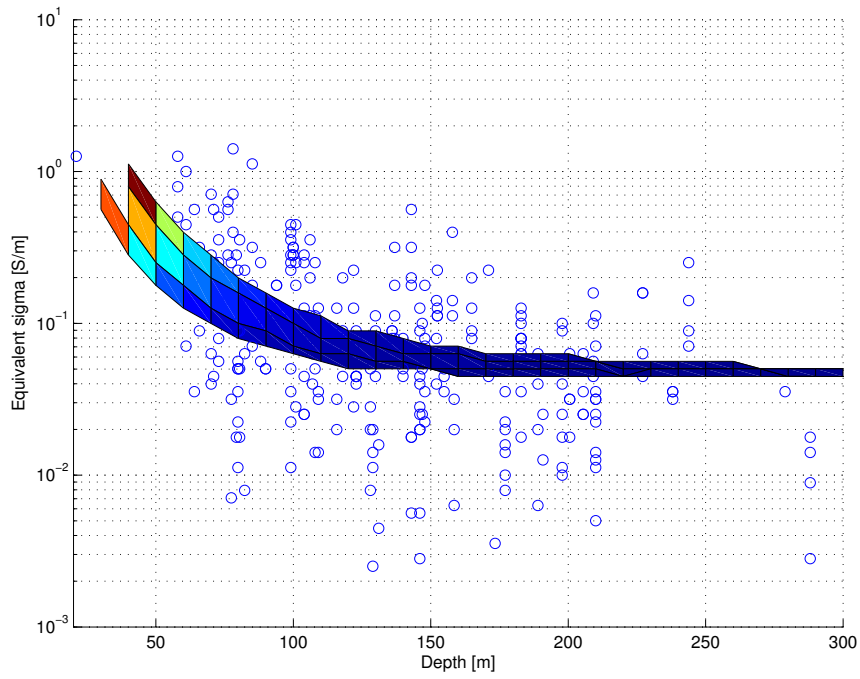
### 4.5.3 Equivalent conductivity

It was calculated the median of equivalent conductivity for all trials by the means of **HHS** model and compared to equivalent conductivities computed from measured data mentioned earlier only the frequencies 630, 1050, 1950 and 3030 Hz. From the images in Figure 4.28, it is possible to infer that simulated scenarios suit real conditions at least up to 300 m depth. Also, it is

possible to infer that the affirmation stated by Lincan in [31] "In the thin sheet model... the highly conducting thin sheet represents possible surface metal structures, such as cables, pipes, cased bore hole, etc., as well as the relatively high conductivity at surface which usually contains more dissolved salt and mineral substances." is possibly mistaken by the observation of high equivalent conductivities in upper overburden when calculated through **HHS** and Q-factor models. This is demonstrated by the simulations carried out in this dissertation, that even not employing any high conductive layer close the surface, still there are higher equivalent conductivities for small depths as it can be seen in Figure 4.28.



(a) 3D view conductivity median vs real data



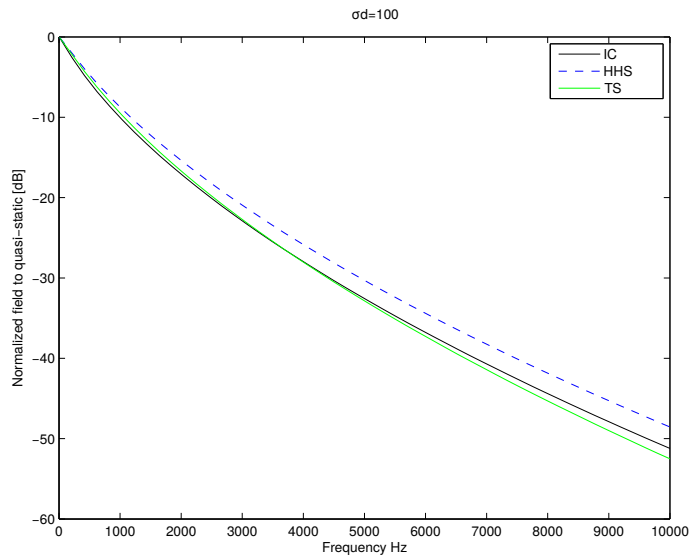
(b) 2D view conductivity median vs real data

Figure 4.28: Median of Equivalent Conductivity compared to real condition data

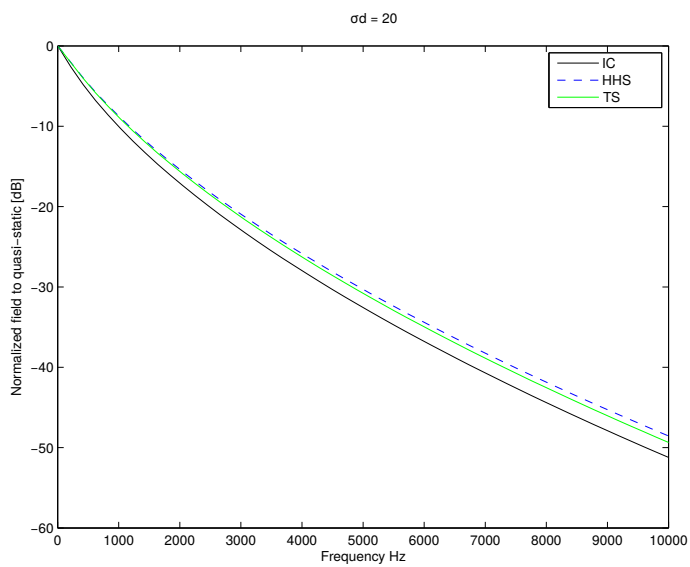
## 4.6 ISSUES SOLVED WHILE USING THE COMMERCIAL SIMULATOR

Several situations were presented while simulation TTE environments. The most remarkable are:

- The use of higher conductivities (higher than 2 S/m) in the first conductive layer for down-link introduces numerical errors in magnetic field calculations. This happens due to inaccuracies in modeling the boundary conditions for a diffusion medium.
- A small proportion between antenna size and the simulation boundary box size also introduces errors on calculation of magnetic field.
- Mesh size of 3D objects must be smaller for more conductive elements.
- The simulation time is reduced while using less layers while using the multi-layer model.



(a) H-field for  $\sigma d = 100$



(b) H-field for  $\sigma d = 20$

Figure 4.3: H-field TS and HHS models variation of parameters  $\sigma d$

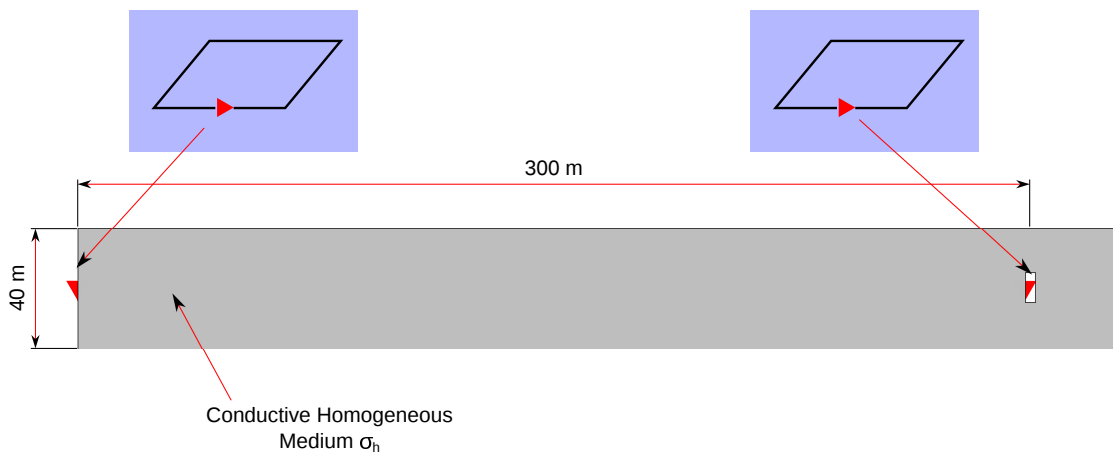
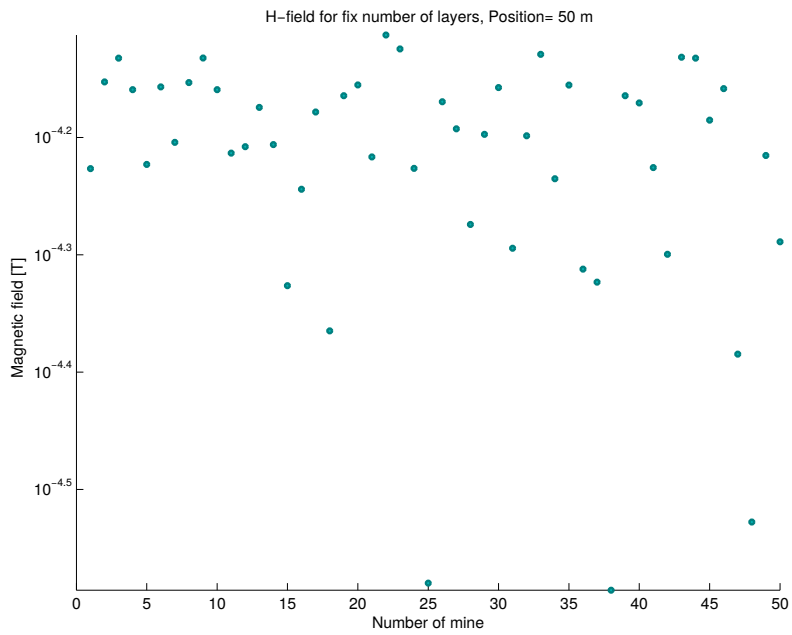
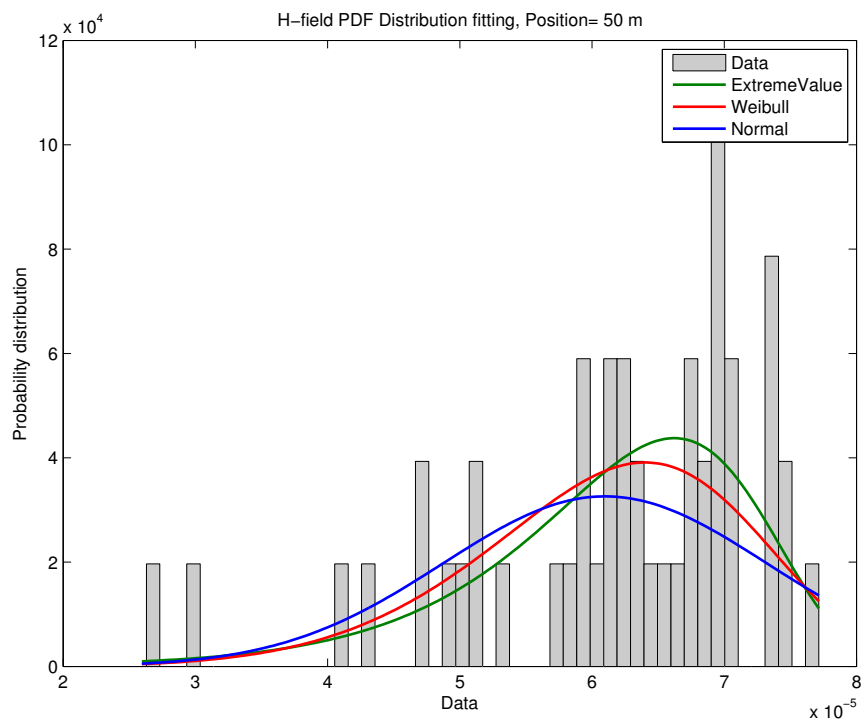


Figure 4.4: Simulation scenario for **HHS** model simulation



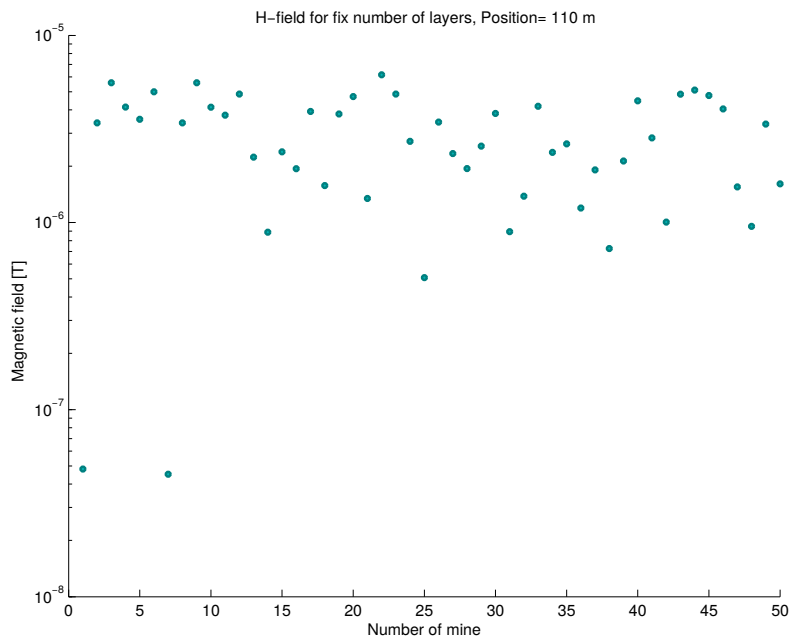


(a) H-field distribution

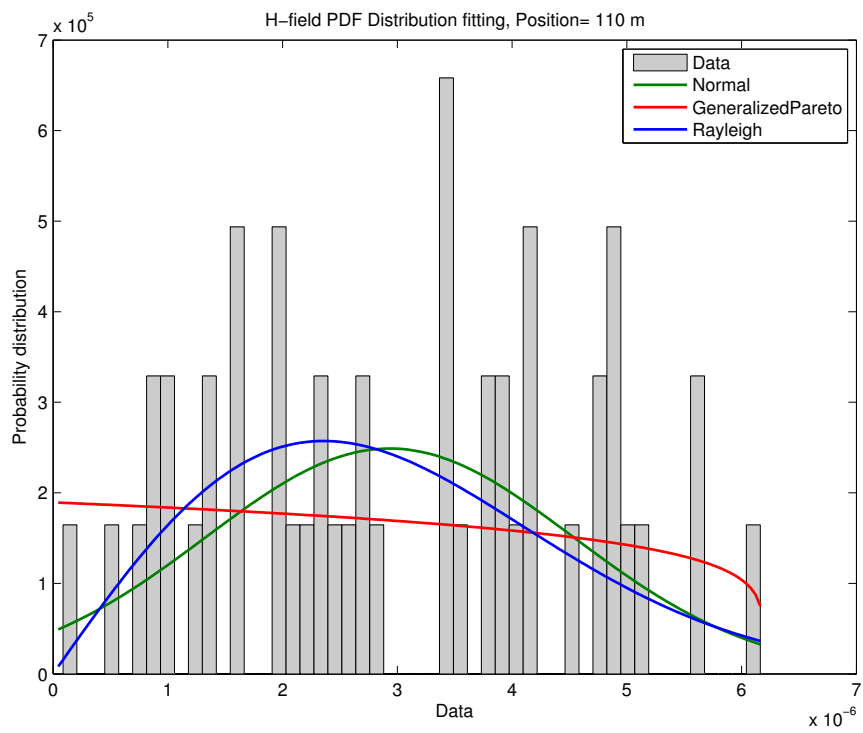


(b) Statistical fitting

Figure 4.6: H-field statistical characterization at 50 m  
Fix number of layers

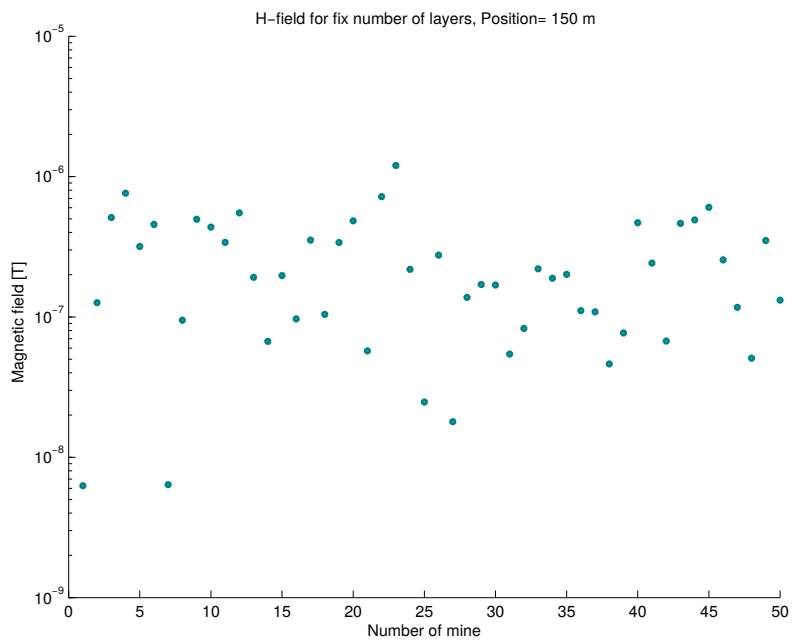


(a) H-field distribution

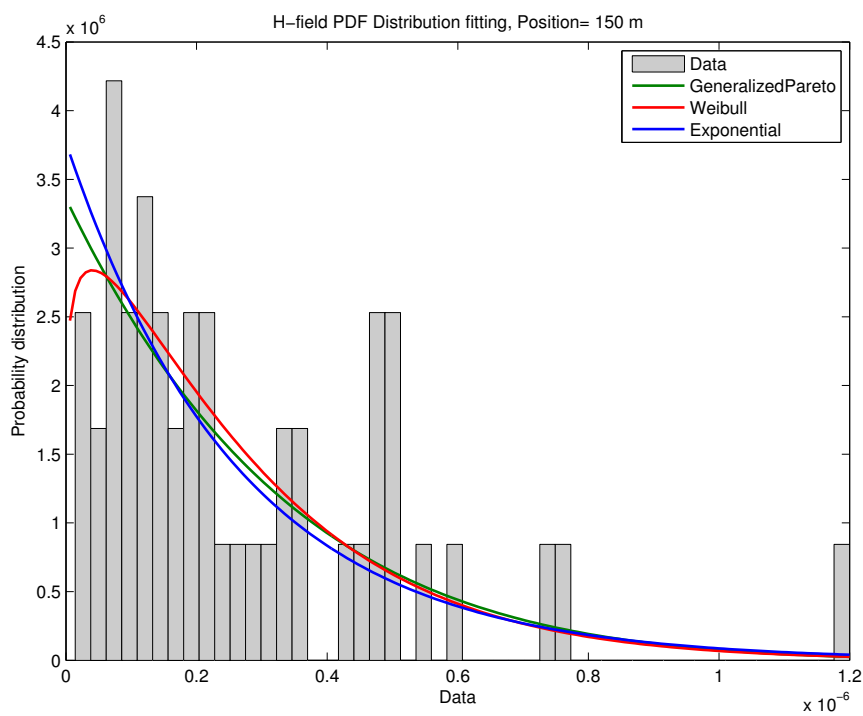


(b) Statistical fitting

Figure 4.7: H-field statistical characterization at 110 m  
Fix number of layers

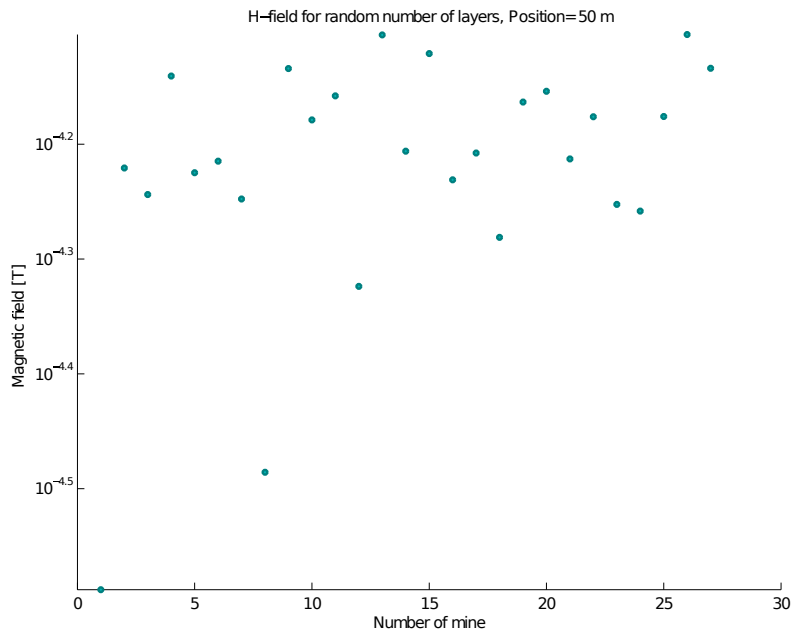


(a) H-field distribution

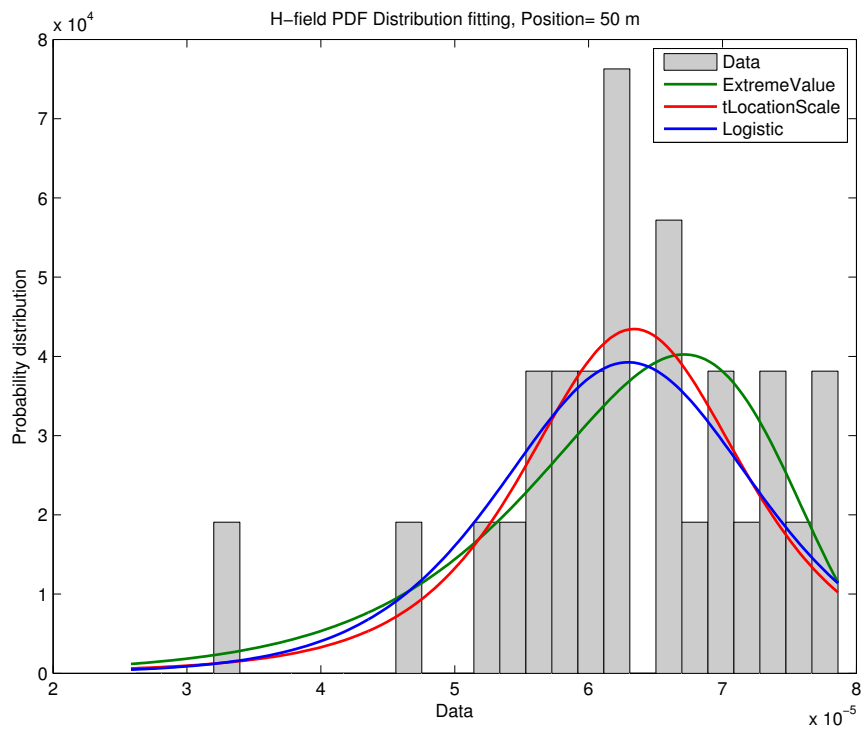


(b) Statistical fitting

Figure 4.8: H-field statistical characterization at 150 m  
Fix number of layers

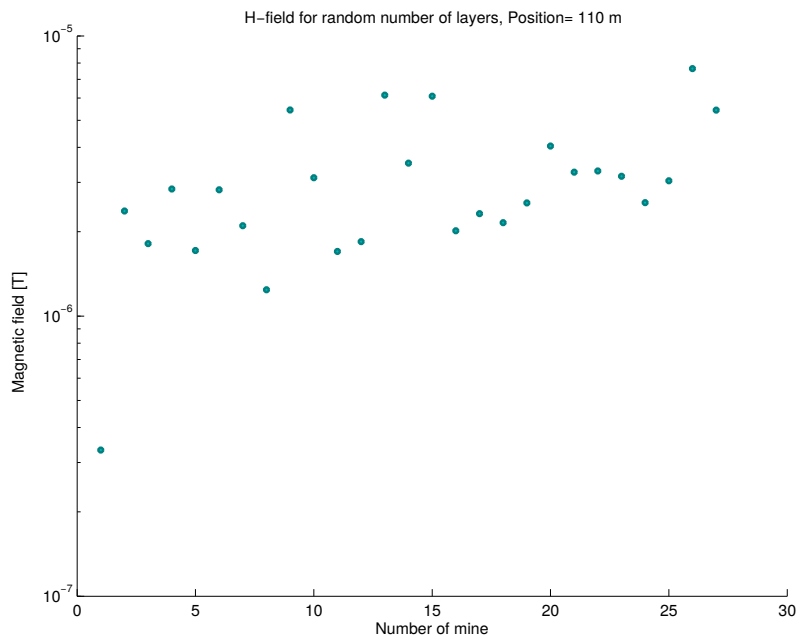


(a) H-field distribution

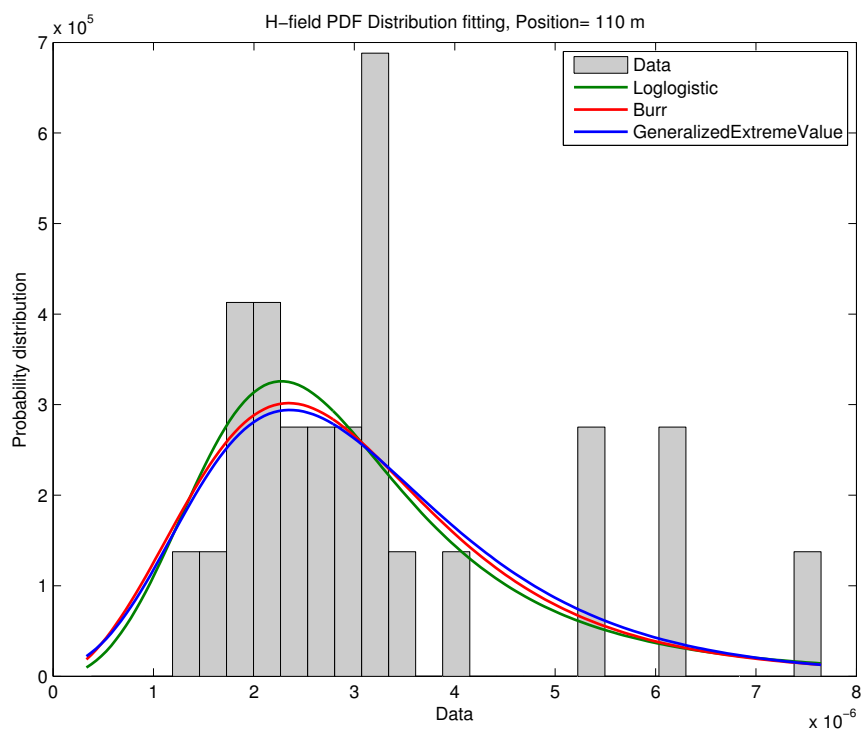


(b) Statistical fitting

Figure 4.9: H-field statistical characterization at 50 m  
Random number of layers

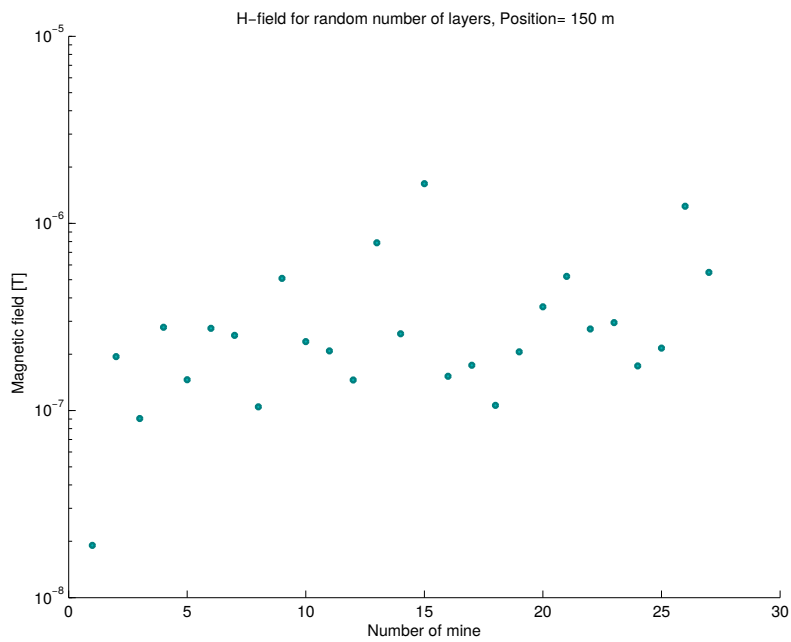


(a) H-field distribution

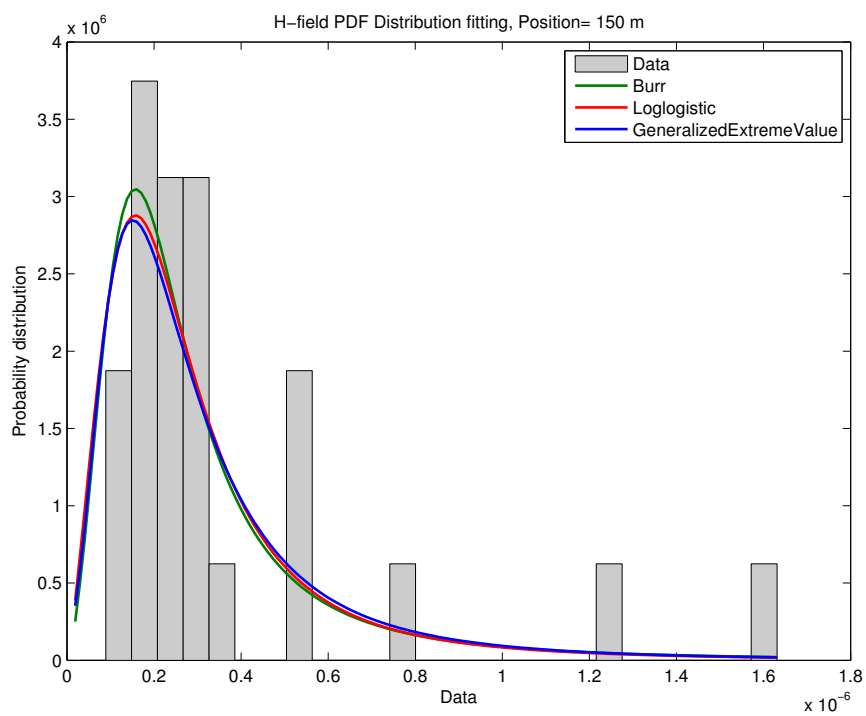


(b) Statistical fitting

Figure 4.10: H-field statistical characterization at 110 m  
Random number of layers



(a) H-field distribution



(b) Statistical fitting

Figure 4.11: H-field statistical characterization at 110 m  
Random number of layers

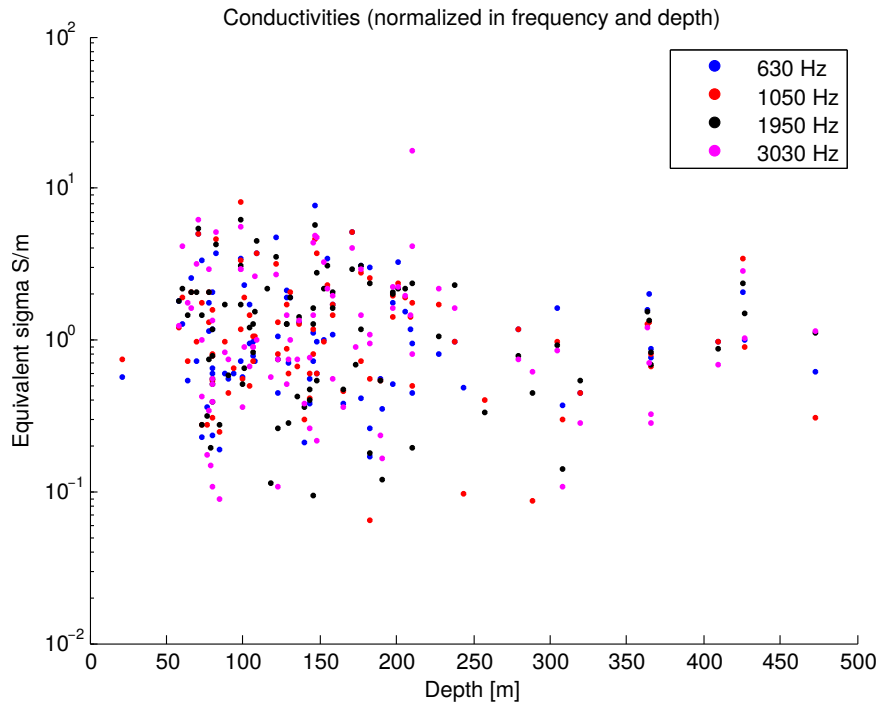


Figure 4.20: Conductivities (normalized in frequency and depth)

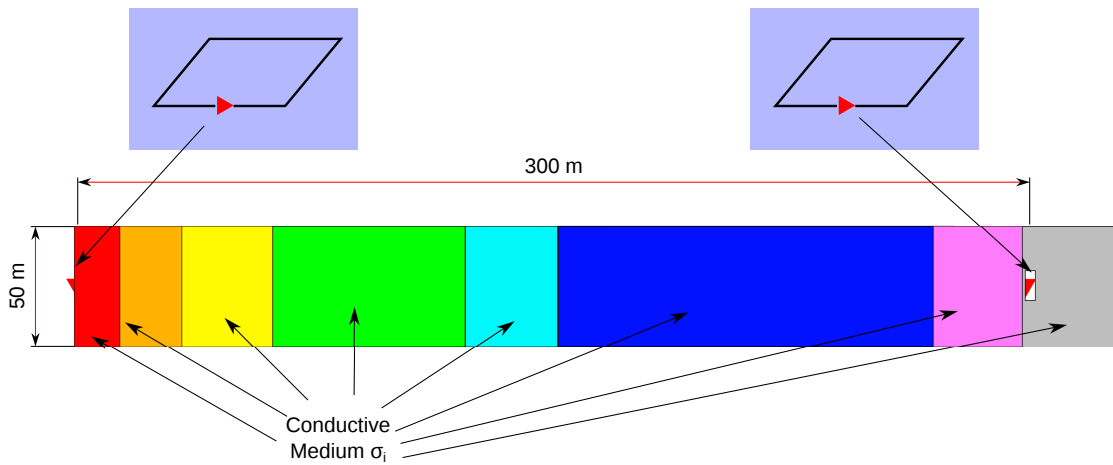


Figure 4.21: Multi-layer TTE scenario

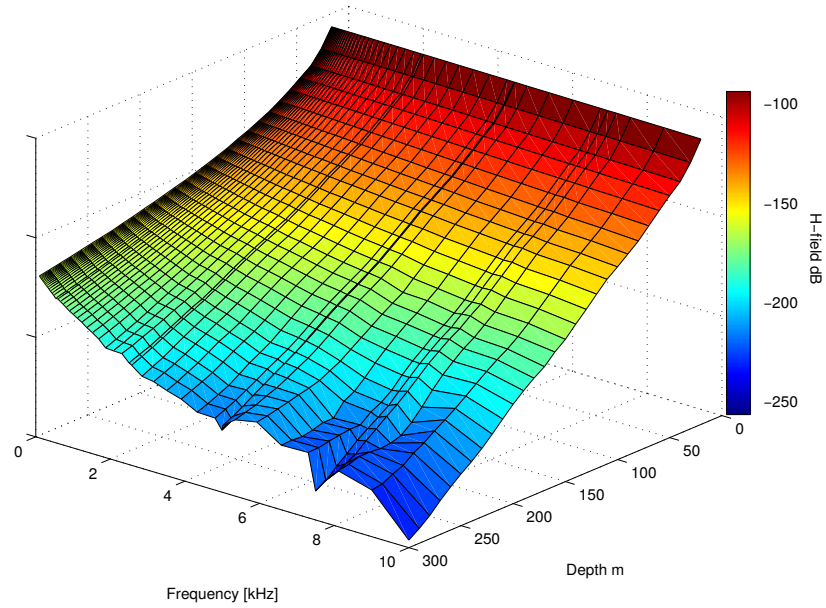


Figure 4.22: H-field variation for a single mine as a function of depth and frequency

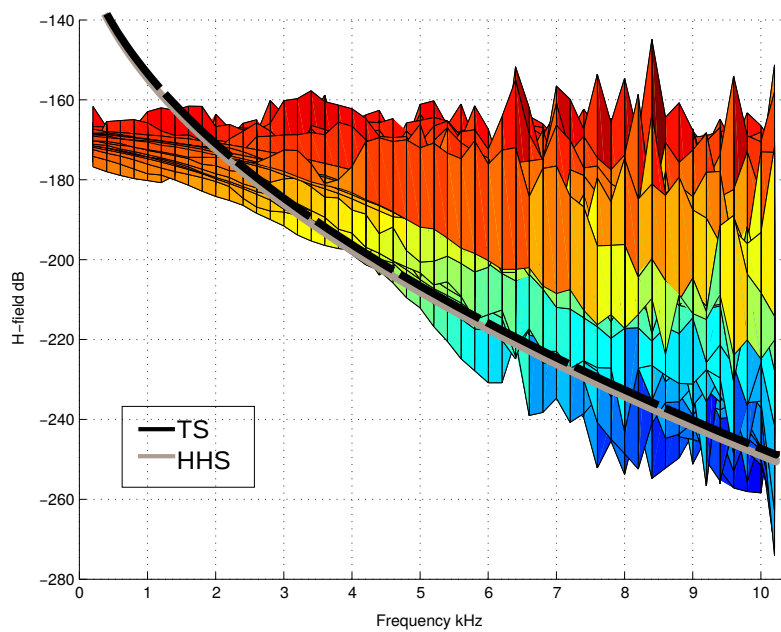


Figure 4.23: H-field variation for a single mine as a function of depth and frequency



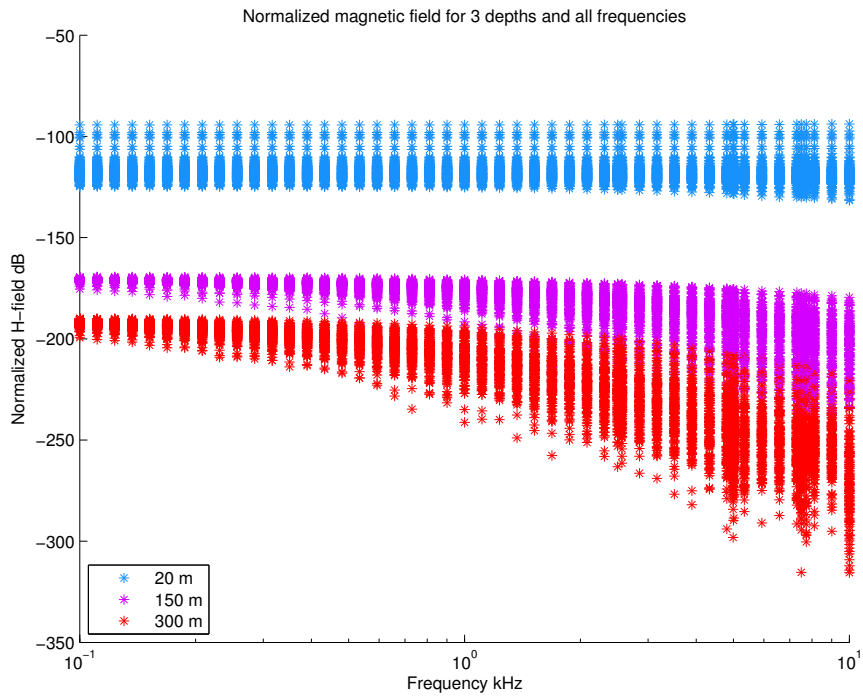


Figure 4.24: H-field variation as a function of depth for 3 positions.

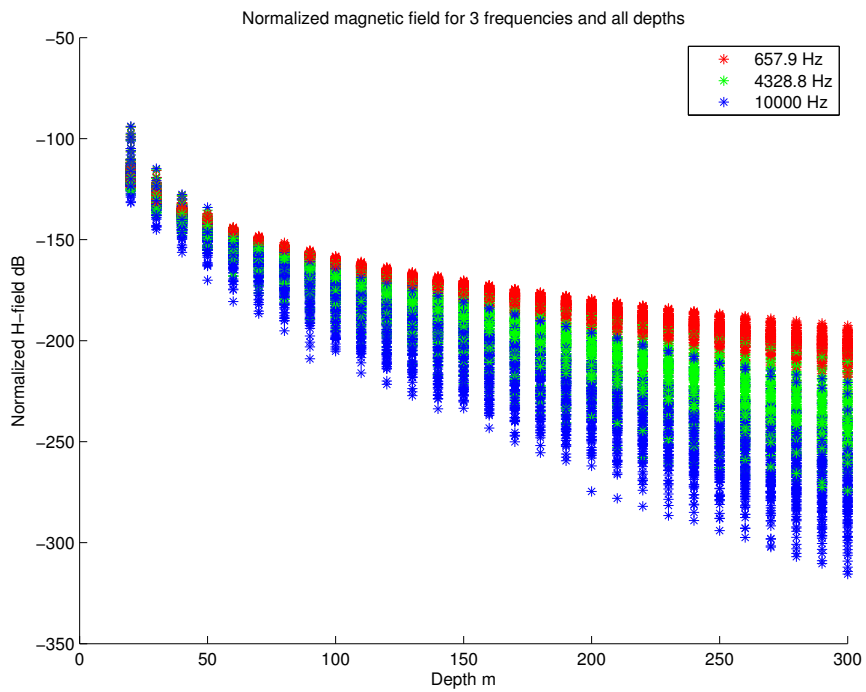


Figure 4.25: H-field variation as a function of frequency.

## 5 CONCLUSION

An alternative to wire based systems in underground mines is the Through-The-Earth communication system, specially in situations where human beings are trapped underground due to tunnel burials that brakes wired links to surface. Other application for the TTE systems is the activation of explosives and automation of equipment for underground mining.

Wireless propagation, especially Through-The-Earth, establishes severe restrictions to the communication system. Using low-frequency signals is essential for reducing the effects of soil attenuation in underground environments. Soil electric characteristics potentiate such attenuation, so having the same information about the environment makes easier the process of planning communication structure for a underground mines.

As it has been shown in this dissertation, theoretical models **TS** and **HHS** does not described properly magnetic field propagation with a variety of media, and other models are too complex to implement that makes almost impossible to used them.

Magnetic field is affected in both depth and frequency dimensions in stratified TTE communication environments. H-field is affected in less proportion for small distances, where frequency (from 0.1 to 10 kHz) does not affect significantly the communication link. For further depths, frequency introduces more variation of H-field for different mine sites, as well as bigger attenuation of signal as it can be seen in Tables 4.15 and 4.16.

Regarding equivalent conductivity, according to **TS** model, equivalent conductivity is higher for smaller depths due to the presence of highly conductive elements. Nevertheless, according to the simulations presented in the previous chapter, for scenarios where no **TS** was contemplated, the equivalent conductivity kept higher values for small depths.

As presented in previous chapters, soil electric conductivity can be an important parameter to be taken into account while transmitting signals through the earth. For an arbitrary mine configuration, after estimating the distance between both endpoints and frequency, it is possible to use the empirical equation of H-field presented in this dissertation for predicting the median of received magnetic field for mines with similar soil characteristics as coal mines. With this information, it is possible to adequate all parameters from the transmitter and receiver for an efficient communication.

TTE communication is a field that has not been extensively studied, therefor there are several topics that can be researched after the present work. Among those topics are the following:

- Propagation channel modeling: as it was seen, **TS** and **HHS** models do not predict magnetic field attenuation and other models are difficult to implement. Because of that, there is a necessity of more accurate and practical models for magnetic field propagating in TTE environments.

- Antennae, transmission/reception circuits and impedance matching circuits: it is necessary to improve the research on high sensibility antennae or magnetic sensor inside conductive medium and all circuits related to them.
- Localization techniques based on multi-sensor networks: this application is vital for sensing mine status prior disasters and after any emergency situation where miners are trapped.
- Studies of field behavior in multi-layer media in quasi-static, near-field, transition and far-field zones to better understand the effect of high equivalent conductivities in upper layers.

## BIBLIOGRAPHICAL REFERENCES

- 1 BARKAND, T. D.; DAMIANO, N. W.; SHUMAKER, W. Through-the-earth, two-way, mine emergency, voice communication systems. In: *IEEE. Industry Applications Conference, 2006. 41<sup>st</sup> IAS Annual Meeting. Conference Record of the 2006 IEEE*. [S.l.], 2006. v. 2, p. 955–958.
- 2 RAAB, F. H.; JOUGHIN, I. R. Signal processing for through-the-earth radio communication. *Communications, IEEE Transactions on*, IEEE, v. 43, n. 12, p. 2995–3003, 1995.
- 3 YENCHEK, M. R.; HOMCE, G. T.; DAMIANO, N. W.; SREDNICKI, J. R. Niosh-sponsored research in through-the-earth communications for mines: a status report. *Industry Applications, IEEE Transactions on*, IEEE, v. 48, n. 5, p. 1700–1707, 2012.
- 4 MINERAL, D. N. de Produção. *Código de Mineração - Capítulo I das Disposições Preliminares*. [Http://www.dnpm-pe.gov.br/Legisla/cm\\_01.htm](Http://www.dnpm-pe.gov.br/Legisla/cm_01.htm). Accessed: 2015-04-22. Available at: <[http://www.dnpm-pe.gov.br/Legisla/cm\\_01.htm](http://www.dnpm-pe.gov.br/Legisla/cm_01.htm)>.
- 5 YARKAN, S.; GÜZELGÖZ, S.; ARSLAN, H.; MURPHY, R. Underground mine communications: A survey. *Communications Surveys Tutorials, IEEE*, v. 11, n. 3, p. 125–142, rd 2009. ISSN 1553-877X.
- 6 (UNDERGROUND), A. M. T. *MAGNETO MINE TELEPHONES*. 2012. <Http://www.britishtelephones.com/atm/atmtel6.htm>. Accessed: 2015-04-15. Available at: <<http://www.britishtelephones.com/atm/atmtel6.htm>>.
- 7 BANDYOPADHYAY, L.; CHAULYA, S.; MISHRA, P. Wireless communication in underground mines. *RFID-Based Sens. Netw*, Springer, 2010.
- 8 SAFETY, N. I. for O.; HEALTH. *Tutorial on Wireless Communication and Electronic Tracking Part 1: Technology Overview*. 2010. <Http://www.msha.gov/techsupp/PEDLocating/WirelessCommandTrack2009.pdf>. Accessed: 2015-04-22. Available at: <<http://www.msha.gov/techsupp/PEDLocating/WirelessCommandTrack2009.pdf>>.
- 9 PATRI, A.; NAYAK, A.; JAYANTHU, S. Wireless communication systems for underground mines—a critical appraisal. *International Journal of Engineering Trends and Technology (IJETT)*, v. 4, n. 7, p. 3149–3153, 2013.
- 10 YIN, Z. J.; CHUNG, K.-S. Multiple access protocol for an underground mobile communication system. In: *Global Telecommunications Conference, 1998. GLOBECOM 1998. The Bridge to Global Integration. IEEE*. [S.l.: s.n.], 1998. v. 4, p. 2217–2224.
- 11 JING, G.; QIANPING, W. Application of hybrid routing protocol for mine WSN. In: *Environmental Science and Information Application Technology (ESIAT), 2010 International Conference on*. [S.l.: s.n.], 2010. v. 3, p. 353–355.
- 12 CHETAN, B.; DESHPANDE, P.; HEGDE, B. G.; SRINIVAS, S.; KUMAR, G. N. Analysis of DSdv amp; aodv for disaster management system in coal mines. In: *Wireless Communications, Networking and Mobile Computing (WiCOM), 2011 7<sup>th</sup> International Conference on*. [S.l.: s.n.], 2011. p. 1–4. ISSN 2161-9646.
- 13 LEI, S.; ZHAO, X.; WENYAN, Z.; XICHENG, C. Model of ad hoc networks for rescuing in mine. In: *Networks Security Wireless Communications and Trusted Computing (NSWCTC), 2010 Second International Conference on*. [S.l.: s.n.], 2010. v. 1, p. 210–213.

- 14 WU, D.; LI, R.; BAO, L. A holistic routing protocol design in underground wireless sensor networks. In: *Mobile Ad-hoc and Sensor Networks, 2008. MSN 2008. The 4<sup>th</sup> International Conference on*. [S.l.: s.n.], 2008. p. 187–194.
- 15 SUN, Y.; LIU, X. Wireless multi-hop ad hoc networks based on olsr for underground coal mine. In: *Wireless Communications and Signal Processing (WCSP), 2010 International Conference on*. [S.l.: s.n.], 2010. p. 1–6.
- 16 WENQI, C.; ZHAO, X. Multi-hop routing for wireless network in underground mines. In: *Wearable Computing Systems (APWCS), 2010 Asia-Pacific Conference on*. [S.l.: s.n.], 2010. p. 337–340.
- 17 JIANG, H.; PENG, J.; PENG, W. Nonuniform clustering routing protocol for tunnel wireless sensor network in underground mine. In: *Wireless Communications Signal Processing, 2009. WCSP 2009. International Conference on*. [S.l.: s.n.], 2009. p. 1–5.
- 18 ZHENG, Z.; HU, S. Research challenges involving cross-layered communication protocol design for underground WSNs. In: *Anti-counterfeiting, Security and Identification, 2008. ASID 2008. 2<sup>nd</sup> International Conference on*. [S.l.: s.n.], 2008. p. 120–123.
- 19 AL., G. S. et. *To the rescue!* 2010. World Coal.
- 20 NEWS, E. *New Through Earth Communication System for Coal Mining*. 2014. Endeavour Magazine.
- 21 FOROOSHANI, A.; BASHIR, S.; MICHELSON, D.; NOGHANIAN, S. A survey of wireless communications and propagation modeling in underground mines. *Communications Surveys Tutorials, IEEE*, v. 15, n. 4, p. 1524–1545, Fourth 2013. ISSN 1553-877X.
- 22 GIBSON, D. *Channel Characterisation and System Design for Sub-Surface Communications*. Tese (Doutorado) — University of Leeds, Feb. 2003.
- 23 BALANIS, C. *Antenna Theory: Analysis and Design*. 3rd. ed. [S.l.]: John Wiley and Sons, 2005.
- 24 GRIFFITHS, D. J. *Introduction to Electrodynamics*. 3a. ed. [S.l.]: Prentice Hall, 1999.
- 25 STARKEY, D. B. Electromagnetic transmission and detection at deep depths. *Sandia Laboratories Report SLL-73-5278*, 1973.
- 26 WAIT, J. R. Electromagnetic induction technique for locating a buried source. *Geoscience Electronics, IEEE Transactions on*, v. 9, n. 2, p. 95–98, Apr. 1971. ISSN 0018-926X.
- 27 WAIT, J. R.; SPIES, K. Subsurface electromagnetic fields of a circular loop of current located above ground. *Antennas and Propagation, IEEE Transactions on*, v. 20, n. 4, p. 520–522, July. 1972. ISSN 0018-926X.
- 28 DURKIN, J. Surface vertical magnetic field produced by a finite loop buried in an earth containing a thin conducting sheet. *Radio Science*, Wiley Online Library, v. 32, n. 1, p. 19–23, 1997.
- 29 ADMINISTRATION, O. S. . H. *Electromagnetic Radiation: Field Memo*. Accessed: 2015-02-22. Available at: <[https://www.osha.gov/SLTC/radiofrequencyradiation/electromagnetic\\_fieldmemo/electromagnetic.html#section\\_6](https://www.osha.gov/SLTC/radiofrequencyradiation/electromagnetic_fieldmemo/electromagnetic.html#section_6)>.
- 30 DA, W. J. H. *Theoretical noise and propagation models for through-the-earth communication*. [S.l.], 1982.
- 31 LINCAN, Y. *Measurements and modeling of the electromagnetic fields in Through-The-Earth (TTE) wireless communications*. Tese (Doutorado) — University of New Mexico, 2014.

- 32 L., H. H.; M., M. J. *Introductory mining engineering*. [S.l.]: John Wiley, 2002.
- 33 HEM, P.; CALDWELL, J. *Block Caving*. Accessed: 2015-01-04. Available at: <<http://technology.infomine.com/reviews/Blockcaving/welcome.asp?view=full>>.
- 34 PRESS, A. *September U.S. Mine Inspections Result in 133 Citations*. 2015. Accessed: 2015-11-5. Available at: <<http://wvpublic.org/post/september-us-mine-inspections-result-133-citations>>.
- 35 RATCLIFFE, M. *Anglo American shares fall as miner completes sale of Norte copper mine after commodities fall hits profits*. 2015. Accessed: 2015-10-01. Available at: <<http://www.cityam.com/224250/anglo-american-completes-sale-of-norte-copper-mine-after-commodities-fall-hits-profits>>.
- 36 ATM MINING TELEPHONES (UNDERGROUND). 2014. Accessed: 2014-09-30. Available at: <<http://www.britishtelephones.com/atm/atmtel6.htm>>.
- 37 AGGARWAL, R.; MOORE, P. Digital communications for protection. iii. fibre optics. *Power Engineering Journal*, v. 8, n. 5, p. 241–246, Oct. 1994. ISSN 0950-3366.
- 38 ON-LINE, C. *95% of municipalities have fiber optics in 5 years*. 2015. Accessed: 2015-12-04. Available at: <<http://www.confirmeonline.com.br/confirme/en/noticias/95-dos-municipios-terao-fibra-optica-em-5-anos>>.
- 39 CONTROL, C. for D.; PREVENTION. *Advanced Tutorial on Wireless Communication and Electronic Tracking: Communication System Performance*. Accessed: 2014-05-12. Available at: <<http://www.cdc.gov/niosh/mining/content/emergencymanagementandresponse/commtracking/advcommtrackingtutorial2.html>>.
- 40 EXCHANGE, P. S. *Transverse Magnetic (TM) and Transverse Electric (TE) modes*. Accessed: 2016-01-02. Available at: <<http://physics.stackexchange.com/questions/78419/transverse-magnetic-tm-and-transverse-electric-te-modes>>.
- 41 PEI, Z.; DENG, Z.; YANG, B.; CHENG, X. Application-oriented wireless sensor network communication protocols and hardware platforms: A survey. In: *Industrial Technology, 2008. ICIT 2008. IEEE International Conference on*. [S.l.: s.n.], 2008. p. 1–6.
- 42 BANDYOPADHYAY, L. K.; CHAULYA, S. K.; MISHRA, P. K. *Wireless Communication in Underground Mines: RFID-based Sensor Networking*. 1<sup>st</sup>. ed. [S.l.]: Springer Publishing Company, Incorporated, 2009. ISBN 0387981640, 9780387981642.
- 43 HUBING, T. H. *Survey of Numerical Electromagnetic Modeling Techniques*. [S.l.], 1991.
- 44 ZHANG, Q.; LI, W. Research on channel characteristics of through-the-earth communication based on fdtd method. *2014 Sixth International Conference on Measuring Technology and Mechatronics Automation*, IEEE Computer Society, Los Alamitos, CA, USA, v. 3, p. 35–37, 2010.
- 45 L, A. N. C. J. A. M. A. L. F. V. J. Through-the-earth magnetic field propagation: Modelling for underground applications,. *Electromagnetics in Advanced Applications, 2009. ICEAA '09. International Conference*, p. 525 – 528, 2009.
- 46 SOUTERWEB. *ASSEMBLY OF THE 2008 DQ RECEIVER BOARDS WITH THE NEW 3496 Hz CLASS-E HIGH EFFICIENCY BEACON DESIGN*. 2008. Accessed: 2016-01-09. Available at: <[http://souterweb.free.fr/boitaoutils/prospection/annexes/NotesOnThe2008\\_DQReceiverBoards.html](http://souterweb.free.fr/boitaoutils/prospection/annexes/NotesOnThe2008_DQReceiverBoards.html)>.
- 47 DURKIN, J. *Apparent Earth Conductivity Over Coal Mines as Estimated From Through-The-Earth Electromagnetic Transmission Tests*. 1984. Available at: <<http://www.cdc.gov/niosh/mining/userfiles/works/pdfs/ri8869.pdf>>.

- 48 LITTLE, I. A. *Detection of trapped miner eLecetromagetec signals above coal mines*. [S.l.], 1980.
- 49 MSHA. *Mine Improvement and New Emergency Response Act of 2006*. 2006. Accessed: 2016-01-06. Available at: <<http://www.msha.gov/mineract/MineActAmmendmentSummary.asp>>.
- 50 FRAGOSO, C. R. *Root mean square error (RMSE)*. Available at: <<http://www.ctec.ufal.br/professor/crfj/Graduacao/MSH/Model%20evaluation%20methods.doc>>
- 51 THE UNIVERSITY OF ALABAMA IN HUNTSVILLE. *The Lognormal Distribution*. The University of Alabama in Huntsville, Shelby Center for Science and Technology, Room 258A, 301 Sparkman Drive, Huntsville, AL 35899, US. Access: 2016-01-30. Available at: <<http://www.math.uah.edu/stat/special/LogNormal.html>>.

# APPENDIX



## I. MINER ACT OF 2006

The following text was extracted from United States Department of Labor website in January 6th 2016 [49]

"The Mine Improvement and New Emergency Response Act of 2006 would require operators of underground coal mines to improve accident preparedness. The legislation would require mining companies to develop an emergency response plan specific to each mine they operate, and require that every mine have at least two rescue teams located within one hour. S. 2803 would also limit the legal liability of rescue team members and the companies that employ them. The act would increase both civil and criminal penalties for violations of federal mining safety standards and would give the Mine Safety and Health Administration (MSHA) the ability to temporarily close a mine that fails to pay the penalties or fines. In addition, the act calls for several studies into ways to enhance mine safety, as well as the establishment of a new office within the National Institute for Occupational Safety and Health devoted to improving mine safety. Finally, the legislation would establish new scholarship and grant programs devoted to training individuals with respect to mine safety.

### **Key Provisions of the MINER Act:**

- Require each covered mine to develop and continuously update a written emergency response plan;
- Promote use of equipment and technology that is currently commercially available;
- Require each mine's emergency response plan to be continuously reviewed, updated and re-certified by MSHA every six months;
- Direct the Secretary of Labor to require wireless two-way communications and an electronic tracking system within three years, permitting those on the surface to locate persons trapped underground;
- Require each mine to make available two experienced rescue teams capable of a one hour response time;
- Require mine operators to make notification of all incidents/accidents which pose a reasonable risk of death within 15 minutes, and sets a civil penalty of \$5,000 to \$60,000 for mine operators who fail to do so;
- Establish a competitive grant program for new mine safety technology to be administered by NIOSH;
- Establish an inter-agency working group to provide a formal means of sharing non-classified technology that would have applicability to mine safety;

- Raising the criminal penalty cap to \$250,000 for first offenses and \$500,000 for second offenses, as well as establishing a maximum civil penalty of \$220,000 for flagrant violations;
- Give MSHA the power to request an injunction (shutting down a mine) in cases where the mine has refused to pay a final order MSHA penalty;
- Create a scholarship program available to miners and those who wish to become miners and MSHA enforcement staff to head off an anticipated shortage in trained and experienced miners and MSHA enforcement;
- Establish the Brookwood-Sago Mine Safety Grants program to provide training grants to better identify, avoid and prevent unsafe working conditions in and around the mines. These grants will be made on an annual, competitive basis to provide education and training for employers and miners, with a special emphasis on smaller mines."

## II. 3D MAGNETIC FIELD SIMULATION ON CST STUDIO SUITE

The following pages present a brief manual on how to build a simulation scenario for a TTE transmission system using the commercial software CST STUDIO SUITE.

For building the TTE transmission simulation computer environment, it is necessary to establish simulator options and constructing the simulation scenario. CST comes with a native application within the application that permit customization and simulation settings in a easy sequence as listed below:

1. Select an application area and a workflow. The application area depends on license purchased. For this investigation was acquired the Microwaves, Radio Frequencies and Optical license. This area opens six workflows: Antennas; Circuit & Components; Radar Cross Section; Biomedical, Exposure, SAR; Optical Applications, and Periodic Structures. Also it is possible to improve the workflow selection through more options according to each item.
2. Select the numerical method solver. According to each workflow, the software will suggest those methods recommended.
3. Select simulation units. For every simulation it is necessary to determine which units will be used for 3D structure building and simulation results.
4. Introduce frequency range or simulation time depending on selected method. In this stage is possible to determine frequency monitors for sensing E-field, H-Field, Power flow, Power losses and Far-field magnitudes.
5. 3D Structure construction. This stage is where physical characteristics of environment are defined. Using several 3D CAD functions is feasible to construct all structures needed. There is a grand material library for choosing from and it is possible to create new materials to fulfill specific conditions. Additionally, external CAD projects can be used to improve structure building velocity.

Aiming an acceptable relation between processing time and accuracy, it is important to select a suitable meshing of all structures and numerical method. CST offers two meshing options, a tetrahedral and hexahedral. Such option controls simulation time and it is available for both time and frequency domain. Figure II.1 shows how meshing adapts to each structure depending on its geometric characteristics. For simpler structures as cubic blocs, this adaptive meshing allows using bigger cells which diminish total node number and reduces time processing.

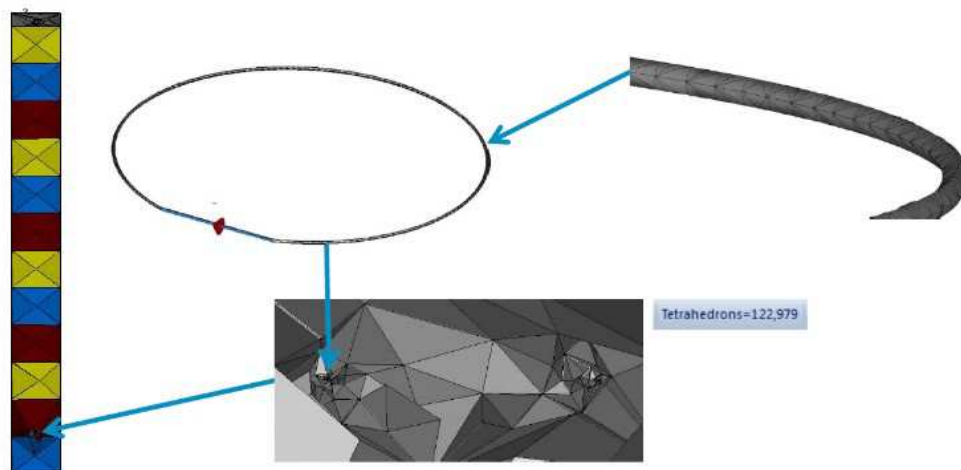


Figure II.1: Tetrahedral meshing

Border conditions are chosen in such way that numerical calculations can converge. That software offers usual conditions as: electric or magnetic planes, free space, conductive walls, periodic characteristic walls and unit cells. In figure II.2, all open boundaries are selected.

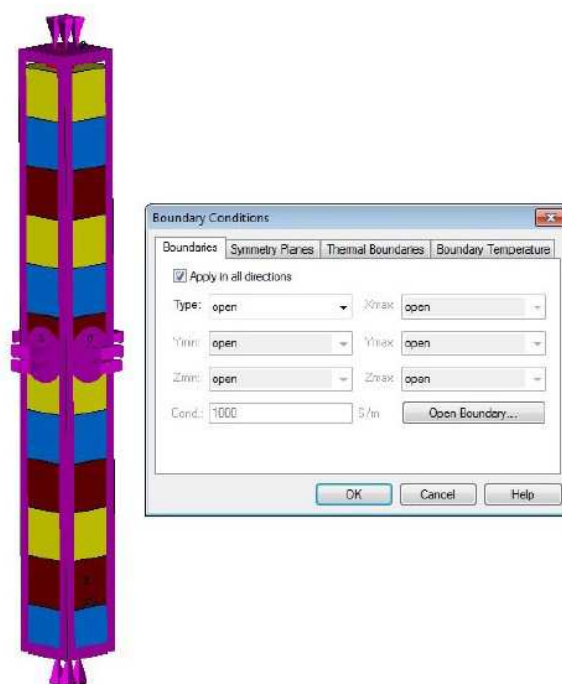


Figure II.2: Border conditions

Field intensities can be measured using probes located on positions of interest. Among that data, it is possible to measure voltages, currents, S parameters, and Z and Y matrix through ports on radiating structures. Generally, those responses are shown in 2D or 3D graphics, which can use several representations as logarithmic, polar, phase and magnitude. Some of them can be visualized as 3D animated images as a function of time and space changing colors for giving

motion sensation. Also, it is feasible to use 3D vector plots with arrows, cones, hedgehog shape lines and streamlines that moves according to field's direction. In figure II.3 is represented a frame of an animated 3D image where is indicated magnetic field variations on space.

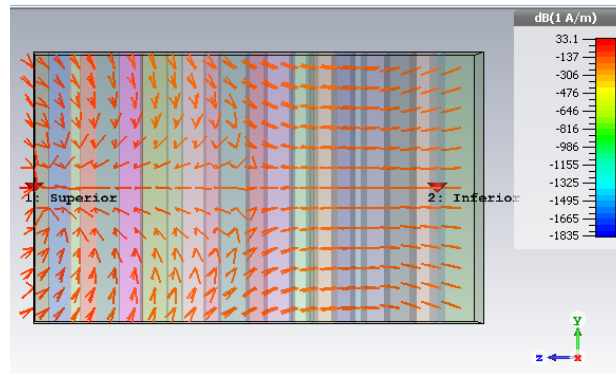


Figure II.3: Magnetic field inside substrates

Commercial software, as CST STUDIO SUITE, have post-processing tools that include programmable routines. Result data can be processed directly at CST for generating new graphics and comparing them to theoretical data without using any other software. Additionally, for some more complex calculation it is possible to use VBA code for upgrading post-processing analysis. Next figure represents a result obtain with CST.

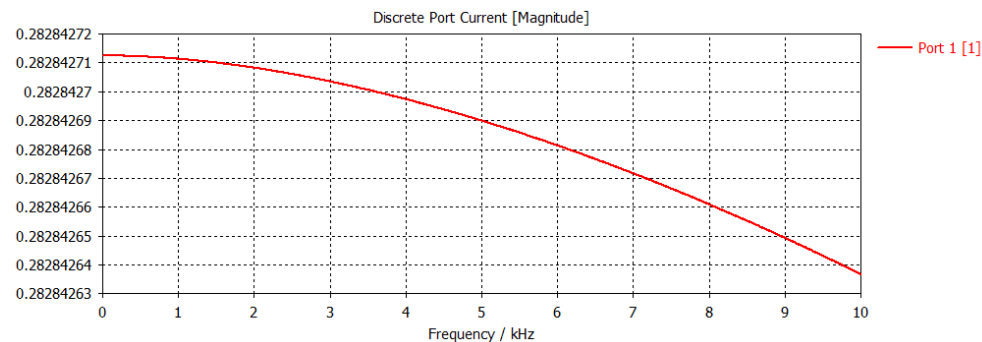


Figure II.4: Current result in linear scale

### III. ROOT MEAN SQUARE ERROR (RMSE)

Fragoso in [50] described the RMSE as follows: "The Root Mean Square Error (RMSE) (also called the root mean square deviation, RMSD) is a frequently used measure of the difference between values predicted by a model and the values actually observed from the environment that is being modeled. These individual differences are also called residuals, and the RMSE serves to aggregate them into a single measure of predictive power.

The RMSE of a model prediction with respect to the estimated variable  $X_{model}$  is defined as the square root of the mean squared error:

$$RMSE = \sqrt{\frac{\sum_{i=1}^n (X_{obs,i} - X_{model,i})^2}{n}}$$

where  $X_{obs}$  is observed values and  $X_{model}$  is modeled values at time/place  $i$ .

The calculated RMSE values will have units, and RMSE for phosphorus concentrations can for this reason not be directly compared to RMSE values for chlorophyll a concentrations etc. However, the RMSE values can be used to distinguish model performance in a calibration period with that of a validation period as well as to compare the individual model performance to that of other predictive models."

## IV. LOGNORMAL DISTRIBUTION

A definition of the UAH in [51] states that: "A random variable  $X$  has a lognormal distribution with parameters  $\mu \in \mathbb{R}$  and  $\sigma \in (0, \infty)$  if  $\ln(X)$  has the normal distribution with mean  $\mu$  and standard deviation  $\sigma$ . The parameter  $\sigma$  is the shape parameter of  $X$  and  $e^\mu$  is the scale parameter of  $X$ ."

In other words,  $X = e^Y$  and  $Y$  has normal distribution with mean  $\mu$  and standard deviation  $\sigma$ . It is possible to rewrite the equation as a function of a normally distributed random variable  $Z$  to obtain:  $Y = \mu + \sigma Z$ . This distribution is used to model continuous random quantities when the distribution is believed to be skewed.

The probability density function (PDF) with parameters  $\mu$  and  $\sigma$  is described by:

$$f(x) = \frac{1}{\sqrt{2\pi}\sigma x} e^{-\frac{[\ln(x) - \mu]^2}{2\sigma^2}}, \quad x \in (0, \infty)$$

1.  $f$  increases and then decreases with mode at  $x = e^{(\mu - \sigma^2)}$
2.  $f$  is concave upward then downward then upward again, with inflection points at  $x = e^{(\mu - \frac{3}{2}\sigma^2) \pm \sigma\sqrt{\sigma^2 + 4}}$
3.  $f(x) \rightarrow 0$  when  $x$  approximates to 0 and when  $x \rightarrow \infty$ .

Then the distribution function  $F$  is given by:

$$F(x) = \Phi \left[ \frac{\ln(x) - \mu}{\sigma} \right], \quad x \in (0, \infty)$$

## V. STATISTICAL PARAMETERS USED

The following parameters were used for each statistical distribution in this dissertation:

### BURR DISTRIBUTION

Table V.1: Burr parameters

Parameter	Description	Support
$\alpha$	Scale parameter	$\alpha > 0$
$c$	First shape parameter	$c > 0$
$k$	Second shape parameter	$k > 0$

### EXTREME VALUE DISTRIBUTION

Table V.2: Extreme value parameters

Parameter	Description	Support
$\mu$	Location parameter	$-\infty < \mu < \infty$
$\sigma$	Scale parameter	$\sigma \geq 0$
$\mu + \sigma\gamma$	Mean	-
$\sigma^2 \frac{\pi^2}{6}$	Variance	-

Where  $\gamma = \lim_{n \rightarrow \infty} \left( -\ln n + \sum_{k=1}^n \frac{1}{k} \right)$  is the Euler-Mascheroni constant.

### GENERALIZED PARETO DISTRIBUTION

Table V.3: Generalized Pareto parameters

Parameter	Description	Support
$\theta$	Location parameter	$-\infty < \mu < \infty$
$\sigma$	Scale parameter	$\sigma \geq 0$
$k$	Shape parameter	$-\infty < k < \infty$
$\theta + \frac{\sigma}{1-k}$	Mean	$k < 1$
$\frac{\sigma^2}{(1-k)^2(1-2k)}$	Variance	$k < 1/2$



## LOG-LOGISTIC DISTRIBUTION

Table V.4: Log-logistic parameters

Parameter	Description	Support
$\mu$	Log Mean	$\mu > 0$
$\sigma$	Log Scale	$\sigma > 0$

## LOG-NORMAL DISTRIBUTION

Table V.5: Log-normal parameters

Parameter	Description	Support
$\mu$	Log Mean	$-\infty < \mu < \infty$
$\sigma$	Log standard deviation	$\sigma \geq 0$

## NORMAL DISTRIBUTION

Table V.6: Normal parameters

Parameter	Description	Support
$\mu$	Mean	$-\infty < \mu < \infty$
$\sigma$	Variance	$\sigma \geq 0$

# VI. NUMERIC METHODS FOR ELECTROMAGNETIC MODELING

Numerical method usage for calculation of magnetic fields, magnetic field densities, impedance, etc. from Maxwell equations has been essential to antennae design and complex propagation media modeling. The most used techniques for such calculations are listed by Todd in [43] and are presented as follows:

## VI.1 FDTD

Finite Difference Time Domain provide a direct solution to Maxwell curl equations VI.1 and VI.2 that depend on time. Through simple central-difference approximations the method evaluates the space and time derivatives in a time stepping procedure.

$$\nabla \times \mathbf{E} = -\mu \frac{\partial \mathbf{H}}{\partial t} \quad (\text{VI.1})$$

$$\nabla \times \mathbf{H} = \sigma \mathbf{E} + \epsilon \frac{\partial \mathbf{E}}{\partial t} \quad (\text{VI.2})$$

The region to be modeled is represented by two interspersed grids of discrete points. The first grid has the points where magnetic field will be evaluated. The other grid contains the points where the electric field will be evaluated.

A simple FDTD grille is represented in Figure VI.1. FDTD stands that for each H-field vector component there are four E-field components. An approximation of first-order central-difference is expressed as:

$$\frac{1}{A} [E_{z1}(t) + E_{y2}(t) - E_{z3}(t) - E_{y4}(t)] = -\frac{\mu_0}{2\Delta t} [H_{x0}(t + \Delta t) - H_{x0}(t - \Delta t)] \quad (\text{VI.3})$$

Where  $A$  is the area of the near face of the cell in Figure VI.1. Due to the time stepping, the only unknown variable is  $H_{x0}(t + \Delta t)$ , which is calculated with E-field values at time  $t$ . Then, a similar process is realized with H-field in equation VI.2 to calculate the next step of E-field.

That calculation is repeated until reaching a steady state solution or desired solution. At each time step, the field components update equations are explicit and no linear equation system is solved. Regarding computer storage and running time, this method is proportional to electrical size of the volume model and grid resolution.

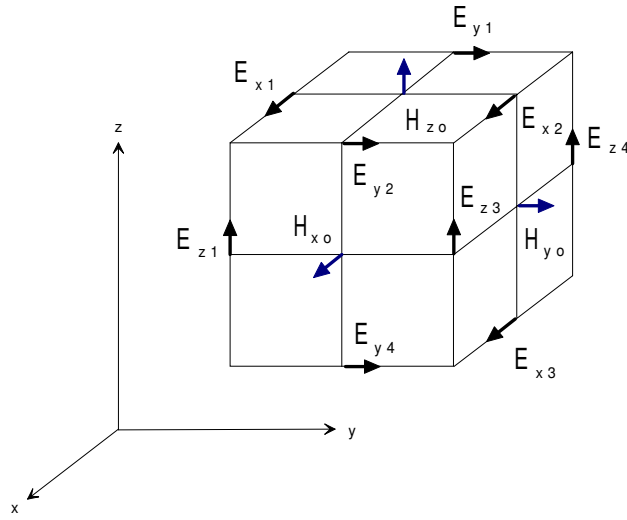


Figure VI.1: Basic Element of FDTD Space segmentation  
Adapted from: Hubing [43]

## VI.2 METHOD OF MOMENTS (MOM)

This method is a technique for solving complex integral equations by means of reducing those equations to a more uncomplicated linear system. MoM uses the technique of "Weighted residuals" which starts with the establishment of a set of trial solution functions with one or more variable parameters. Then, the residuals are a measure of the difference between the trial solution and the real solution. Aiming the minimization of those residuals, the variable parameters are determined in such a way that the best fit of the trial functions is guaranteed.

The equation solved by MoM has the form of the Electric Field Integral Equation (EFIE) or the Magnetic Field Integral Equation (MFIE). Both forms can be derived from Maxwell's equations, considering the problem of a scattered field by a PEC (Perfect Electric Conductor) or PMC (Perfect Magnetic Conductor) surface. Such equations have the following form:

$$EFIE : \mathbf{E} = f_e(\mathbf{J}) \quad (VI.4)$$

$$MFIE : \mathbf{M} = f_m(\mathbf{J}) \quad (VI.5)$$

The left-hand side terms of these equations are the incident fields and  $J$  is the induced current. Such equations are flexible in the terms of adaptation to several scenarios as thin-wire structures or metal plates. Generally, they are expressed in the frequency domain, nonetheless MoM can be used in time domain.

The first step in the MoM solution process is expanding  $J$  as a finite sum of expansion functions,

$$\mathbf{J} = \sum_{i=1}^M J_i b_i \quad (\text{VI.6})$$

where  $\mathbf{b}_i$  is the  $i^{\text{th}}$  basis function and  $J_i$  is an unknown coefficient. After that, a set of  $M$  linearly independent testing functions,  $w_j$  are set. An inner product of each testing function is built using both sides of the equation that is been solved. Regarding MFIE, this inner product results in a set fo  $M$  independent equations as:

$$\langle w_j, \mathbf{J} \rangle = \langle w_j, f_m(\mathbf{J}) \rangle \quad j = 1, 2, \dots, M \quad (\text{VI.7})$$

Then, expanding  $J$  through equation VI.7, a set of  $M$  equations in  $M$  unknowns is obtained:

$$\langle w_j, \mathbf{J} \rangle = \sum_{i=1}^M \langle w_j, f_m(\mathbf{J}_i, \mathbf{b}_i) \rangle \quad j = 1, 2, \dots, M \quad (\text{VI.8})$$

Which can be expressed by its matrix form:

$$[\mathbf{H}] = [Z][\mathbf{J}] \quad (\text{VI.9})$$

where:

$$\begin{aligned} Z_{ij} &= \langle w_j, f_m(b_i) \rangle \\ \mathbf{J}_i &= J_i \\ \mathbf{H}_j &= \langle w_j, \mathbf{H}_{\text{inc}} \rangle \end{aligned}$$

Vector  $\mathbf{H}$  contains the known incident field quantities and the terms of  $Z$ -matrix the geometry functions.  $J$  vector contains the unknown coefficients of the induced current. Such values are obtained solving the equation system. Other parameters as the scattered magnetic and electric fields can be estimated directly from the induced currents.

Modifying those integral field equations, MoM can be applied to structures with conductors only, homogeneous dielectrics only, or specific conductor-dielectric geometries. This method is not very effective when applied to non planar structures or arbitrary configurations with complex geometries or non-homogeneous dielectrics.

### VI.3 FINITE ELEMENT METHOD (FEM)

Similarly to MoM, this method is used to solve nonlinear magnetic and electrostatic problems. The first step for solving a problem is dividing the configuration into a number of small homogeneous elements. Figure VI.2 shows an example of this segmentation. The model has information

about object geometry, material constants, excitations and boundary conditions. Those pieces can be smaller in places with more detailed geometries and much larger in other places. For each finite element, a simple (usually linear) variation of field quantity is assumed. All corners of the elements are called "nodes". The main objective of FEM is to determine the field quantities at the nodes.

Commonly FEM analysis finds the solution for the unknown field quantities by minimizing an energy functional. This energy functional is an expression that describes all energy associated with the configuration under analysis. For a 3-Dimension, time-harmonic problems this functional can be represented by:

$$F = \int_V \left( \frac{\mu |\mathbf{H}|^2}{2} + \frac{\epsilon |\mathbf{E}|^2}{2} - \frac{\mathbf{J} \cdot \mathbf{E}}{2j\omega} \right) dv \quad (\text{VI.10})$$

The first two terms in the integral represent the energy stocked in the H and E-field, and the third term is the energy dissipated by conduction currents.

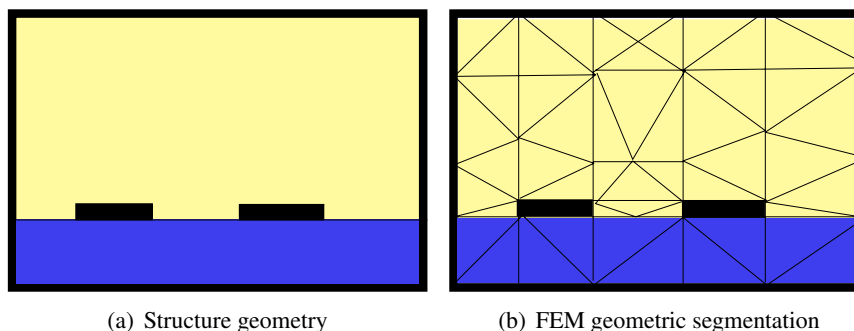


Figure VI.2: FEM segmentation example  
Adapted from Hubing [43]

An equation of the form of  $f(\mathbf{J}, \mathbf{E}) = 0$  is obtained by setting to zero the derivative with respect to  $\mathbf{E}$  and expressing  $\mathbf{H}$  in terms of  $\mathbf{E}$ . An approximation of the function  $f$  of order  $k$  is applied to each of  $N$  nodes and boundary conditions are enforced, which results in the following equation system:

$$\begin{bmatrix} J_1 \\ J_2 \\ \vdots \\ J_n \end{bmatrix} = \begin{bmatrix} y_{11} & y_{12} & \dots \\ y_{21} & y_{22} & \dots \\ \vdots & \vdots & \\ \cdot & \cdot & y_{nn} \end{bmatrix} \begin{bmatrix} E_1 \\ E_2 \\ \vdots \\ E_n \end{bmatrix} \quad (\text{VI.11})$$

The values of  $\mathbf{J}$  on the left-hand side of the equation system are called "source terms" which present the known excitations. The elements of the  $\mathbf{Y}$ -matrix are functions of problem's geometry and boundary conditions. Due to each element interacts only with those elements close to it, the  $\mathbf{Y}$ -matrix is usually sparse. Vector terms on the right-hand side represent the unknown E-field at each node that are obtained by solving the equation system. Another parameters, as H-field,

induced currents, and power loss can be calculated from the E-field values. In order to obtain a unique solution, field values must be constrained at every boundary nodes. A notable limitation of FEM is the relative difficulty of modeling open configuration (i.e. where fields are not known at every spot in a closed boundary). To overcome this limitation, absorbing boundaries are used in practical applications. In the other hand, the main advantage of FEM is the the electrical and geometric properties of each element can be defined independently. This permits the segmentation of the problem to have smaller elements in regions with more complex geometries and bigger elements in relatively open regions. Also, it is possible to model more complicated geometries and arbitrary shaped dielectric regions fairly efficiently. Choosing between time and frequency domain will depend on the characteristics of the studied scenario and the solution needs.

## VII. MAGNETIC FIELD MEASUREMENTS FROM 94 AMERICAN COAL MINES

According to [48], the following tables shows the measurements, carried out by the American Bureau of mines in 1970, of Magnetic field and Magnetic moment from 94 coal mines for several depths, adapted to meters, and frequencies.

Table VII.1: Surface Vertical Magnetic Field signal levels vs. Overburden Depth from 94 Coal Mine Sites RMS Signal levels in dB reference  $1 \mu$  A/m. Adapted from [48].

Mine No.	State	Depth (m)	Frequency [Hz]			
			630	1050	1950	3030
1	KY	182.87	20.7	14.3	5.9	0.5
2	KY	122.83	32.3	29.3	23.6	17.9
3	KY	122.83	30.3	27.0	20.8	10.9
4	IL	243.83	-7.7	-8.9	-15.9	-24.8
5	KY	425.80	3.3	F <sup>1</sup>	0.0	-7.0
6	KY	205.43	24.1	20.7	13.0	-9.9
7	VA	158.49	31.1	29.3	24.6	23.7
8	KY	60.95	48.8	49.0	44.1	45.8
9	OH	80.46	41.2	41.4	37.5	34.7
10	OH	77.41	46.3	40.1	42.2	40.3
11	WV	80.46	44.0	45.0	42.0	43.0
12	WV	76.19	38.6	32.8	30.4	26.2
13	PA	103.93	36.0	36.0	36.0	31.0
14	PA	135.94	33.0	30.0	19.0	9.0
15	PA	182.87	17.0	16.0	12.0	10.0
16	PA	210.00	10.0	7.0	5.0	-3.0
17	PA	72.84	45.0	42.0	36.0	34.0
18	PA	64.00	48.0	48.0	42.0	44.0
19	PA	106.07	23.0	22.0	18.0	14.0
20	PA	103.93	35.0	35.0	30.0	28.0
21	PA	99.05	30.0	25.0	17.0	5.0
22	WV	173.43	32.3	30.1	25.1	23.9
23	VA	365.75	-6.3	-9.7	-12.9	-13.4
24	KY	82.29	39.0	37.5	35.5	36.0
Continued on next page						

<sup>1</sup>SYMBOLS: N= No test measurement performed. F=Failure to detect transmitted signal

**Table VII.1 – continued from previous page**

Mine No.	State	Depth (m)	Frequency[Hz]			
			630	1050	1950	3030
25	VA	129.84	33.0	31.0	20.0	18.5
26	VA	210.00	19.0	17.0	14.0	9.0
27	VA	210.00	21.0	19.0	17.0	16.0
28	VA	157.88	14.0	19.0	8.5	8.0
29	VA	177.08	28.0	25.0	22.0	19.5
30	KY	99.05	35.0	33.0	32.0	33.0
31	VA	188.97	23.0	21.0	17.0	17.0
32	WV	100.88	32.0	31.0	24.0	31.0
33	WV	70.10	26.0	29.0	32.0	31.0
34	WV	409.04	-2.0	-8.0	-20.0	-24.0
35	WV	99.05	43.0	42.0	37.0	35.5
36	WV	65.83	53.0	53.0	51.5	49.0
37	PA	145.99	33.0	32.0	26.0	21.0
38	WV	238.04	22.0	17.0	5.0	-11.5
39	WV	154.83	29.0	26.0	18.0	13.0
40	AL	142.95	38.0	33.0	26.1	20.8
41	AL	147.82	21.5	21.5	15.5	13.5
42	AL	109.11	35.0	36.0	31.0	29.0
43	AL	89.91	43.0	36.0	34.0	29.1
44	AL	79.85	48.0	47.0	44.0	41.0
45	TN	288.03	16.0	9.0	10.0	-6.0
46	TN	363.01	6.0	1.0	-3.2	-17.0
47	KY	79.85	43.0	41.5	40.0	33.0
48	KY	307.84	13.0	8.0	4.0	0.0
49	KY	145.99	30.5	29.5	27.0	24.0
50	IL	227.07	4.0	-7.0	0.0	-16.0
51	IL	85.03	26.0	33.0	29.0	30.0
52	IL	139.90	29.0	25.0	20.0	14.0
53	IL	197.81	20.0	10.0	10.0	-4.7
54	IL	93.87	40.0	37.0	26.0	23.0
55	IL	88.08	44.0	43.0	37.0	34.0
56	WV	128.93	35.0	33.0	29.0	27.0
57	WV	320.03	18.0	14.0	7.0	3.0
58	WV	177.08	27.0	24.0	19.0	15.0
59	WV	117.95	30.0	30.0	23.0	21.0
Continued on next page						



**Table VII.1 – continued from previous page**

Mine No.	State	Depth (m)	Frequency[Hz]			
			630	1050	1950	3030
60	WV	106.98	40.0	38.1	37.0	35.0
61	WV	257.86	N	N	N	N
62	WV	209.09	6.0	4.0	0.0	-6.0
63	WV	147.82	30.0	26.0	16.0	18.0
64	WV	107.89	34.0	34.0	31.0	31.0
65	WV	71.01	44.0	44.0	40.0	40.0
66	WV	78.02	16.0	17.0	15.0	16.0
67	WV	128.01	38.0	36.0	31.0	29.0
68	WV	136.85	18.2	17.6	12.1	7.9
69	WV	131.06	F	F	32.0	25.0
70	WV	278.89	F	F	-6.0	F
71	PA	72.84	54.0	52.0	43.0	39.0
72	PA	146.91	26.0	24.0	18.0	16.0
73	PA	190.80	F	26.0	21.7	F
74	PA	145.99	28.0	25.0	F	15.0
75	PA	200.55	27.0	15.0	12.0	3.0
76	DT	364.84	2.4	2.0	-14.0	-24.1
77	DT	304.79	1.1	-0.4	-8.6	-13.8
78	DT	365.75	13.0	7.0	2.0	-5.0
79	CO	427.02	-1.6	-11.0	F	F
80	OH	152.39	23.9	9.0	7.0	-7.0
81	OH	182.87	15.0	11.0	2.0	-11.0
82	OH	142.95	8.0	8.0	1.0	-9.0
83	OH	164.89	15.0	12.0	6.0	-3.0
84	OH	170.99	13.0	20.0	12.0	5.0
85	KY	79.24	45.0	44.0	39.0	40.0
86	KY	152.09	26.0	24.0	18.0	14.0
87	KY	121.91	30.0	28.0	24.0	24.0
88	KY	115.82	29.0	28.0	26.0	23.0
89	AL	197.81	22.0	20.0	16.0	10.0
90	AL	472.74	-2.0	-9.0	-12.0	-16.0
91	KY	57.91	44.0	41.0	36.0	33.0
92	KY	79.85	47.5	46.5	44.0	38.0
93	KY	21.03	57.0	56.0	53.0	52.0
94	KY	99.97	27.5	20.0	7.0	-4.0

Table VII.2: In-mine Collins Transmitter RMS Magnetic Moment at Fundamental Operation frequency vs. Frequency and Depth from 94 Coal Mine Sites  
 RMS Signal levels in dB reference ( $A\text{-}m^2$ ). Adapted from [48].

Mine No.	State	Depth (m)	Frequency [Hz]			
			630	1050	1950	3030
1	KY	182.87	1599	1206	741	495
2	KY	122.83	618	528	370	261
3	KY	122.83	618	528	370	261
4	IL	243.83	1438	1097	680	456
5	KY	425.8	1545	1172	724	484
6	KY	205.43	1545	1172	724	484
7	VA	158.49	1613	1232	765	513
8	KY	60.95	1410	1079	671	450
9	OH	80.46	847	698	468	323
10	OH	77.41	847	698	468	323
11	WV	80.46	766	619	405	277
12	WV	76.19	847	698	468	323
13	PA	103.93	1197	948	608	413
14	PA	135.94	1264	995	635	430
15	PA	182.87	931	759	502	345
16	PA	210	847	698	468	323
17	PA	72.84	1142	909	587	399
18	PA	64	970	774	501	341
19	PA	106.07	415	339	224	154
20	PA	103.93	1173	931	599	407
21	PA	99.05	759	631	427	296
22	WV	173.43	1346	1049	663	447
23	VA	365.75	1688	1279	789	527
24	KY	82.29	549	474	338	240
25	VA	129.84	1192	932	591	399
26	VA	210	1203	952	611	414
27	VA	210	1017	929	727	546
28	VA	157.88	1746	1325	818	547
29	VA	177.08	1727	1269	764	507
30	KY	99.05	1197	948	608	413
31	VA	188.97	1410	1079	671	450
32	WV	100.88	1089	870	563	383
33	WV	70.1	141	137	125	108
34	WV	409.04	2045	1526	929	619

Continued on next page

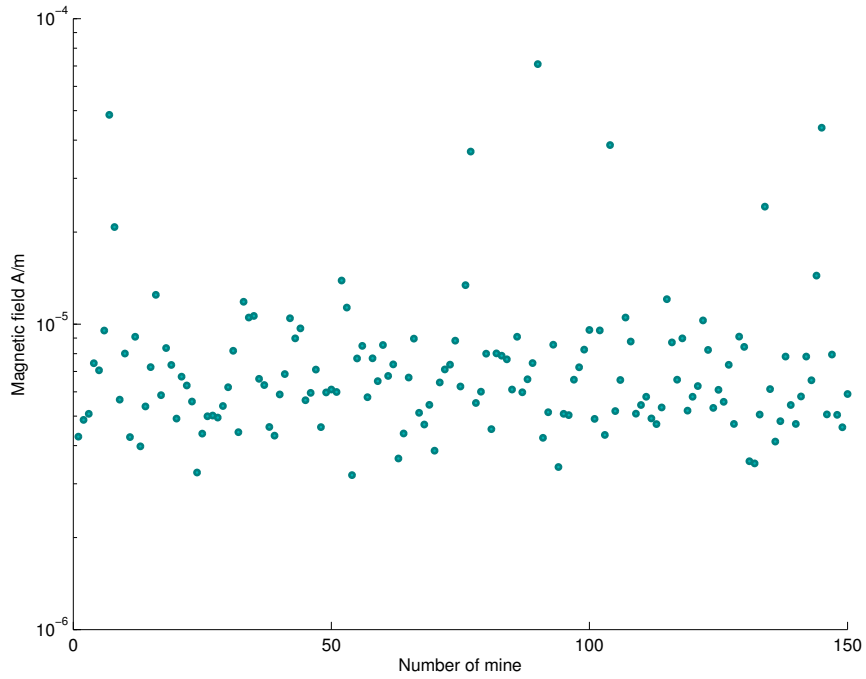
**Table VII.2 – continued from previous page**

Mine No.	State	Depth (m)	Frequency[Hz]			
			630	1050	1950	3030
35	WV	99.05	1324	1037	658	445
36	WV	65.83	1310	1026	651	440
37	PA	145.99	1444	1119	704	474
38	WV	238.04	2216	1639	992	659
39	WV	154.83	1197	948	608	413
40	AL	142.95	1099	870	558	379
41	AL	147.82	847	698	468	323
42	AL	109.11	815	672	451	312
43	AL	89.91	618	528	370	261
44	AL	79.85	906	741	493	339
45	TN	288.03	1265	986	623	420
46	TN	363.01	1123	896	580	395
47	KY	79.85	639	543	379	266
48	KY	307.84	1319	1020	641	431
49	KY	145.99	926	755	501	344
50	IL	227.07	1299	1017	646	437
51	IL	85.03	718	601	410	285
52	IL	139.9	858	706	471	325
53	IL	197.81	1516	1169	731	492
54	IL	93.87	926	756	501	344
55	IL	88.08	1444	1119	704	474
56	WV	128.93	855	700	466	321
57	WV	320.03	1412	1081	672	451
58	WV	177.08	1028	816	524	356
59	WV	117.95	847	698	468	323
60	WV	106.98	1025	826	540	369
61	WV	257.86	936	760	501	344
62	WV	209.09	936	760	501	344
63	WV	147.82	1102	878	567	386
64	WV	107.89	1055	846	550	375
65	WV	71.01	936	760	501	344
66	WV	78.02	936	760	501	344
67	WV	128.01	1439	1115	701	472
68	WV	136.85	847	698	468	323
69	WV	131.06	1220	957	609	412
Continued on next page						

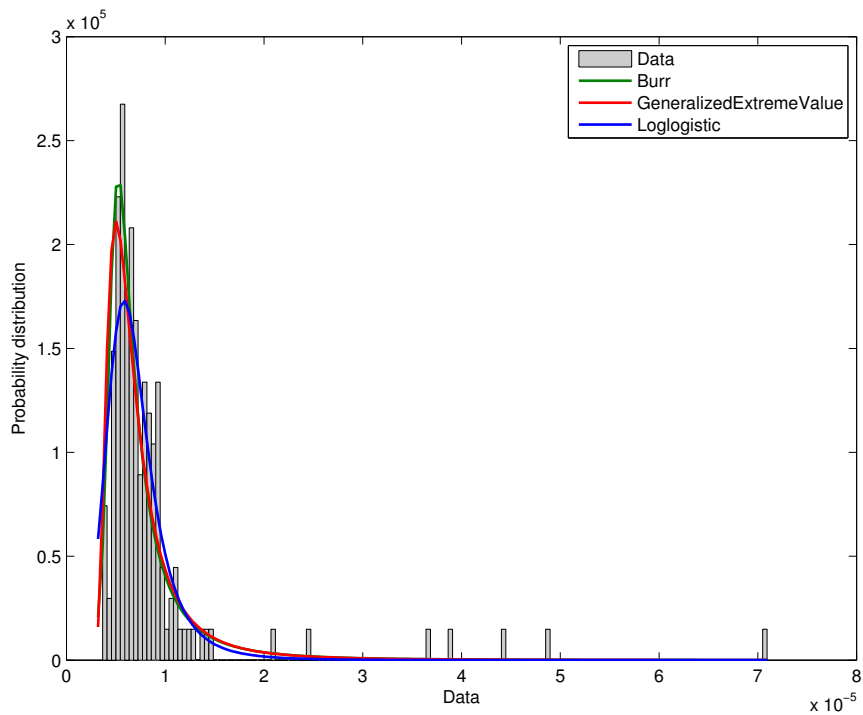
**Table VII.2 – continued from previous page**

Mine No.	State	Depth (m)	Frequency[Hz]			
			630	1050	1950	3030
70	WV	278.89	1467	1132	709	477
71	PA	72.84	1141	890	563	380
72	PA	146.91	888	726	482	331
73	PA	190.8	2047	1527	930	620
74	PA	145.99	1324	1037	658	445
75	PA	200.55	1471	1134	710	478
76	UT	364.84	1031	819	527	358
77	UT	304.79	1220	957	609	412
78	UT	365.75	2047	1527	930	620
79	CO	427.02	1342	1039	653	440
80	OH	152.39	847	698	468	323
81	OH	182.87	558	481	342	243
82	OH	142.95	959	779	513	352
83	OH	164.89	815	672	451	312
84	OH	170.99	964	782	515	353
85	KY	79.24	1087	871	565	385
86	KY	152.09	1324	1037	658	445
87	KY	121.91	1087	871	565	385
88	KY	115.82	531	457	323	229
89	AL	197.81	906	741	493	339
90	AL	472.74	2047	1527	930	620
91	KY	57.91	735	612	415	288
92	KY	79.85	1324	1037	658	445
93	KY	21.03	193	143	87	58
94	KY	99.97	447	306	176	115

# VIII. H-FIELD STATISTICAL DISTRIBUTIONS FOR FREQUENCY AND DEPTH

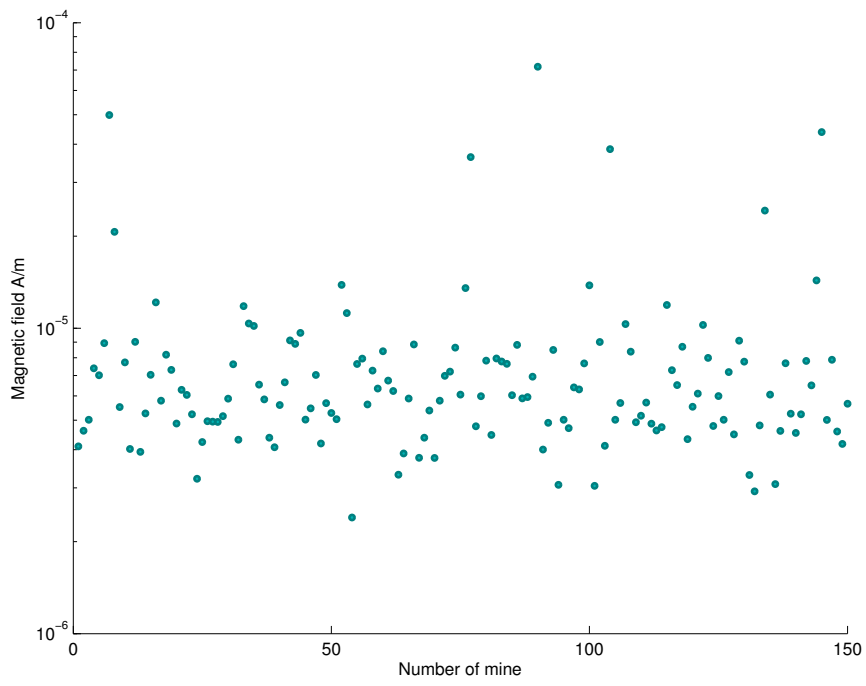


(a) H-field distribution

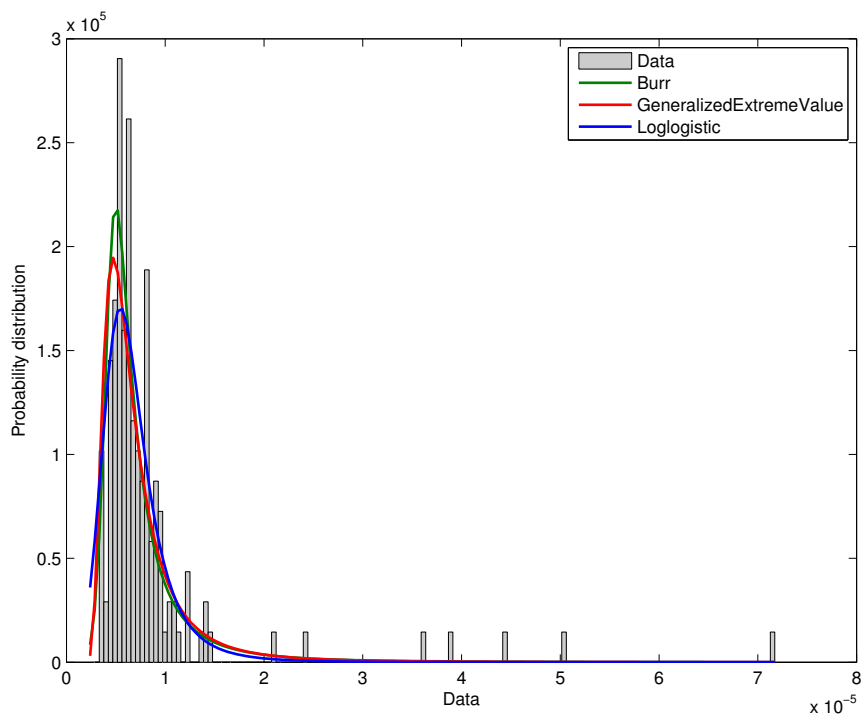


(b) Statistical fitting

Figure VIII.1: H-field statistical characterization at 20 m and 657.9 Hz

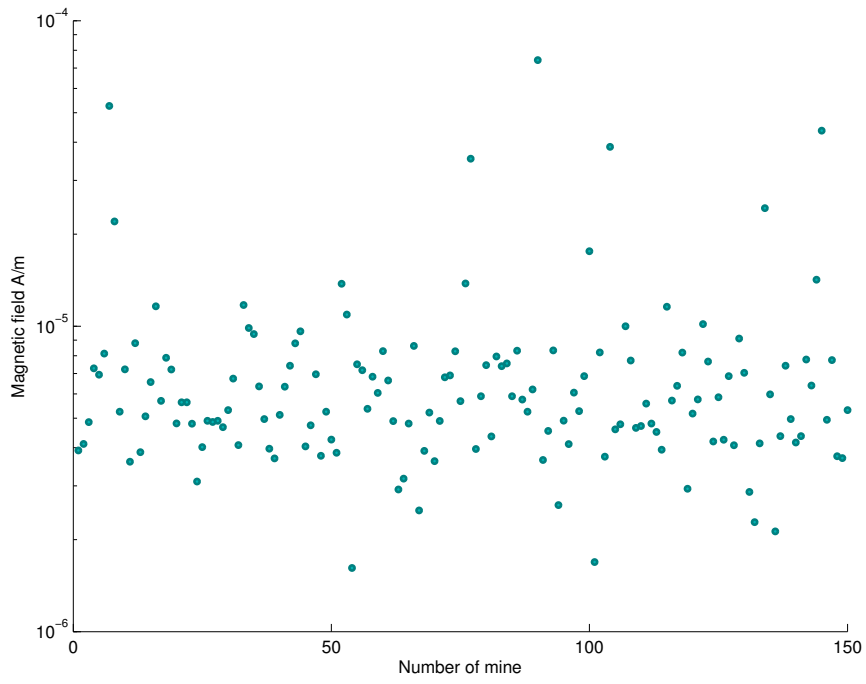


(a) H-field distribution

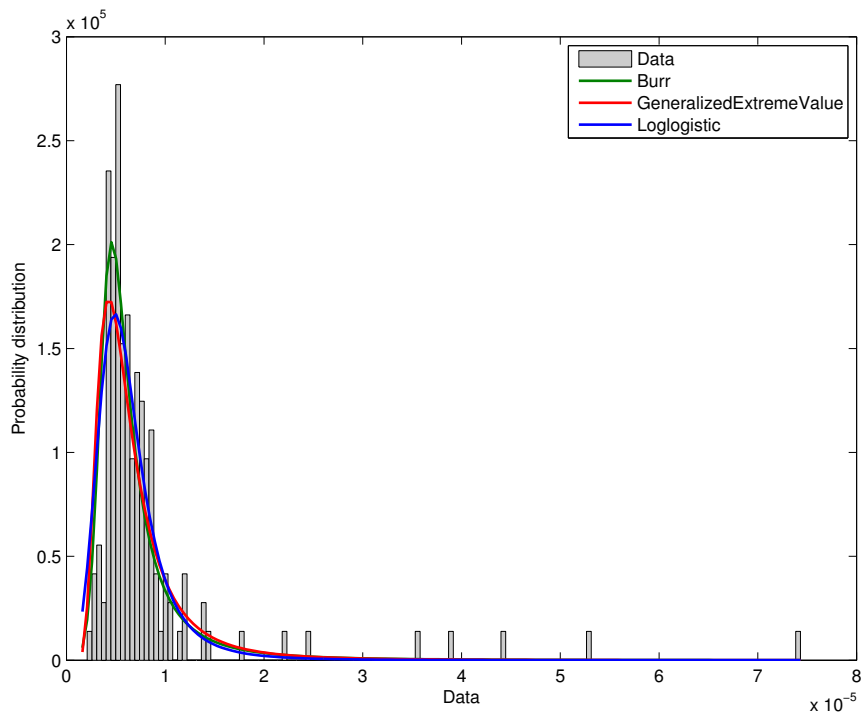


(b) Statistical fitting

Figure VIII.2: H-field statistical characterization at 20 m and 4328.8 Hz

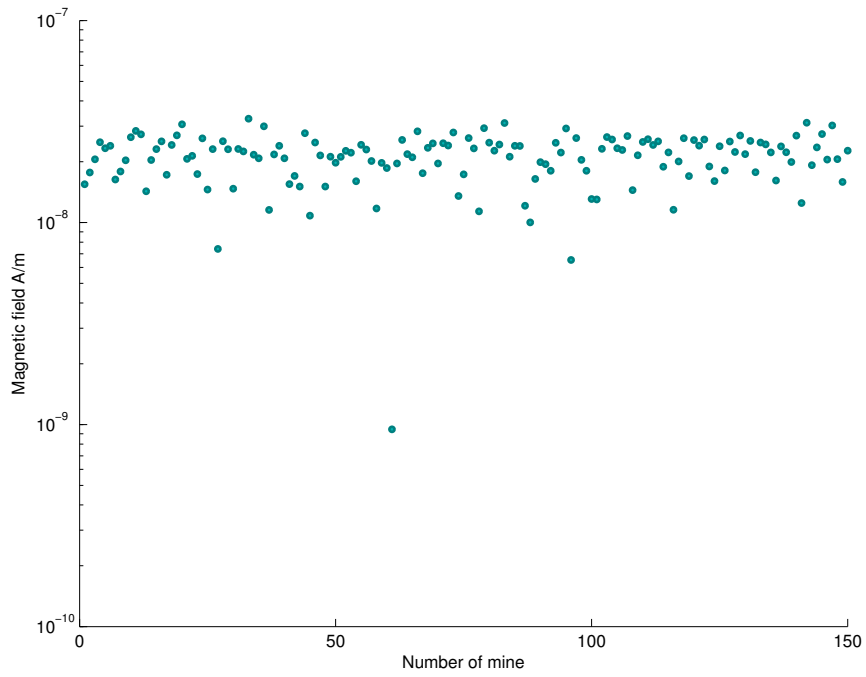


(a) H-field distribution

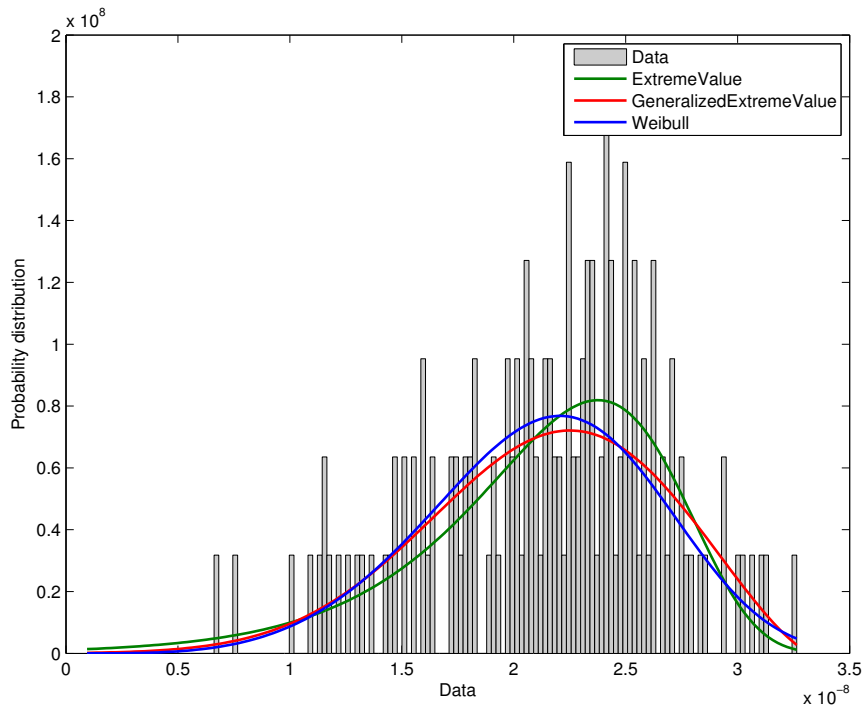


(b) Statistical fitting

Figure VIII.3: H-field statistical characterization at 20 m and 10000 Hz



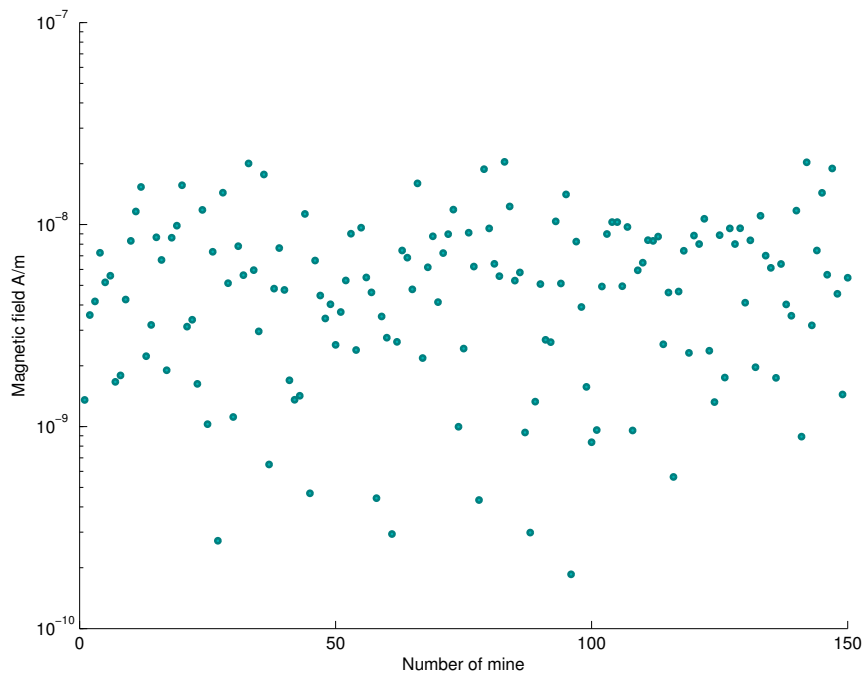
(a) H-field distribution



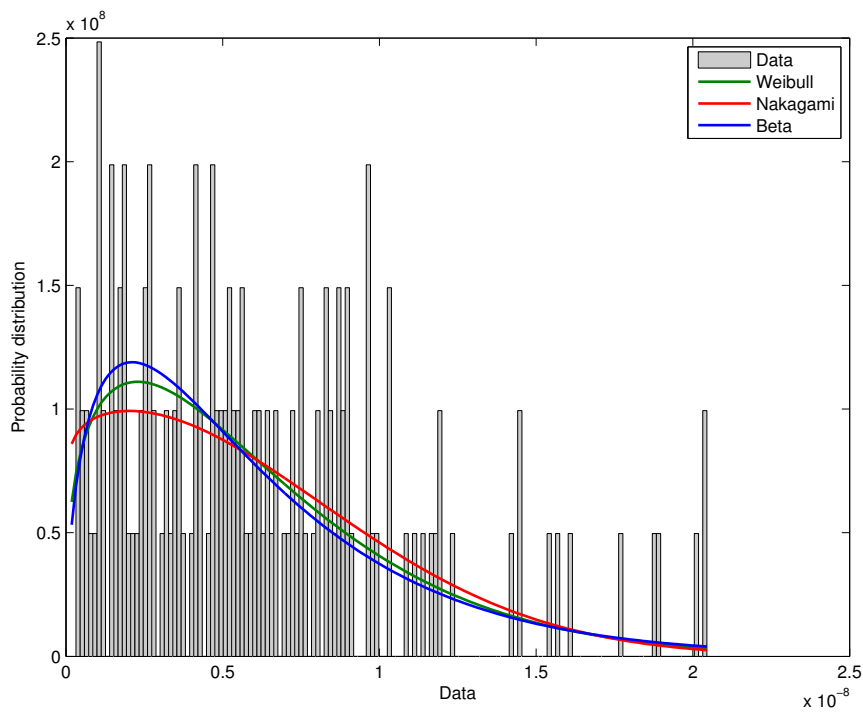
(b) Statistical fitting

Figure VIII.4: H-field statistical characterization at 150 m and 657.9 Hz



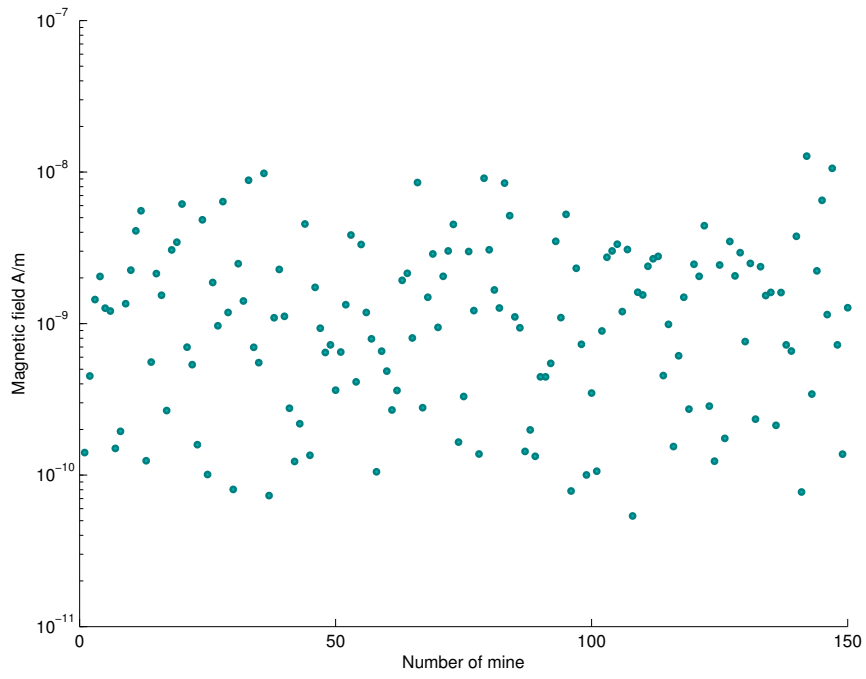


(a) H-field distribution

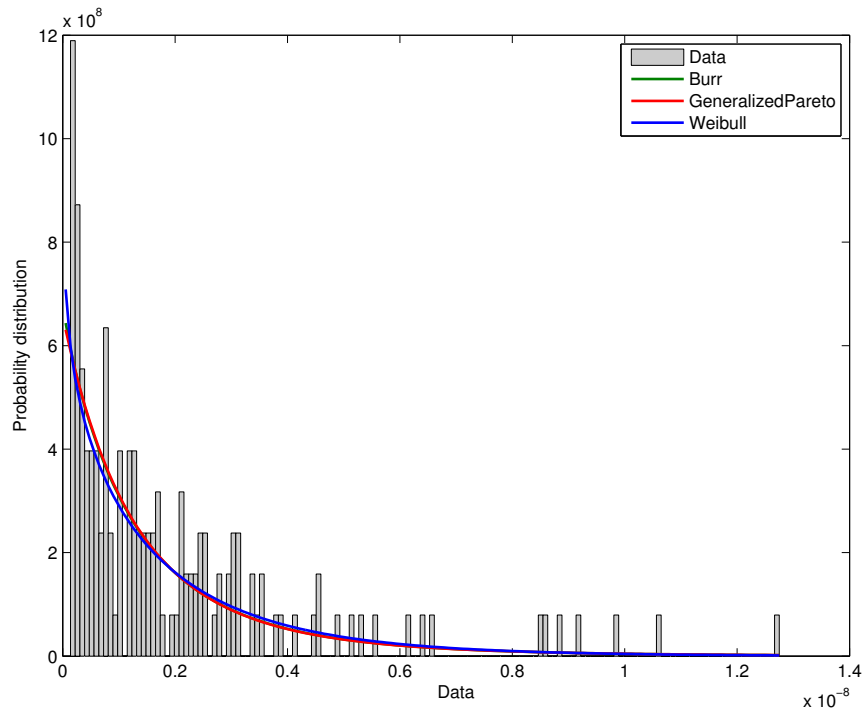


(b) Statistical fitting

Figure VIII.5: H-field statistical characterization at 150 m and 4328.8 Hz

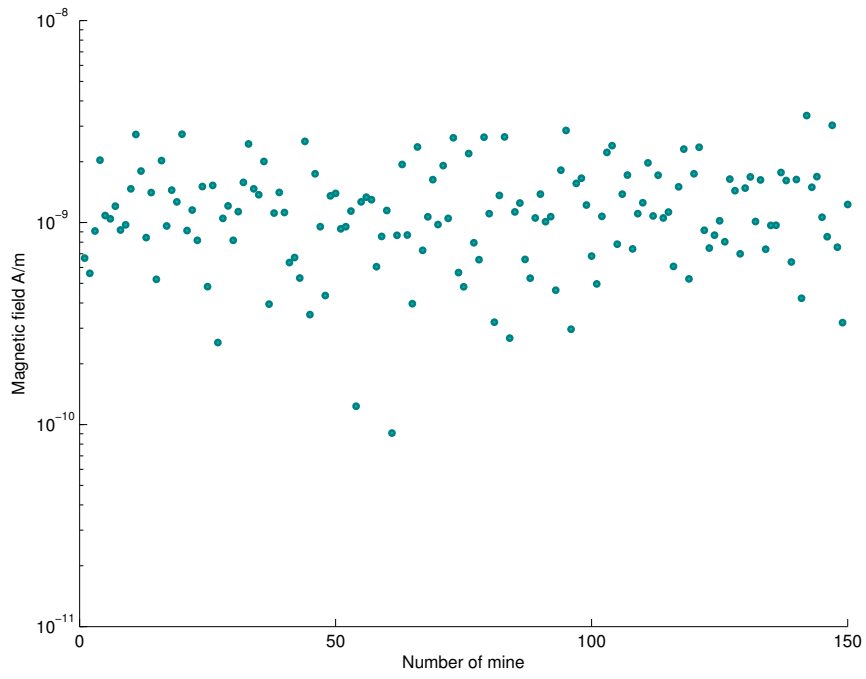


(a) H-field distribution

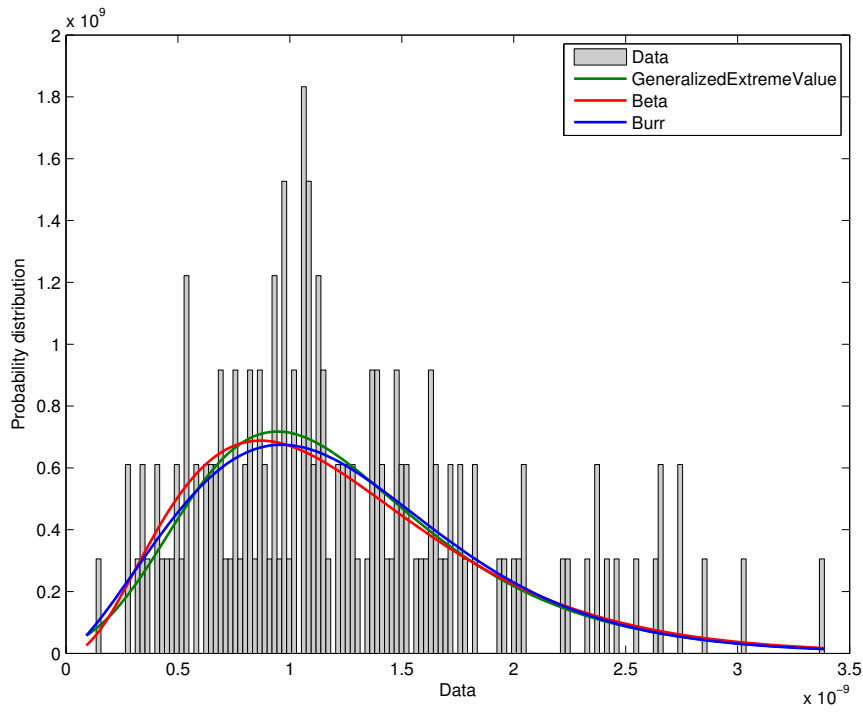


(b) Statistical fitting

Figure VIII.6: H-field statistical characterization at 150 m and 10000 Hz

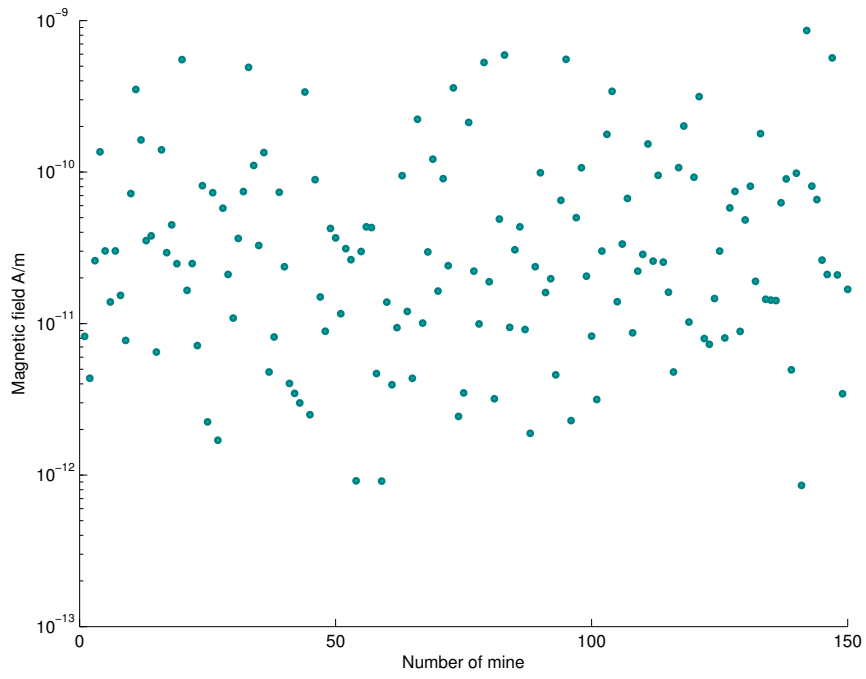


(a) H-field distribution

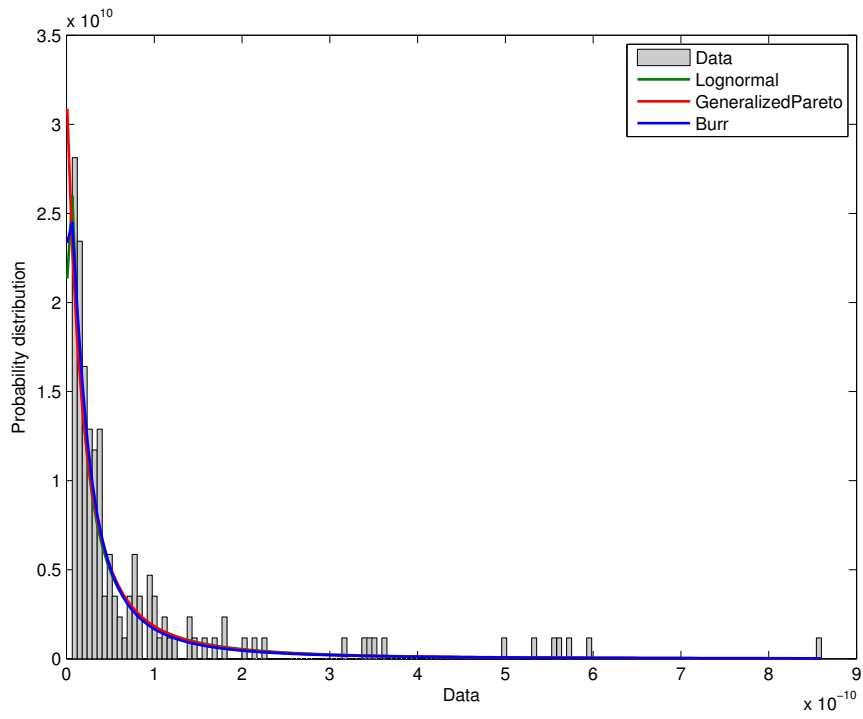


(b) Statistical fitting

Figure VIII.7: H-field statistical characterization at 300 m and 657.9 Hz

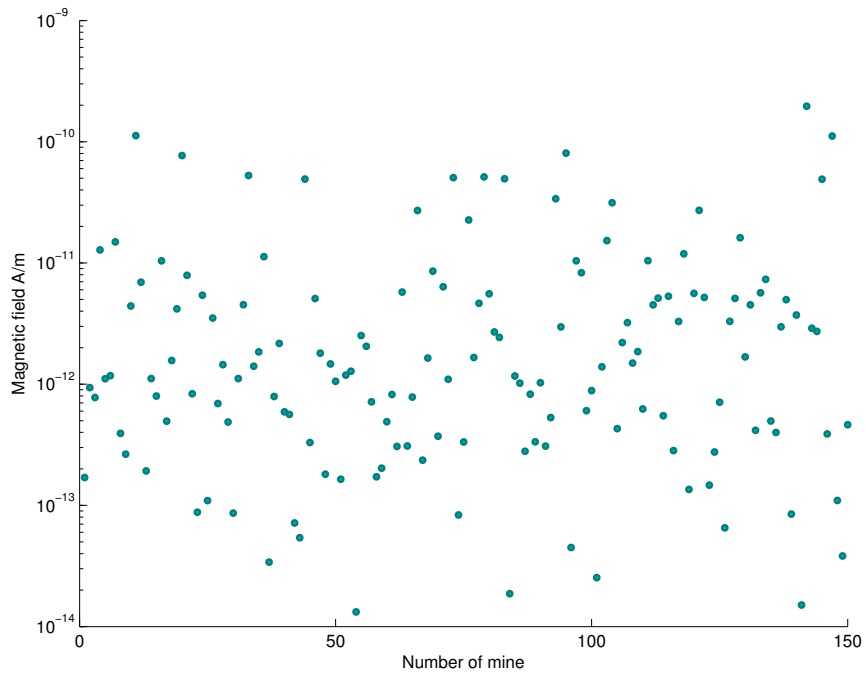


(a) H-field distribution

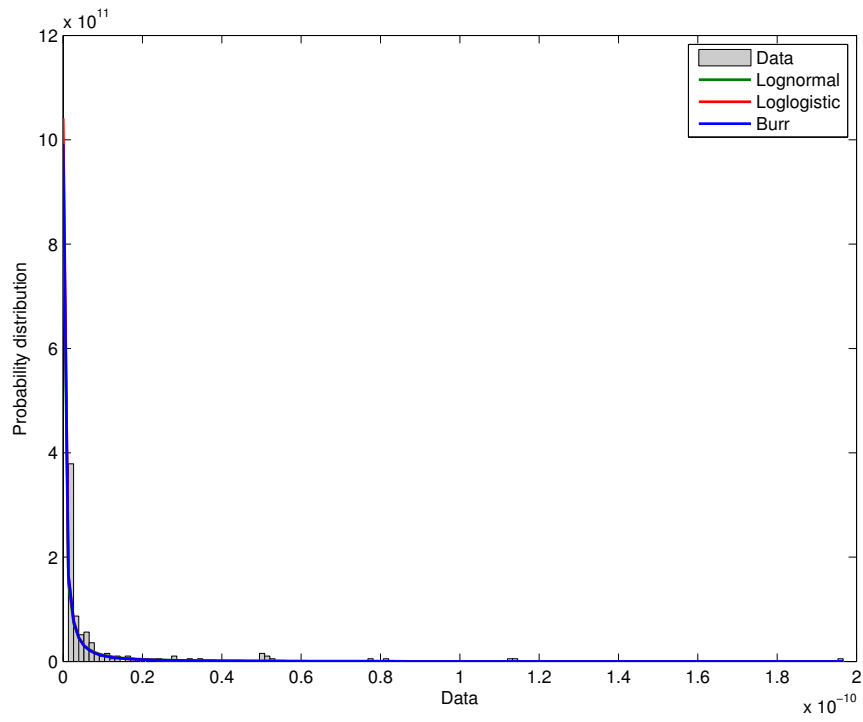


(b) Statistical fitting

Figure VIII.8: H-field statistical characterization at 20 m and 4328.8 Hz



(a) H-field distribution



(b) Statistical fitting

Figure VIII.9: H-field statistical characterization at 300 m and 10000 Hz